REPORT DOCUMENTATION PAGE

Form Approved
OMB No. 0704-0188

1. AGENCY USE ONLY (Leave blank)	2. REPORT DATE	3. REPORT TYPE AND DATES COVERED
	July 1972	Ph.D Thesis

4. TITLE AND SUBTITLE

Ion Drainage in High Power Klystrons

5. FUNDING NUMBERS

6. AUTHOR(S)

J. K. Smith

7. PERFORMING ORGANIZATION NAME(S) AND ADDRESS(ES)

Ph.D Thesis
University of Cambridge
Cambridge, England

8. PERFORMING ORGANIZATION REPORT NUMBER

9. SPONSORING/MONITORING AGENCY NAME(S) AND ADDRESS(ES)

Cambridge University,
English Electric Valve Co,
Chelmsford, England

10. SPONSORING/MONITORING AGENCY REPORT NUMBER

11. SUPPLEMENTARY NOTES

12a. DISTRIBUTION/AVAILABILITY STATEMENT

Unlimited

12b. DISTRIBUTION CODE

13. ABSTRACT *(Maximum 200 words)*

This experimental Ph.D thesis measures ion current in a high power klystron. The ion current is collected through a small hole in the cathode. Both oscilliatory & steady state ion current is measured & results in steady state are compared with applicable theory.

14. SUBJECT TERMS

Microwave tubes, Ion noise, Ions in Microwave tubes

15. NUMBER OF PAGES

145

16. PRICE CODE

17. SECURITY CLASSIFICATION OF REPORT	18. SECURITY CLASSIFICATION OF THIS PAGE	19. SECURITY CLASSIFICATION OF ABSTRACT	20. LIMITATION OF ABSTRACT
Unclassified	Unclassified	Unclassified	Unlimited

ION DRAINAGE IN HIGH POWER KLYSTRONS

by

J.K. SMITH

Trinity Hall, Cambridge

A dissertation submitted for the degree of Doctor of Philosophy at the University of Cambridge

July 1972

TABLE OF CONTENTS

Preface 1

Chapter 1 Introduction
1.1 Ions in High Power Electron Beam Devices 1
1.2 Review of Previous Investigations 4
1.2.1 Neutralised Beams 4
1.2.2 Unneutralised Beams 5
1.3 Proposed Research 8

Chapter 2 Description of the Experimental Apparatus
2.1 The Klystron 12
2.1.1 Physical Description 13
2.1.2 Modification to the Valve 14
2.1.2.1 External Modifications 14
2.1.2.2 Internal Modifications 17
2.1.3 Electrical Operation of the Klystron 19
2.2 The Vacuum System 21
2.3 Valve Voltage Supplies 23
2.4 Equipment for Ion Current Measurements 24
2.5 Overall Electrical Arrangement 29

Chapter 3 Ion Formation and Motion in the Drift Tube
3.1 Ion Formation by Collision 32
3.2 Trajectories of Collision Products 35
3.3 Losses of Ions and Ejected Electrons from the Beam 42
3.4 Ion Drainage to the Cathode 44
3.4.1 Space Charge Storage in the Beam 48
3.4.2 Neutralisation Pressure 49
3.4.3 Partial Neutralisation of the Beam Potential Depression 49
3.4.4 Voltage Gradient in the Drift Tube 49
3.5 Summary 50

Chapter 4 Preliminary Experimental Results
Introductory Remarks 51
4.1 Steady State Measurements 54
4.1.1 Dependence of the Ion Current upon Residual Gas Pressure 55
4.1.2 Faraday Cage Effects 58
4.1.3 Ion Current Dependence on the Magnetic Field 64
4.1.4 Ion Current Dependence on Beam Voltage and Current 65
4.2 Build-up Time to the Steady State 69
4.2.1 Build-up Time Dependence on Pressure 70
4.2.2 Build-up Time at Lowered Beam Currents 71
4.2.3 Charge Storage in the Beam 72
4.3 Oscillation in the Ion Drainage Current 74
4.3.1 Oscillations during Low Beam Current Measurements 75
4.3.2 Oscillations during Normal Beam Current Measurements 76
4.3.3 Oscillations with a Negative Collector 79
4.3.4 Oscillation at Different Beam Currents 80
4.3.5 Summary 81
4.4 Body Interception Current 83
4.4.1 Body Current at High and Low Pressures 84
4.4.2 Drift Tube Interception and Ion Current Oscillations 85

Chapter 5 Experimental Results with Drift Tube and Collector Bias

5.1 Introduction 87
5.2 Experimental Results with Variable Collector Bias 87
5.2.1 Positive Collector Bias 88
5.2.2 Negative Collector Bias 88
5.2.2.1 Spatial Distribution of Ion Formation 91
5.2.2.2 Potential Gradient Reversal 93
5.2.2.3 Increase in the Ion Current at Small Depression 94
5.2.2.4 Build-up Time and Charge Storage Measurements with Negative Collector 98
5.3 Drift Tube Section Biasing 101
5.3.1 DC Positive Bias 102
5.3.2 Positive Pulsing of the Drift Tube Sections 103
5.3.2.1 Methods and Typical Responses 103
5.3.2.2 Determination of Ion Formation Distribution 108
5.3.2.3 Experiments with Integration to Determine Faraday Cage Efficiency 110
5.3.2.4 Potential Gradients due to Ionic Charge 114

Chapter 6 Summary and Conclusions

6.1 Steady State Ion Current 117
6.2 Ion Current Build-up Time 119
6.3 Charge Storage in the Beam 120
6.4 Oscillations 121
6.5 Spatial Distribution of Ion Formation 122
6.6 Suggestions for Further Research 122

Appendix I Circuit Diagrams for Ion Measurements 125
Appendix II Rogowski Belt Construction 126
Appendix III Drift Tube Pressure Differential 128
Appendix IV Axial Potential in Drift Tube Biasing 134
Bibliography 135

PREFACE

This dissertation describes work carried out by the author in the Department of Engineering at the University of Cambridge (CUEL) between October 1968 and October 1971. The project originated as a result of correspondence between Professor A.H.W. Beck, CUEL, and M. Esterton, EEV, Chelmsford, which recognised the importance of establishing research into ion phenomena in high power valves. This correspondence resulted in the offer of the loan of a high power klystron to CUEL.

The work described in this dissertation deals with measurements made of the ion current draining to the cathode, which is the first stage of research which will eventually explore the relationship between drainage and the noise effects in the klystron by simultaneous measurements. This final design goal required that modifications be made to the klystron without affecting its RF performance, and a large part of the time spent on this study was involved with these modifications, and designing and building a measurement system.

Account is taken of the work of previous experimenters, and credit is given whenever the results and predictions of others are used in this dissertation. But this dissertation is based upon original work with a high-powered valve, and investigates the drainage of ions from a higher power electron beam than has been examined before, to the best of the author's knowledge. The explanations for the effects observed are also original, except as acknowledged.

Grateful thanks are given to my many colleagues in the Engineering Department for helpful discussions, and occasionally, muscle power, and in particular to:

Professor A.H.W. Beck, for his constant help, encouragement, and supervision.

English Electric Valve Co., Chelmsford, who provided not only the klystron which was modified for these experiments, but also advice

and construction without which this research could not have been completed. Especially to be thanked are M. Esterton and R. Heppinstall.

Messrs. A.R. Tubby, P. Mackenzie and D. Shaw and others of the staff of CUEL who applied great skill and patience to the problems which arose in the course of research.

Mr. and Mrs. John Thouron, who generosity in providing scholarships for exchange between the University of Pennsylvania and British universities provided my maintenance during the course of this research.

And lastly, to my wife for her patience and help.

This dissertation has not been submitted previously to any other university, either as a whole or in part.

July 1972 J.K. Smith

CHAPTER 1

INTRODUCTION

1.1 Ions in High Power Electron Beam Devices

High power electron beam devices find a great deal of usage in the fields of communications and radar as a source of high power microwave signal. They are characterised by their use of a dense electron beam as a means of signal amplification, and include in their class such devices as klystron power amplifiers and travelling wave tubes. The electron beam of these devices is formed within a vacuum envelope, and is usually prevented from spreading due to space charge forces by some system of electric and magnetic fields. The signal amplification is produced by a velocity modulation of the beam, and an RF circuit couples the power into the output load. Devices of this sort serve as what is presently the most efficient and least noisy method of producing high power microwave energy.

One of the problems which they all have in common is the ionisation by the electron beam of the residual gases which are present in the vacuum envelope. The residual gases are those left in the envelope after the normal valve degassing and pumping are completed. Although these valves are generally pumped down to pressures of 10^{-6} to 10^{-8} Torr, or better, the high beam current and long drift tube lengths may produce ions in such numbers that they can interfere with both signal fidelity and cathode life. These problems have been reported often in the literature (1,2,3,4,5,6,7,8) and are well known to valve manufacturers.

The interference which the ions cause to the desired signal usually takes the form of an AM or FM modulation of the RF output of the device. The modulation which has been observed falls into one of two classes: a higher frequency oscillation in the region of a couple of hundred kilohertz to one or two megahertz; and a much lower frequency, relax-

ation type of phenomena whose frequency ranges from tens of kilohertz down to almost DC. The oscillation may have discrete frequency components, but these are of changing frequency. The modulation can often be 10% of the carrier, and ranges up to close to 100% in some cases(9). Recent interest in generating signals with spurious sidebands very low even close to the carrier has revealed ion-related oscillations even in valves which are small in size and have been pumped very hard. The presence of these oscillations is in general discovered by observation of modulation effects on the RF. But at pressures higher than would normally be observed in a valve, these oscillations are sometimes found in measurements of the body current and collector current.

Bohlen and Dubravec (6) have demonstrated that the storage of ions within the beam can cause non-linearities in klystron-amplifier operation in the case of a valve rather similiar to the one considered in this dissertation. An interaction between the ionic oscillation about the axis and a transmitted signal causes changes in the beam diameter which result in increased gain in synchronism with the oscillations. It was found that draining some of the ions from the drift tube by depressing the collector had the effect of reducing the non-linearity.

Cathode life is affected by the impact on the cathode of ions draining from the drift tube, where the majority of ions are formed. Having drained from the drift space, the ions are accelerated across the full beam voltage, and then possess sufficient kinetic energy to do physical damage to the cathode. This effect is familiar to users of high power electron valves, and of any valves in which there is a high gas pressure (and hence more ions formed). A visual examination of cathodes removed from high power devices reveals a central area in which coatings have been removed, and in some cases, deeper damage done. The emissivity of this area is degraded and the life of the valve shortened. The sputtered coatings may cause undesired emission from

new surfaces, and the central change is emissivity has the effect of changing the focusing properties of the gun. Experiments by Cutler and Saloom (9) simulated this effect and showed increased body interception. Some manufacturers, including EEV (English Electric Valve Co.) in the case of Model K 376, the valve used in these experiments, anticipate this problem and reduce cathode damage due to sputtering by cutting a hole in the center of the cathode. A cup placed behind this hole confines most sputtered atoms. Observation of the cathodes removed from K376's and other valves after thousands of hours of operation reveal a region surrounding this central hole which is discoloured (10). Although the specific nature of the chemical change which causes the discolouration is undetermined, the phenomenon would indicate that not all ions are being collected by the cup.

Both the physical and electrical problems mentioned above are presently minimized by the obvious solution: more careful processing of the valve to ensure that the pressure remains as low as possible. But both the higher power and more stringent demands for low noise performance and longer life justify research to attempt to understand more adequately the processes of ion formation and drainage. The research which has been reported to date, which is reviewed briefly later in this chapter, has concentrated largely on low power devices.

Although a detailed explanation of the process of ion drainage will be attempted in Chapter 3, a very brief outline of the most obvious characteristics of ion drainage in valves of this type is necessary*. The electron beam emitted from the large area of the cathode is focused into the far narrower beam diameter, and accelerated to a high velocity. The narrow beam then travels along a long drift tube

* Details of the operation of these valves may be pursued in any of a variety of texts, e.g. A.H.W. Beck, Space Charge Waves, Pergammon Press, London, 1958.

in which it maintains a relatively constant diameter. It is in this region that the RF interaction takes place. The drift tube is generally cylindrical and is maintained at the same potential as the accelerating anode. After leaving the drift tube the beam electrons hit the collector, which is often also held near anode potential, although interest in increased efficiency is making the use of depressed collectors more common. Collisions between beam electrons and residual gas molecules along the beam path and on the walls of the collector may create ion-electron pairs. The ions which are thus generated along the length of the drift tube are mostly confined within the beam by the negative space charge fields of the beam. However, an axial flow of ions out of the drift tube must take place or else the continued generation of ions would neutralise the beam, resulting in a plasma state in the drift tube. This phenomenon is not observed in any but very gassy valves, or those in which a special arrangement of axial potential prevents the ions from draining. Once a steady state has been achieved, the average rate at which ions leave the drift tube must equal the rate at which they are being produced. This rate of production will be dependent on the path length and the pressure, as well as the species of residual gases which are present.

1.2 Review of Previous Investigations

1.2.1 Neutralised Beams

Much of the previous study of ions in electron beams has been associated with attempts to use the ionic charge to neutralise the space charge potential depression of the beam, and thus remove the need for heavy focusing systems which are normally necessary to confine electron beams. Field, et al (11) indicated early success in this endeavour with the use of trapping potentials on a low current (50 ma) beam in a specially designed experimental apparatus. Measurements of the spread of the electron beam in the absence of magnetic

fields were used as the means to determine the amount of beam neutralisation. However, the use of residual gas ions for neutralisation was shown not to be repeatably successful due to various instabilities which appear to be inherent in the attempt to neutralise the beam (12, 13,14). Further work on neutralised systems (15,16,17) dealt with the theory and some limited experimentation in the regime of neutralised and over-neutralised beams, and the sort of build-up to neutralisation which would be predicted. The most successful results reported with the use of neutralisation were those of Zinchenko and Zhigailo (18). They demonstrated the use of high residual gas pressures (10^{-4} to 10^{-5} Torr) in reducing transverse debunching. For the low voltage and high modulation case studied by them, beam diameters decreased to less than the unmodulated beam diameter.

Barford (19) analysed the case of ion drainage in linear flow beams, but the presence of magnetic field and the large potential depression in valves of interest to this dissertation violate his initial conditions, and predictions from the theory were shown not to be applicable to this experimental equipment.

In all of the work mentioned above, the gas pressure was much higher than that which would be expected in ordinary electron beam devices. Furthermore, since the advantages of doing away with the heavy focusing system are greatest in the case of low power devices (1 KW or less), which do not need the large cooling systems characteristic of higher power devices, most of the experiments performed in the study of beam neutralisation were done on low current and low voltage devices. The experimental work was also done without magnetic fields, and these three characteristics indicate that any application of the results of this work to high power valves must be carefully examined.

1.2.2 Unneutralised Beams

Although it is more relevant to the problem at hand, there has been

less work published on the study of ions in unneutralised beams. These are distinguished from neutralised systems by a lower pressure and a confining magnetic field.

Cutler (1) discusses RF modulation effects which he has observed in low power TWT's and examines them in greater detail with the use of a special apparatus. The experimental apparatus, however, is not capable of RF modulation, and oscillations can be observed only by measurement of the collector current. The oscillations observed by this method are divided into three classes: those which occur at the ion undulation frequency for the device, and are thus a function of beam current but not pressure; those occuring at a lower range of frequencies which appear to be relaxation oscillations, and are caused by change between complete neutralisation and loss of ions to a less neutralised state; and those which appear to be strictly electronic effects and are related to the number of beam secondaries. The second type are found to be common at 10^{-5} Torr and uncommon at 10^{-7} Torr. It is important to realise that these oscillations are fluctuations in the collector current, and represent losses to the body by beam diameter changes, or temporary storage within the beam itself. The cathode itself did not exhibit current fluctuations.

Sutherland (3) observed oscillations in the operation of a low power, high perveance TWT with magnetic confinement. As in the case of Cutler, collector current measurements were used as the means of detecting these oscillations. Unlike the oscillations mentioned just above, however, this phenomenon occurs at very low pressures, and could not be demonstrated above a critical pressure in the neighbourhood of 10^{-7} Torr unless the collector were depressed. Furthermore, the oscillations were observable in the cathode current as well as the collector current, although the latter was more sensitive. This is an indication that the thermionic emissivity of the cathode is affected as well as the beam

transmission. The oscillations occur at low frequencies between .1 and 3 KHz. Sutherland performed more extensive experiments with a specially constructed beam device which had a similiar high perveance gun, but no confining magnetic field. With those experiments he reached the conclusion that the oscillations are due to a transition between two or more solutions possible for the electron beam flow. Transition to a condition in which a virtual cathode forms allows ions to accumulate in the region of the virtual cathode until the minimum is overcome and the beam flow changes, thus expelling the ions, which in turn allows the virtual cathode to re-form. Volosok and Chirikov reached similiar conclusions (20).

Hartnagel and his associates report continuing work on this same problem (2,21,22). Experimental data were obtained on low power TWT's and klystrons, and oscillations in the collector current at frequencies between 1 Hz and 1 KHz were observed. Explanations put forward suggest that any electron beam which exhibits scalloping will demonstrate the oscillation phenomena at some pressures, but that the reduction of scalloping will serve to reduce the amplitude of the oscillations. It is suggested that the absence of oscillations of this type above a certain pressure occurs when the ion current is sufficient to prevent a potential well from forming again after an initial draining of the well has occured.

In terms of power, Senise's work with a 10 KV, 1 Amp beam is closest to that with which this dissertation deals. His observations of the collector current showed that an improvement in beam transmission occured as the potential minima caused by scallops stored ionic charge within the beam. Oscillations at high pressures were again observed, and some experimental evidence was found to suggest that although ion concentrations were found in the beam, they were shifted in position with respect to the beam scallops (23).

Hines, et al (24) applied the formulas of Field, et al (11) to determine the nature of ion drainage from drift tubes which have a longitudinal magnetic field, and found agreement in experimental work. The experiments use a 950 volt, 14.5 ma TWT in which a wire ion collector at the centre of the electron collector is used to determine the ion drainage by actual measurement of ion current. Pulsed experiments are used to determine the build-up of the ion drainage current to its steady state value, and by raising the pressure, neutralisation is observed. The work of Hines, et al is the only one relating to unneutralised beams which employs direct measurement of the ion current.

1.3 Proposed Research

The research reviewed above is felt to have the following limitations:

1) All experimenters except Senise (23) worked at low power. There are many reasons to suspect that high power devices might give results different from those obtained from low power devices. Firstly, the large size of high power devices makes it more difficult to obtain the low pressures common in small devices. Secondly, the large beam currents produce more ions (in direct proportion to the current), and they create large potential depressions. Whereas in the case of low current beams these depressions tend to be on the order of the energies due to the thermal and collision effects, they are far larger in the case of heavy current beams, ranging to hundreds of volts. Thus the confining effect of the fields created by the depression is far more significant, and furthermore, the fields are of such magnitude that they may impart velocities to collision products which would make those particles capable of further ionizing collisions. Thirdly, the high accelerating voltages which are used for the electron beam cause ions draining out of the drift tube to do more damage to the cathode. Finally, manufacturers observe ion-related effects far more frequently in

high power devices than in low power devices.

2) The vast majority of published work contains results obtained from indirect measurement of ion drainage and oscillation, as for example the measurement of collector current to observe oscillations. The effects of ion drainage are being measured rather than than the ion drainage itself. Such measurements as those of collector current, body interception current, and visual determination of beam diameter, are inaccurate means of studying the ions, and furthermore are effective only in measuring time-varying phenomena. In contrast, direct measurement of ion current within the beam as was done by Hines, et al (24) provides a sensitive measurement which does not have large background currents which require time dependence to distinguish ion effects from normal tube phenomena.

3) No attempt has been made to correlate the ion-related noise seen in some microwave amplifier outputs with the flow of ion current out of the drift tube. The present concern for high spectral purity in microwave signals for both radar and communications requirements has resulted in the evolution of measurement techniques which permit observation of spurious signals originating in microwave amplifiers with very great sensitivity (25). Use of these techniques therefore provides a very useful tool for the observation of ion-related noise effects, especially oscillation. The relationship between the amount of ion current within the beam and these noise effects has not been examined at all.

It is with the nature of ion drainage and the measurements made on an example of a high power klystron that this research is concerned. The work was planned to extend earlier researches and eliminate the limitations mentioned above. A high power (25 KW CW) klystron with a 17.5 KV, 4.6 A beam was kindly furnished by EEV, Chelmsford for the purpose of conducting these experiments. The only modifications made to the valve were to provide for a de-mountable electron gun, contin-

uous pumping, and direct measurement of ion drainage to the cathode with a Faraday Cage behind the central hole. The study is to consist of two parts: a first stage in which the experimental equipment is constructed and data on the ion drainage measured; and a second stage which will continue the work of the first and also make simultaneous measurements of the RF behaviour and the ion drainage. This dissertation reports on the first stage of this study.

The decision to use an operable valve to make this investigation rather than equipment specially designed for measurements of such a beam was made in order to provide a piece of equipment which was capable of simultaneously measuring ion current and RF noise and modulation for the second stage of the study. It was felt that the disadvantage of less flexibility for the measurement of ion current which is inherent in the use of an operable valve was outweighed by the importance of constructing equipment which was capable of simultaneous measurements. A further advantage in using an operable valve is that the information which it provides is expected to be of immediate application to other valves of similiar size and power. This is not always true of special experimental equipments.

Because the valve provides a Faraday Cage opening for the direct measurement of ion current, it is possible to measure such characteristics of the ion drainage as the total ion drainage to the cathode, the build-up times, charge storage within the beam, the spatial distribution of ion formation, and the dependence of these characteristics on various experimental conditions. In addition, the enhanced sensitivity for the measurement of oscillations mentioned above is gained by this direct measurement method for ions.

The goal of this first stage of work, in which no RF measurements are made, is to learn as much as possible concerning the formation and drainage of ions in the drift tube and collector. Since it is hoped that

the information gained in this investigation will be useful in suggesting methods to reduce degradation in valve performance caused by ion effects, some experiments are immediately suggested. The first of these is the measurement of the ion current drainage to the cathode under normal operating conditions. The dependence of this current upon residual gas pressure and beam current can be used to verify currently used approximations and theory. It is clear that attempts to measure oscillation present in the ion current are also of great interest.

The experimental data taken during measurements of these basic parameters of ion drainage in turn suggested other measurements and various techniques which could take advantage of the unique valve construction, and provide further knowledge and greater accuracy for the basic measurements. Results gained from these experiments are interrelated and require a certain amount of interpretation, which in turn leads to certain insights concerning the ion drainage process. The following chapters deal with the measurement and interpretation of these results.

CHAPTER 2

DESCRIPTION OF THE EXPERIMENTAL APPARATUS

The equipment used in these experiments centres around a 25 KW Tv transmitting klystron which was modified for continuous pumping and ion drainage-current measurement. The large size of this high power device meant that both electrical and mechanical problems had to be solved. The ion current measurement problem itself is difficult since it involves measuring very small currents at very high potentials and in the presence of large currents and voltages. The discussion of the equipment and the experimental set-up is most easily broken down into four parts: the valve itself, the equipment associated with maintaining and measuring the vacuum within it; the voltage supplies for the valve and the associated timing system; and the circuits for ion current measurements. This chapter deals with a discussion of all these aspects, excepting certain measurement problems which seem best discussed during explanations of individual measurements, and thus fall in later chapters.

2.1 The Klystron

The valve which was used in these experiments was an EEV Type K376 ceramic-metal klystron which was made available to CUEL by EEV, Chelmsford (Figure 1). The klystron is usually employed in television transmission and operates between 470 and 610 MHz, producing 25 KW RF power. The gain is 42 db. Four external tunable cavities are normally fitted, but these were not used during the experimentation described in this dissertation.

The normal beam voltage is 17.5 KV, and the electron gun has a microperveance of 1.97 (beam current = 4.56 Amps). The cathode is run negatively with respect to earth, and the body section and collector are at earth potential. The beam is magnetically focused in a field of about 400 Gauss, which is provided by a K4054 magnet assembly which

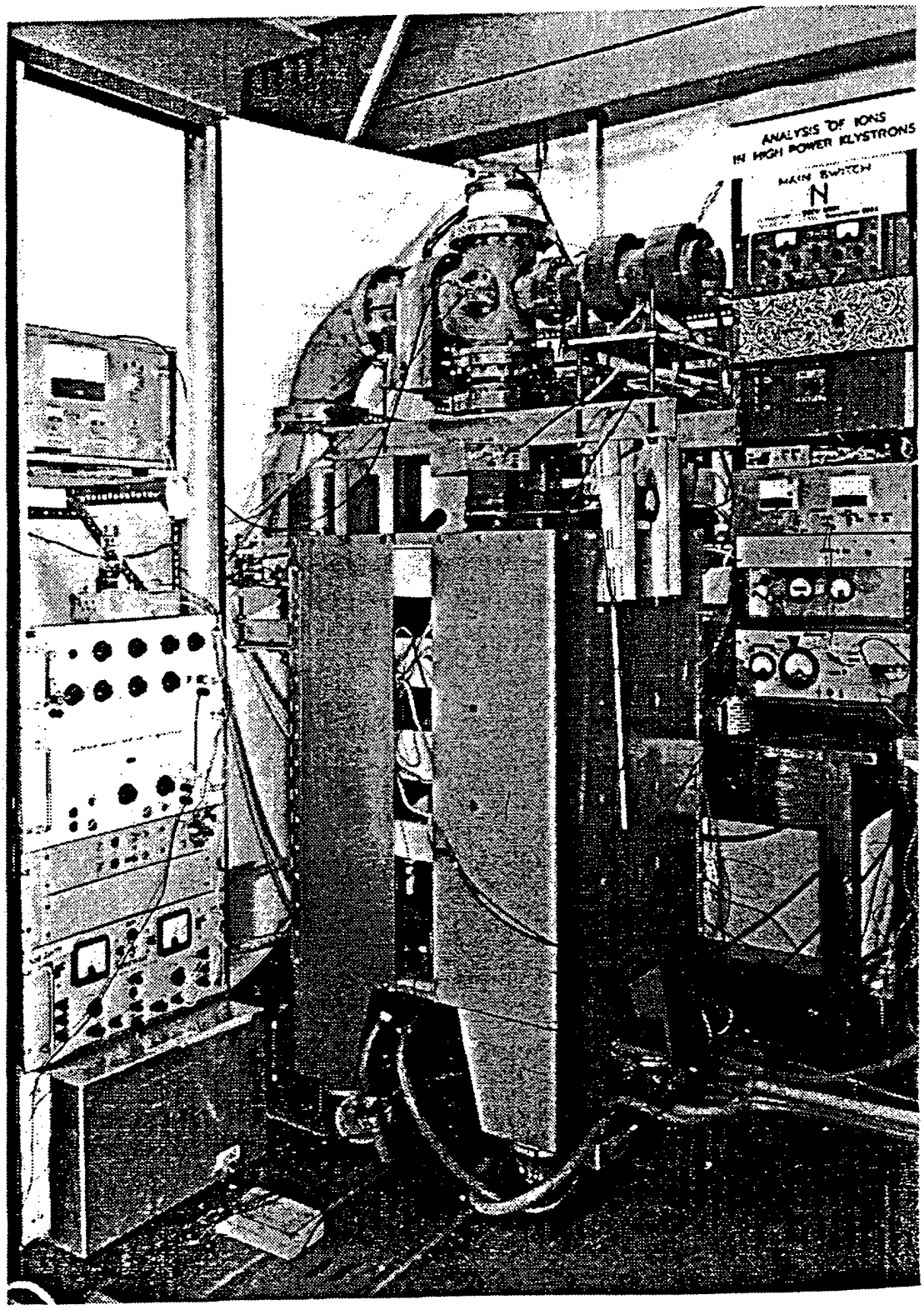

FIGURE 1 THE KLYSTRON

also supports the valve. The beam is focused from a cathode of 8 cm diameter to approximately 2 cm diameter.

2.1.1 Physical Description

The unmodified valve has an overall length (from header plate to collector) of 1.465 meters, most of which is the drift tube, which is .8825 meters in length (Figure 2). The metal sections of the K376, which comprise the header plate, the modulating anode, five drift tube sections, and the collector, are separated from one another by ceramic sections. These provide the necessary high voltage insulation, and furthermore, facilitated the biasing experiments which were performed. The drift tube sections, which along with the collector are water-cooled, have gaps of varying length between them, the gap usually being about 1 inch. The internal diameter of the drift tube sections is 1 inch*.

A full size view of the gun end of the valve before modification is shown in Figure 3. Observe in particular the header plate, which supports the electron gun, and has filament connections and a vacuum seal-off port. The plate required considerable modification for use in this study. The gun 'pot' consists of the cathode, which is of elliptical cross-section and .0745 m in diameter, the associated heater windings and heat shields, and the heavy iron cylinder of .0952 m diameter. This cylinder provides magnetic shielding for the cathode.

The cavities used are external and separate in the middle to be clamped between the drift tube sections (DTS). The valve is operated with the gun end upwards and is supported at the bottom of the magnet

* The reader will please excuse the mixture of metric and English systems which occasionally occurs in this dissertation. Calculations are invariably in MKS units, with the exception of the use of Torr, but when dimensions such as the drift tube diameter are exactly an English unit, it seems to be unnecessarily rigorous to convert then to a non-integal metric unit. Although calculations may be most easily done in the MKS system, this valve and the modificiations made to it were specified in practical engineering units.

OUTLINE

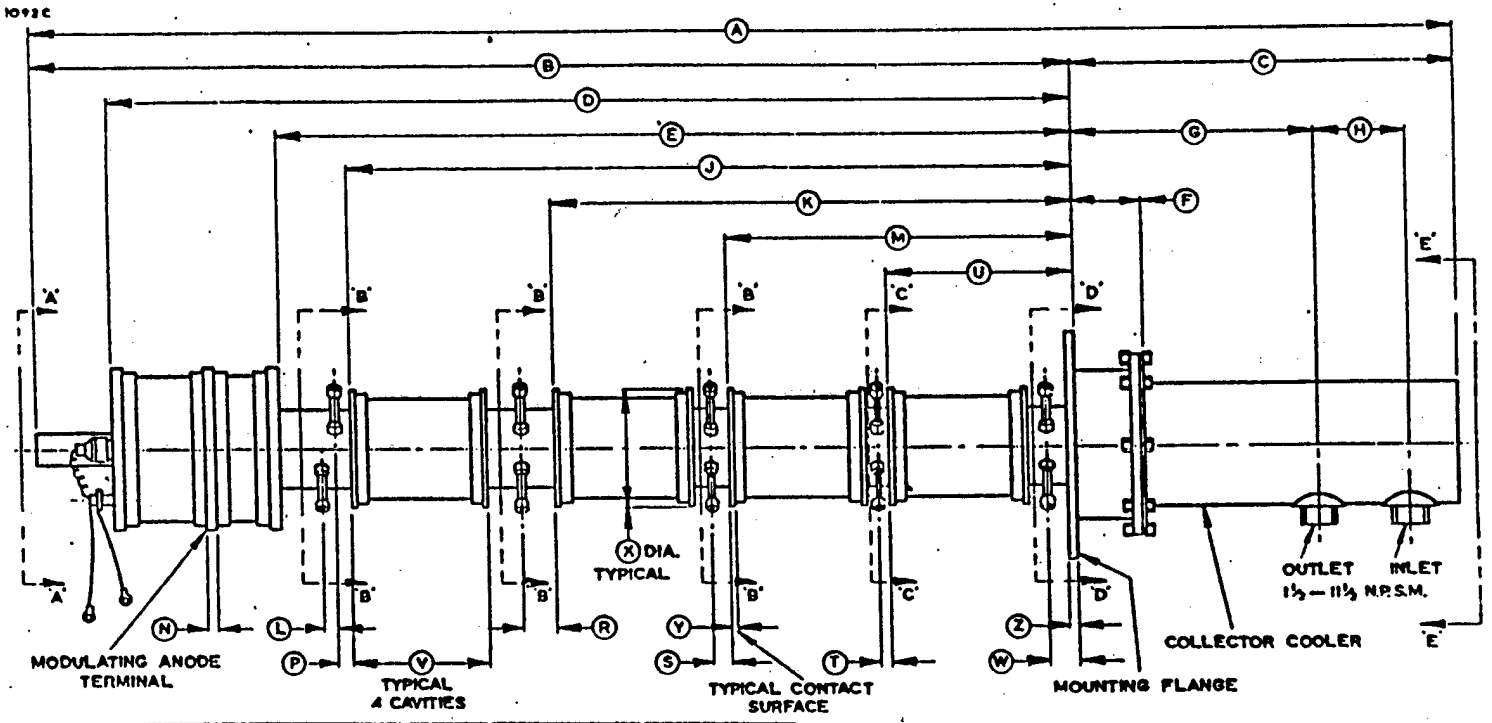

Ref.	Inches	Millimetres	Ref.	Inches	Millimetres
A	61·59	1564	N	0·500	12·70
B	45·11	1146	P	0·657	16·69
C	16·48	418·6	R	1·433	36·40
D	41·90	1064	S	0·875	22·23
E	34·47	875·5	T	0·437	11·10
F	2·912	73·96	U	8·124	206·3
G	10·35	262·9	V	6·000	152·4
H	4·000	101·6	W	1·125	28·58
J	31·34	796·0	X	5·125	130·2
K	22·50	571·5	Y	0·250	6·35
L	0·606	15·39	Z	0·375	9·53
M	15·00	381·0			

Millimetre dimensions have been derived from inches.

NOTES

(*a*) A modulating anode terminal ring with an 8–32 U.N.C. connecting screw is supplied with the klystron.

(*b*) The unions of the water connections to the five body sections are threaded 5/8–24 N.E.F.

FIG. 2 K376 KLYSTRON

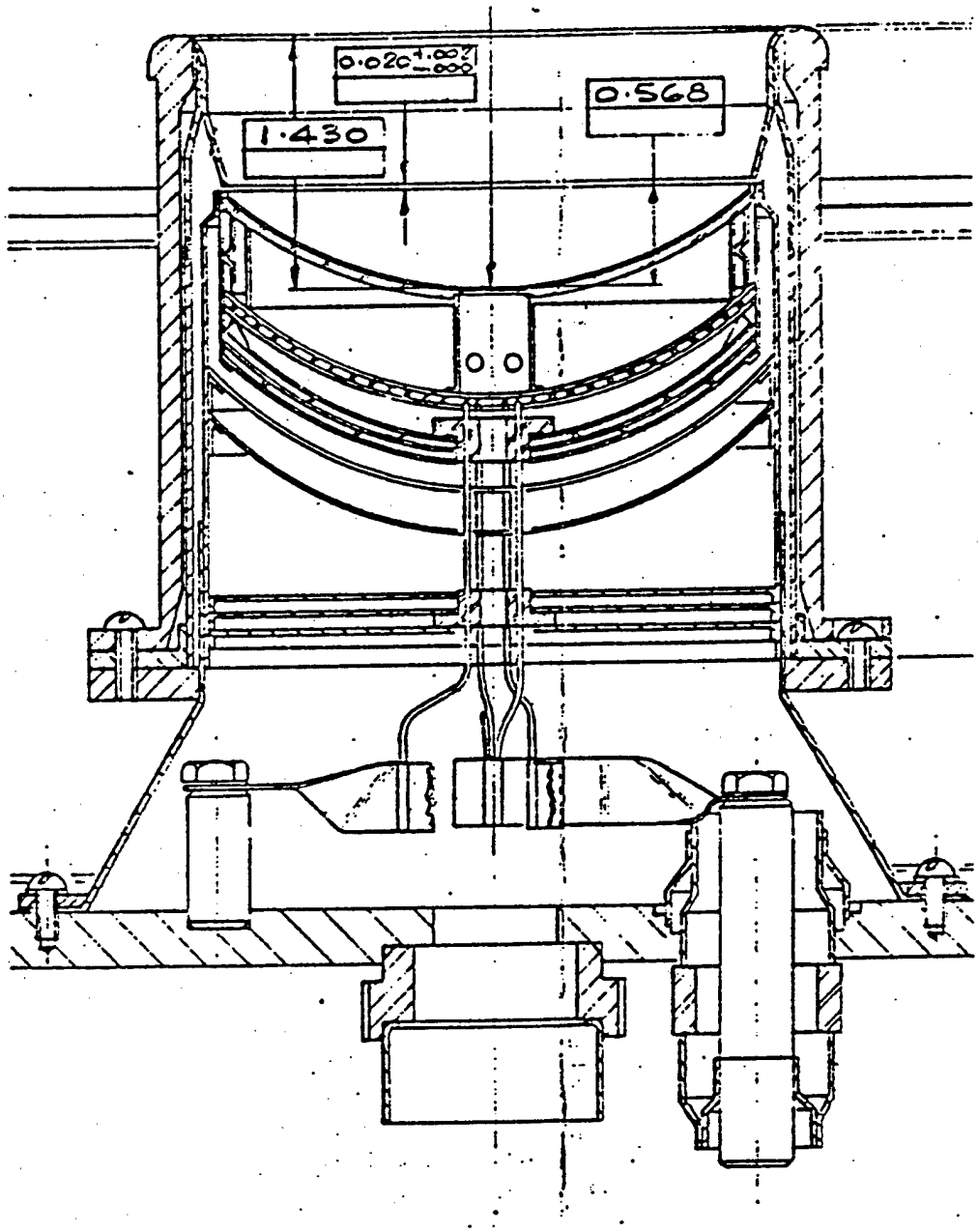

FIG. 3 GUN BEFORE MODIFICATION

coil assembly. The coil assembly surrounds the entire valve plus cavities (Figure 1). It also provides pole pieces at each end for magnetic field shaping. Fine adjustments of the position of the upper shield were made before experimentation to reduce body interception to a minimum.

2.1.2 Modification to the Valve

2.1.2.1 External Modifications

The objectives to be obtained in modifying the valve were 1) to provide a connection to the valve for continuous pumping; 2) to make provision for a demountable cathode; and 3) to provide for equipment which could monitor the ions draining to the cathode. These modifications were to be made so as to not interfere with normal valve operation.

Figure 2, which is part of the standard literature describing this valve, indicates the original length, and the location of the ceramics. It was decided to place a pumping port behind the gun. Since it was anticipated that the valve would be pumped during operation, it was necessary to incorporate a section at earth potential between the gun and a new header plate, which has a potential of -17.5 KV. This section would serve as the connection point for the pumping system.

By consulting with EEV at Chelmsford it was found that two ceramic sections identical to those used in the unmodified valve were available, and that their facilities for normal valve manufacture would be available to perform the special welding operations used in making metal-to-ceramic joins.

It was thus decided to add ceramic sections to extend the length of the valve at the cathode end, and use a metal section for pumping and other access ports. To provide a platform for mounting the cathode, a ceramic section and a standard header plate were attached above this metal pumping section. Figure 4 illustrates these modifications.

In detail, the original header plate was replaced by a modulating

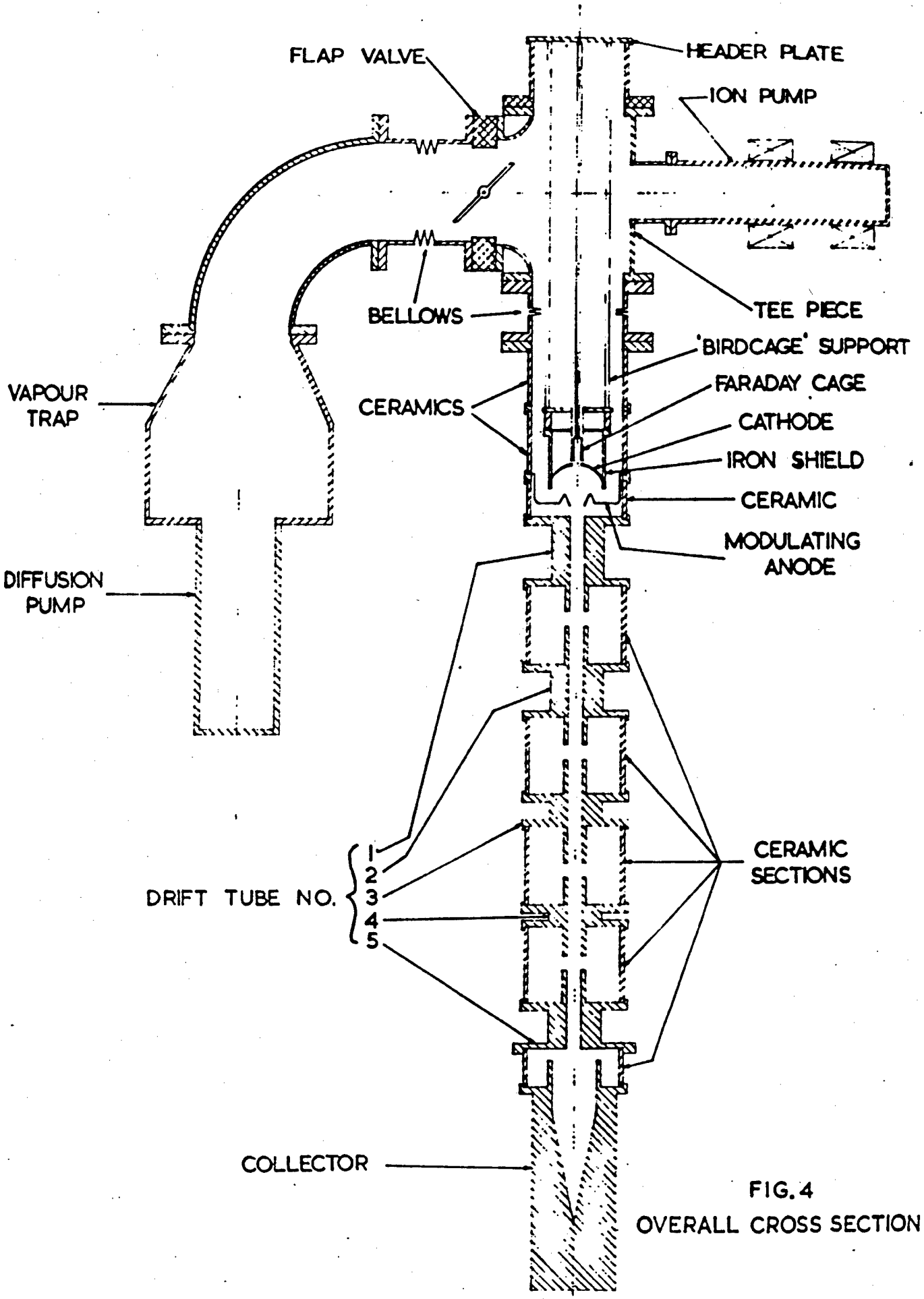

FIG. 4
OVERALL CROSS SECTION

anode ring which had been bored out to the diameter of the ceramics (Figure 5). This provided a method of attaching one ceramic to another, and allowed a new ceramic section to be added above the cathode location.

Above this ceramic section of the modified structure is a stainless steel flange 10" in diameter, which was attached to the ceramic in the same way as a normal header plate. Figure 6 illustrates this sort of flange and join. This flange and all other metal parts were made of a non-magnetic stainless steel (type En58J) in order to avoid any distortion of the magnetic field used in focusing the beam.

The added metal sections are connected to this flange and centre about a modified 6" diameter 'tee piece', which in addition to the large port which forms the 'tee' also has a 4" diameter tube leading to the ion pump, and a 4" diameter access flange. The access flange is located directly above the intersection of the axes in Figure 4, and is visible in Figure 1. It is used to mount an ionisation guage head. The tee piece is attached to the adjoining sections by 10" diameter flanges (Figure 6). These incorporate a crushed copper gasket seal which employs a .010" thick by $\frac{1}{4}$" wide annealled copper ring which is compressed between a knife edge and a mating groove. These must be machined to .001" concentricity tolerance, and are compressed by 16 bolts around the flange, but have proven reliable in producing a leak tight seal. These seals are, of course, bakable.

The tee piece is connected to the rest of the valve by a stainless steel bellows made by Palatine Precision, which is edge-seamed, and very flexible. These were included to assist in the assembly of the valve, which entailed lowering the assembled tee piece and associated pumps, which weigh 400 pounds, onto the main body of the valve, which was already located in the magnet frame. As the ceramics are very strong for longitudinal compressive loads, but weak for shearing stresses, this

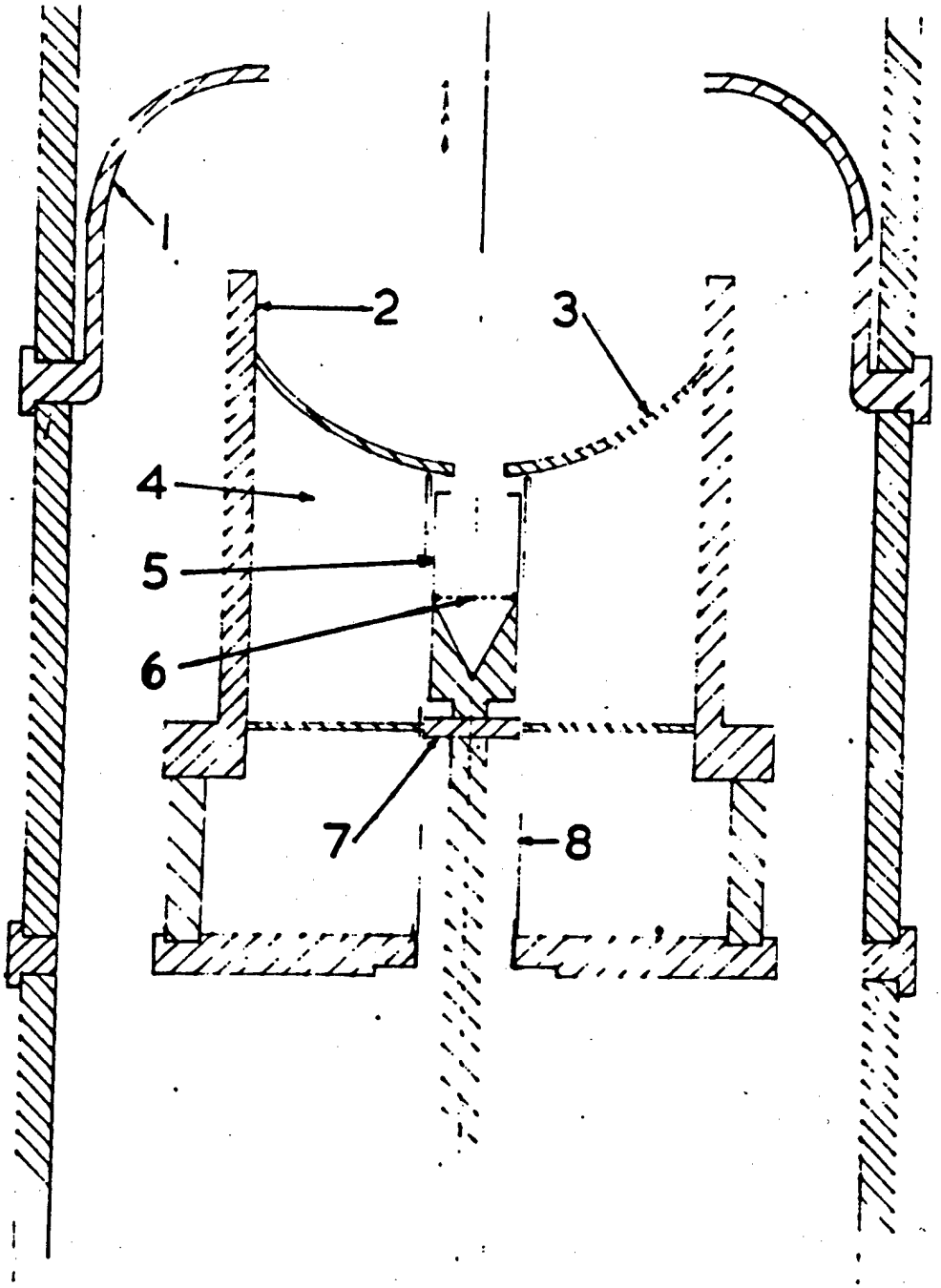

1. MODULATING ANODE
2. IRON SHIELD
3. CATHODE
4. HEATER
5. FARADAY CAGE
6. MESH
7. CERAMIC
8. MOLY TUBE

FIG. 5 GUN AFTER MODIFICATION

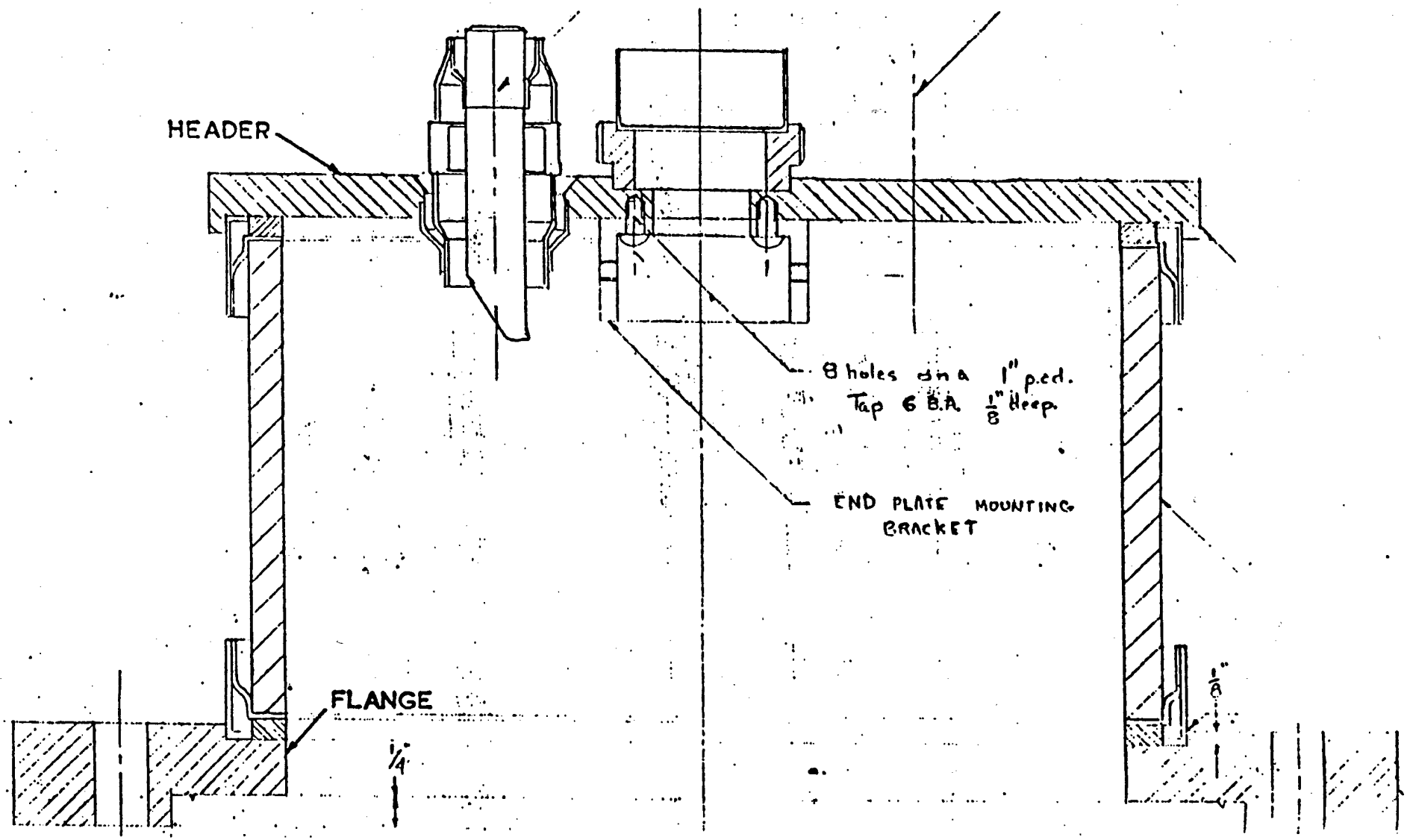

FIG. 6 HEADER PLATE AND 10" FLANGE

was a very necessary addition. The bellows themselves are not capable of supporting the force of the atmospheric pressure, which is 400 pounds on a 6" diameter. To maintain the length of the bellows constant when this force is exerted, they were held at a fixed length by four adjustable bolts. Adjustments of these bolts also make possible small adjustments in the longitudinal cathode position.

Another flange and ceramic are attached to the top of the tee piece, and these support the header plate (Figure 6). This is of standard design except that the holes for evacuation and ion pump are blocked off, and holes have been drilled to allow a special support for the cathode to be attached.

To the left of the tee piece in Figure 4 a flap valve and pumping system are attached. The flap valve attachment to the tee piece had to be made with a Viton 'O' ring, as this is part of the design of the commercial flap valve selected (Edwards QSB6). To the left of this flap valve is another Palatine bellows, which is in turn connected by another flange to a 90° stainless elbow which leads to the cold trap and diffusion pump. The six-inch diameter is maintained in this tubing. The adjustable bolts which extend along the bellows here provide for small adjustments while connections between the heavy diffusion pump and elbow are being made, and were designed as a way of relieving stress should the valve body become sufficiently hot during operation that thermal expansion tended to shift the weight to difference support points. The pumps and associated tubing present a very unbalanced mechanical load if the fulcrum is considered to lie on the valve longitudinal axis. To avoid the chance of breaking a ceramic or distoring a copper flare, it is essential that this load be independently supported. The support is provided at three points: beneath the centre of the ion pump, beneath the flap valve, and

beneath the vapour trap. The vapour trap is mounted in a 'U' harness. All points of support are made adjustable over the range of a few inches by the use of studding. The studs are connected to a Dural frame, which is bolted to the magnet frame (Figure 1). The construction has been found totally adequate. Furthermore, it introduces no new materials into the valve, other than the very small surface of 'O' ring exposed.

2.1.2.2 Internal Modifications

Once the original header plate was removed from the valve, it was necessary to find a new way to support the cathode 'pot'. The term cathode 'pot' is meant to include not only the actual cathode itself, but the associated iron shielding pot and the heater coils which it contains (See Figure 5). The tolerances on the positioning of the cathode pot are .008" along the axis, and .005" in concentricity. Furthermore, the weight of the pot is five pounds. To allow RF operation a rigid mounting of the cathode is necessary, or external vibration will tend to cause an AM modulation on the RF output. Thus a rigid support structure was necessary. The structure arrived at consisted of six $\frac{1}{4}$" diameter, parallel, stainless steel rods arranged to lie along the circular walls of an imaginary cylinder, and brazed to discs at the ends and partway along the longitudinal dimension of the structure. It is called a 'birdcage' in Figure 4. Its radius was made as large as possible while maintaining sufficient distance from low potential parts of the valve to prevent electrical breakdown. This would be particularly dangerous in the case of the bellows, which have only a .008" wall thickness. Breakdowns might result in a leak. The birdcage design is very open and does not interfere with the pumping speed. It also allows room in the centre for the subsequent placement of measurement equipment. Adjustments at the base permit mechanical corrections to meet the concentricity specification. Measurements

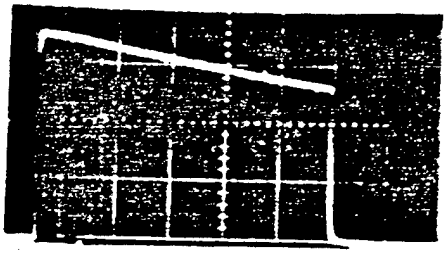

BEAM VOLTAGE

5 KV/ DIV

200 μS/DIV

FIG. 12

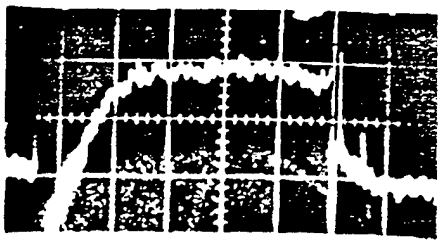

ION CURRENT

110 μA/DIV

100 μS/ DIV

FIG. 26

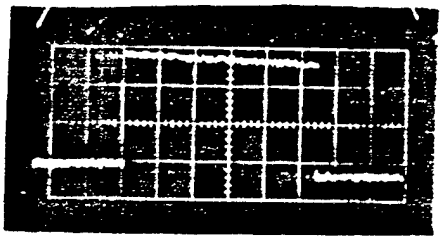

A) 1 MA

200/μS/DIV

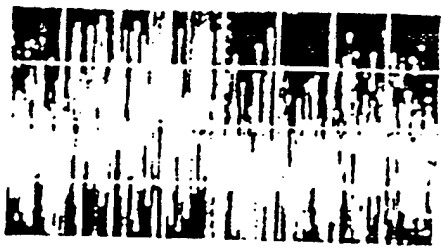

B) 10 μA

200 μS/DIV

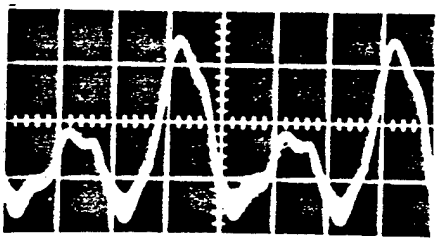

C) NO SHIELD

5 MS/DIV

180 μA/DIV

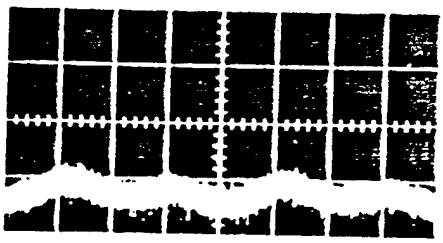

D) MAG. SHIELD

5 MS/ DIV

36 μA/DIV

FIG. 14 ROGOWSKI BELT RESPONSES

made prior to the insertion of the gun in the klystron demonstrate the meeting of mechanical specifications for cathode positioning. Electrical measurements of perveance further demonstrate the accuracy of this positioning.

The heater lead-in from the header plate provides a good support for the brittle wire which leads to the heater, and for this reason a modified header plate was used below the cathode pot (Figure 7). In an unmodified valve the cathode pot is attached to the header plate by a metal collar. Because the collar had a base too large to fit through the bellows when the cathode was being inserted in the valve, it was necessary to mount the cathode pot on posts above the modified header plate. The plate was further modified to include a groove to mate with the 'birdcage'. Holes were drilled in the modified header plate to improve pumping speed.

In the centre of the 'birdcage' a stainless steel hollow rod was used to provide support for the Faraday cage. A ceramic rod was inserted in the end to attach to the Faraday cage and provide insulation and fine adjustments to the height. The central support rod itself can be positioned laterally by adjustment of three fingers attached to one of the discs of the birdcage.

As was mentioned above, a 3/8" diameter hole in the centre of the cathode is a standard feature of this valve. The hole is usually baked by a molybdenum cap of about ½" depth. To make use of the hole for measurements of ion drainage to the cathode, it was necessary to remove the cup and to cut a 3/4" diameter central hole through the heat shields behind the cathode. Figure 3 depicts the unmodified cathode pot, and may be compared to Figure 5. It was also necessary to cut away part of the heater winding to make this hole. The winding was reduced from the normal 100.75" to 86.7".A .010" wall, 3/4" diameter tube of molybdenum was mounted to the modified header plate

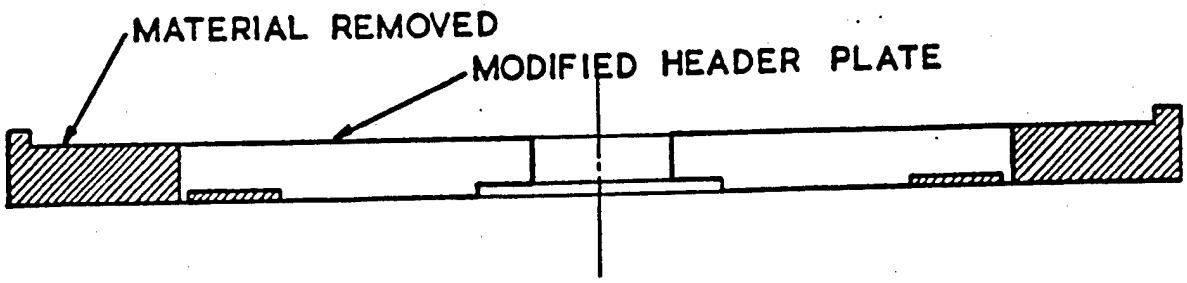

FIG 7 HEADER PLATE CROSS-SECTION

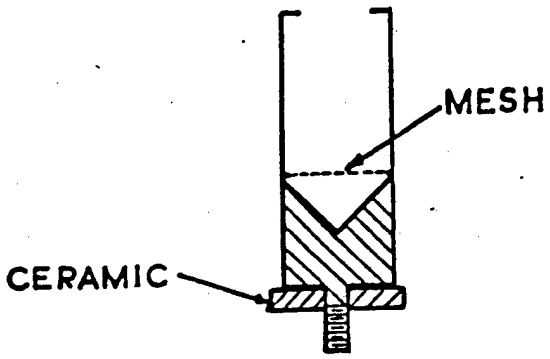

FIG 8 FARADAY CAGE CROSS-SECTION

by a small flange and extended into this hole to within a few mm's of the back of the cathode.

The Faraday cage itself was machined from a 5/8" rod of stainless steel. Figure 8 depicts the cage. The central cone was chemically polished. The deep angle of the cone, the use of the mesh to provide a region of low electric fields, and re-entrant mouth were designed to minimize both ion and electron escape from the cage. The ceramic mounted at the bottom centres the cage in the tube. The top of the cage is positioned approximately .080" behind the cathode back surface. Electrical contact to the Faraday cage is made by two spring wire contacts attached to the base of the rod on which the Faraday cage sits. These spring outward and make contact with the reamed out anode ring which separates the ceramics and is exactly opposite the modified header plate. These are held in as the cathode pot is being lowered past the bellows. Electrical contact with the ring can be checked before sealing the valve.

The performance of the Faraday cage during measurements, especially with respect to the number of secondary electrons escaping and the efficiency with which the total drainage current was collected, required special measurements which are discussed in later chapters.

2.1.3 Electrical Operation of the Klystron

The valve normally requires extensive forced air and water cooling, but the pulsed operation of this valve with low duty cycles reduced the requirements for these, and the configuration used for most experiments consisted of a 2 gallon/minute water flow to the collector, no water to the body sections, and a small flow of air from a compressed air line to the cathode area. The temperature of the ceramics opposite the cathode, which would be the hottest, was not observed to rise above 100°C. No warming of the drift tubes was noticed.

Normal anode interception current is 2 ma, and was measured to be

5 ma for this specimen. The current to the rest of the body was 144 ma at the beginning of beam pulses, as compared to a spec maximum value of 150 ma, but it was found that the interception current depends on partial neutralisation of the beam charge, so this figure for the beginning of the pulse is perhaps not the most appropriate measurement. This is discussed in detail in Section 4.5.2.

At voltage somewhat below the rated maximum voltage it was demonstrated that the micro-perveance was close to 1.97, the design value. This indicates an accurate placement of the cathode in the valve, and together with the interception measurements would indicate that the operation of this valve is fairly typical of the normal operation. The axial magnetic field of the standard assembly was measured and is illustrated in Figure 9.

Difficulty was encountered in obtaining the normal emission from the cathode. Two cases must be distinguished: the first a case in which the cathode had been exposed to the atmosphere after its initial activation; and the normal case in which the cathode was fresh, and activated for the first time in the valve.

In both cases normal emission was not obtained immediately after activation (re-activation in the first case). Activation is a long process, taking about six hours for this cathode. The normal procedure calls for only the application of normal heater voltages, and predicts that a cathode which completes the procedure will be capable of full normal emission.

In the case of the re-activated cathode, departure from this behaviour is expected since exposure to the atmosphere results in some of the BaO in the cathode being converted to $Ba(OH)_2$, which does not break down under the influence of the temperatures available alone. However, improved performance is obtained if the cathode temperature is increased as much as possible. It was necessary to increase the

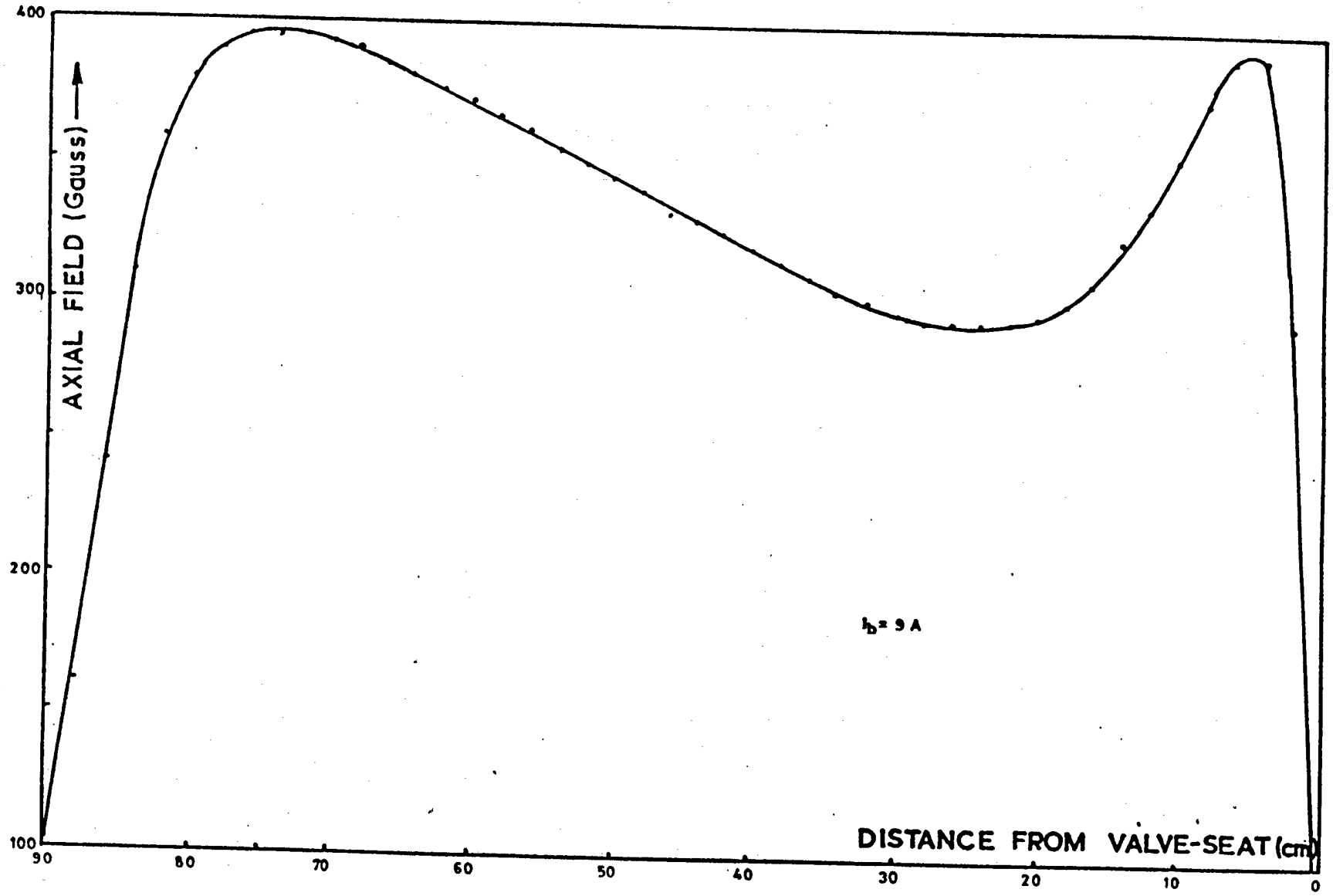

FIG 9 MAGNETIC FIELD

heater power input to 125% above the normal 286 watts before significant emission could be obtained. Even at this temperature, emission from the re-activated cathode was limited to 2.5 A. Continued usage over a period of months increased this value to 3.4 A. Drawing current from the cathode is an important part of the activation process, but since the duty cycle used during these experiments is .01 at the most, it would require very long operation to duplicate normal usage.

The second cathode which was activated, this one for the first time, demonstrated the same characteristics to a lesser degree, and with a shorter time scale. Figure 10 shows emission from this second cathode at two different heater voltages, the lower one being the normal operating voltage. Emission is obviously limited in both cases when the beam voltage rises above about 12 KV. Most experimental data obtained in this dissertation was based on the lower heater voltage, a precaution used to reduce the chance of burning out the shortened heater wire.

2.2 The Vacuum System

The vacuum system is composed of a high speed system designed to quickly pump the system down to operating pressures from atmospheric pressure, and a lower speed system capable of an ultra high vacuum. As is shown in Figure 4, the high speed section, which consists of a 30 l/sec Edwards ED33 backing pump, a 600-650 l/sec Edwards 6M3A mercury diffusion pump and an Edwards NTM6 liquid nitrogen cold trap, may be separated from the rest of the system by a large capacity flap valve. With the cold trap fitted, the pumping speed of this section drops to 260-290 l/sec. The large volume of the system, 40 liters, and the large volume of gas evolved during activation of the cathodes, necessitated the incorporation of the high speed system, although most measurement work

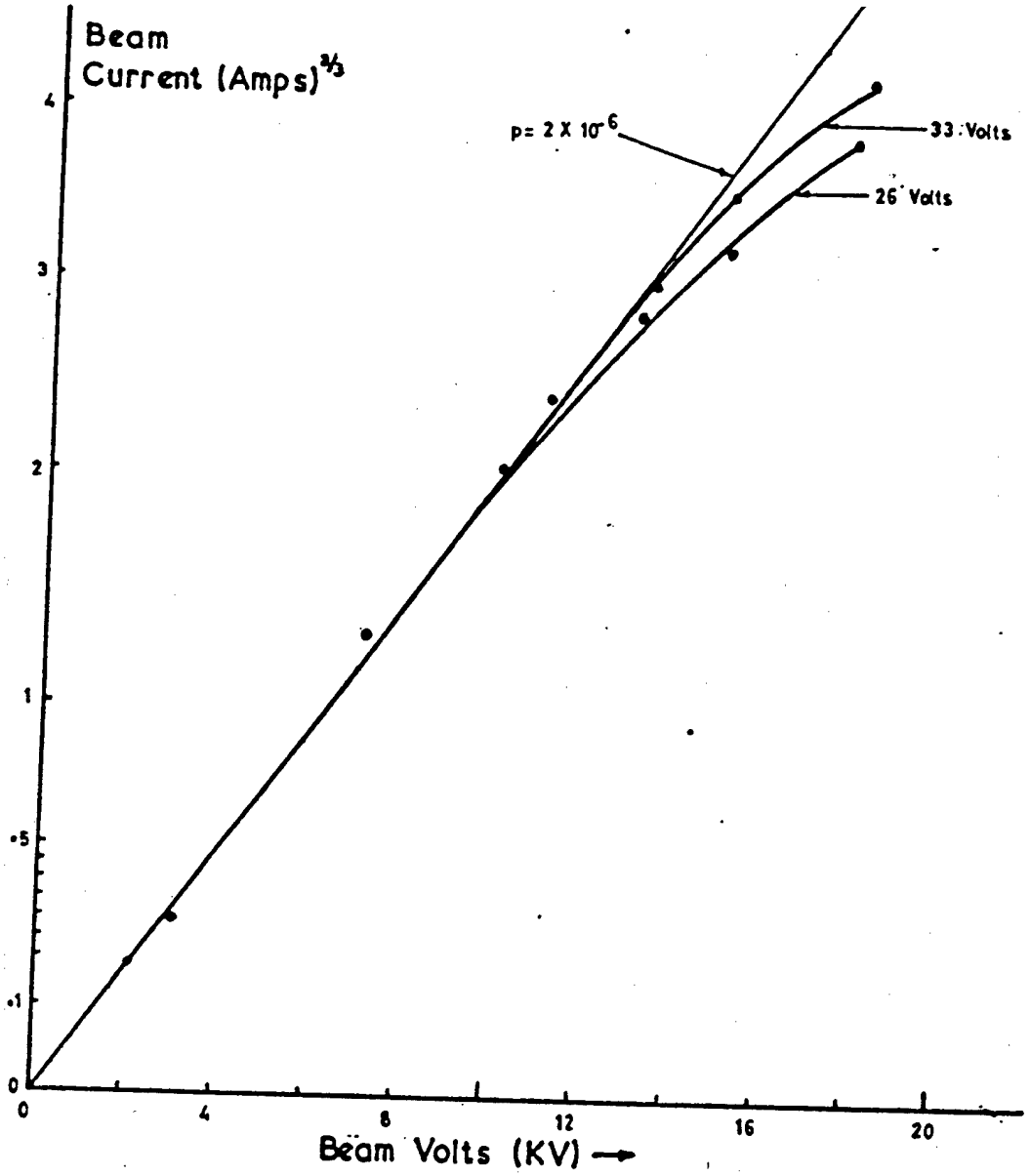

FIG.10 PERVEANCE TEST

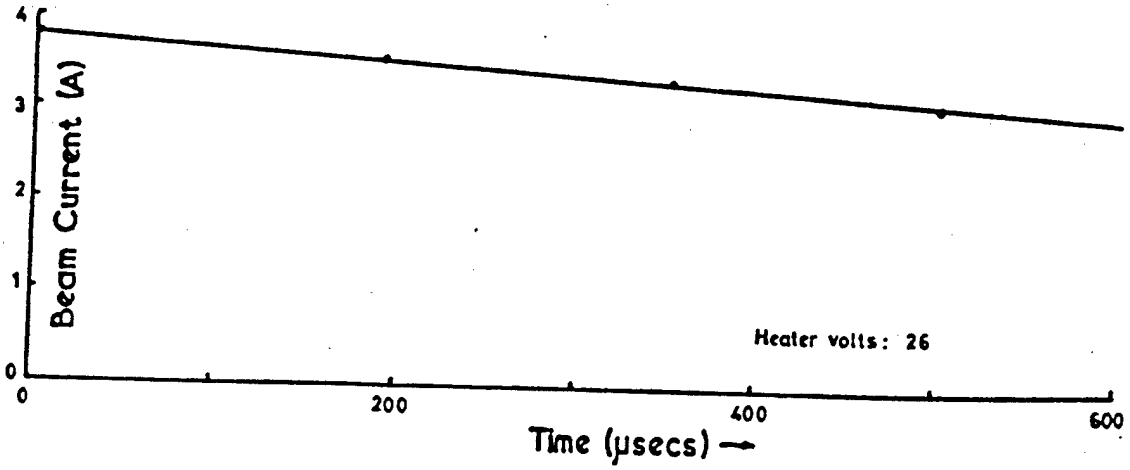

FIG.13 BEAM CURRENT DROOP

was done with the flap valve closed and the pressure controlled by the ion pump.

The getter ion pump used for maintaining and adjusting the pressure after operating pressures had been reached is a Ferranti 40 l/sec model. The predicted pumping speed at the pressures involved is actually 33 l/sec. It is connected to the "tee piece" by a short length of 4" diameter tubing. In the experiments which were conducted with the first electron gun, it was necessary to use the ion pump as a pressure measuring apparatus.

At the same time as the second gun was put into the klystron, a nude Bayard-Alpert ionisation gauge was installed at the centre of the "tee-piece" (Figure 4). This was used along with an Edwards Model 5M gauge supply for more accurate pressure measurements. Long outgassing periods were used to ensure that not only the head, but the surrounding metal parts were all outgassed. The gauge was used to calibrate the ion pump for use as a pressure measurement device. Figure 11 shows the calibration curve of the ion pump current vs. pressure for pump voltages of 3.4 KV and 1 KV. Also shown is the pump maker's data for 3.4.KV, which is the rated voltage. His original figures have been reduced by 6% to account for the pressure differences which exist between the ionisation gauge head and the pump entrance due to the finite conductances. It was found that the original calibration data was not very accurate. Furthermore, a certain amount of care must be taken in using ion pump readings as a way of measuring the pressure, especially after the pump has just been turned on, or the pump voltage raised. The processes seem to evolve a certain amount of gas from the pump itself, which means that the pump indicates higher pressure readings than actually exist in the valve. A temporary rise in the ion current draining to the cathode and the ionisation pressure gauge readings

are also observed when such changes are made.

It was found that by lowering the voltage on the ion pump it was possible to lower the pumping speed and thus increase the pressure in a controlled way. Voltages ranging down to hundreds of volts were used in various experiments to raise the pressure. Although these voltages are so low that the discharge within the pump will not start itself, it is possible to start the discharge at a higher voltage and thus obtain the desired variable pumping speed.

2.3 Valve voltage supplies

The DC operating conditions for the K 376 are 17.5 kV and 4.56 Amps, beam voltage and current respectively. To limit the average power dissipation and to study the build up of ion current, pulsed power supplies were designed for this valve, although the normal operating condition is, of course, CW. The wide range of experiments which were planned required that a very flexible power supply be designed which would provide variable beam voltage, variable pulse length, and variable PRF (pulse repetition frequency). These specifications indicated that a driver-power-amplifier type of supply be built, rather than a line-pulsing type. Figure 60 in Appendix I shows a circuit diagram of the unit which was constructed. The principles of operation of this type of supply are expounded in many texts (26). The voltage amplitude was controlled by the variable positive DC supply, and the amount of grid drive by the amplitude of the pulse amplifier output. A problem which is inherent with this type of supply is that a droop will always be present on the output pulse due to the capacitive discharge. For the case of a space charge limited load following the 3/2 law, it can be shown that the pulse voltage will decay as :

$$V(t) = V_o \left[\frac{2C}{p\sqrt{V_o}t + 2C} \right]^2 \qquad 2.1$$

where V_o is the initial voltage, C the capacitance, and p the perveance of the load. For the case of this valve these quantities are 0.75 μF and 1.97 x 10^{-6} pervs.

Figure 12 shows the measured voltage waveform, and Figure 13 is a detailed plot of measured beam current vs. time. The limited emission which the cathode exhibited caused minor departure from the behaviour indicated in Equation 2.1. The voltage is measured using a Tetronix Type 50 high voltage probe, and the current with a precision 10 Ohm resistance between the collector and earth. When connected to a resistive load with low capacitance cable, the voltage pulse has a 10%-90% rise time of 2 μsecs. The 5 μsec rise time when connected to the valve is longer due to the shielding of the lead-in cable, the heater transformer capacitance, and the inherent capacitance of the valve itself. The supply is capable of pulsewidths between 20 and 1200 μsecs at any duty cycle which produces an average power of 500 watts or less. The voltage output is variable from 2 KV to 20 KV.

The cooperation of T.P. Lennox in the design and construction is gratefully acknowledged.

2.4 Equipment for Ion Current Measurements

For the purposes of this study it was essential that an oscilloscope picture of the ion current drainage be made available. The small clearance between the cathode and the Faraday cage which was used to collect ions required that the Faraday cage be biased to a high negative potential close to that of the cathode, and thus the measurement problem is seen to be a difficult one. In addition to the problems which are posed in measuring pulsed signals on the order of 10 μamps, these signals are biased to about 17.5 KV, and are in close proximity to the large beam and magnetic field currents.

A number of solutions were considered. The usual technique of

putting a resistor in the lead to the Faraday cage to measure the current using a differential oscilloscope was not useful because of the capacitive charging currents to the Faraday cage, even if it was assumed that probes capable of cancelling the beam voltage were available. The Faraday cage itself has a 10 pf capacitance to earth, and a 41 pf capacitance to the cathode. The most promising technique seemed to be the one which used some form of magnetic coupling of the current from the lead, and thus made electrical isolation problems much smaller. Furthermore, it could be used to cancel the capacative current, as shall now be discussed.

A so-called Rogowski Belt (27), which is essentially a simple transformer, was constructed to accomplish this magnetic coupling. Figure 64 in Appendix II illustrates the belt, which is a torus encircling the high potential wire which carries the ion current. With appropriate external circuitry this belt couples the ion current signal to low potential amplifying circuits. The detailed electrical operation of this circuit is discussed in Appendix II, the selection of turns ratio and load resistor is discussed, and the values which were selected given. The response of the belt to a 1 ma square 1100 μsec pulse is shown in Figure 14a, and the performance is aspredicted in Equation II.6. The low input currents expected require an amplifier to be connected to the Rogowski belt output. Operation of the belt and amplifier as described above was satisfactory when the valve and other high current devices were turned off, but required further improvements before it would function adequately with them on.

Noise, or perhaps more generally, unwanted signals from the Rogowski Belt, fall into two groups: mains or PRF coherent; and thermal and amplifier noise. The coherent signals are caused by both unwanted magnetic and electric coupling. Since the Rogowski belt operates by

magnetic coupling of microampere signals, it is not surprising to find that the 15 Amperes of the heater supply, the 9 amperes of the confining magnetic field, the beam pulse itself, and the mains current leading to electronic equipment, all contribute a large signal to the Rogowski belt through their magnetic fields. At the same time, electric coupling from the 17.5 KV pulses would give ambiguous results. It was found experimentally that it was necessary to reduce the magnitude of both effects if measurements in the range of 10 μamps were to be made. The electric coupling was largely eliminated by surrounding the Rogowski belt by a brass shield also in the shape of a doughnut. This doughnut was made in two halves and provided with a shielded output lead which connected directly to the amplifier box. Figure 15 is a cross section of the Rogowski belt and associated equipment. The many turns required on the belt use more than one revolution about the torus axis, and thus provide a second loop which picks up stray signals. This source of pickup was cancelled by starting the coil winding with an equal number of revolutions in the opposite direction. Magnetic shielding was provided by an iron box of 3/8" wall in a cubic shape which enclosed the belt (Figure 15). A further 3/8" thickness between the belt and the magnet suppressed the particularly bothersome 300 Hz component of the 3 phase magnet supply. The Rogowski Belt response with and without the magnetic shield are shown in Figure 14 C and D.

Since a large part of the interest in these measurements is directed to oscilloscope observation of the ion current signals, further steps were necessary to reduce mains coherent signals. If a signal has a PRF which is not synchronized to the mains, the mains contributes a varying initial value to the signal, and it is not possible to observe the signal without confusion except on a single-shot-and-storage basis. Even this does not eliminate the mains

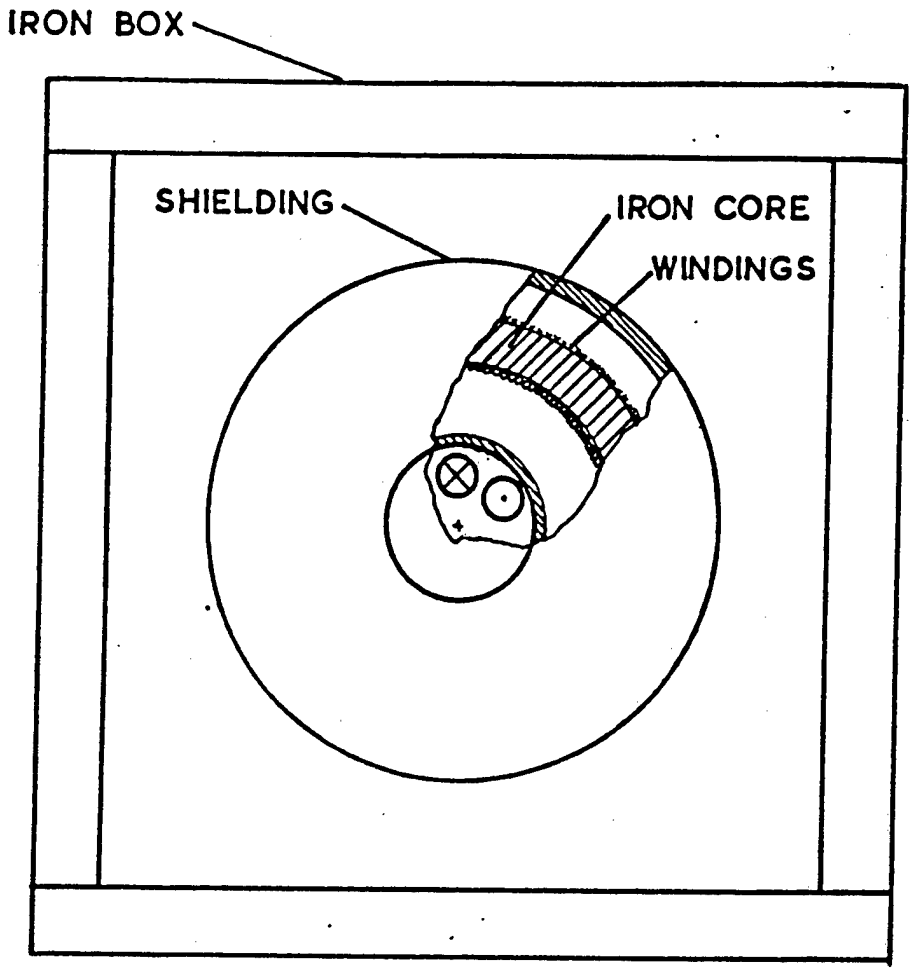

FIG. 15 ROGOWSKI BELT CROSS-SECTION

coherent baseline slopes, and if, as is usually the case, one wants to watch a repeated signal, the lack of synchronization will cause the starting value of the signal to vary from pulse to pulse. This will not interfere with a sample and hold circuit, but will prevent accurate observation of the time dependence of the signals on the oscilloscope. Thus mains synchronization was seen as a necessity. It is extremely important that an adjustable delay be provided for this synchronization, as it is then possible to find a flat portion of the mains rippled baseline to use for a pulse. A flat baseline is obviously a necessity for accurate measurement. The shorter the pulse duration, the easier this is to find, but it was possible to find portions suitable for 1 msec pulses. In conjunction with the other two improvements, it was possible to reduce interference from these coherent sources to below that from the amplifier noise. The mechanisation of this synchronization is discussed in Section 2.5.

The noise from the amplifier provides the most basic limitation to accurate observation of signals from the Rogowski belt. Some low level signals were seen to have average values which are less than the r.m.s. noise voltage. This makes accurate determination of the signal levels by oscilloscope observation alone almost impossible. In the case of long pulses having lengths of hundreds of μses, simple low pass filtering techniques remove a great deal of the noise, but only at the expense of losing the frequency response which may show changes of interest which can be observed only on an oscilloscope. To make unambiguous measurements of low signal levels while at the same time retaining the full bandwidth of the measurements system for oscilloscope observation, coherent wide-band detection was employed. The technique which was applied to this problem was to use a sample and hold network and average the output to enhance the signal-to-noise ratio.

The sample and hold network operated at variable delay within the

pulse of ion current. The unit tracks the signal during the sample command pulse and then holds the instantaneous value at the end of the pulse as a DC output. The signal is re-measured at the same point in each succeeding pulse, and the DC output is changed to a new value. The need for this circuit which proved a great help in making ion current measurements, arose not only because of measurements which had to be made in the neighbourhood of low signal to noise ratio, but from the difficulty of making repeatable oscilloscope measurements. The sensitivity of the Rogowski belt circuit and the need for signal enhancement may be seen in Figure 14b, which depicts the Rogowski belt response to a 10 ua flat pulse of 300 usec duration. The sample and hold output may be averaged and displayed with a meter, as is shown in Figure 62 of Appendix 1. This integration technique provides a signal to noise ratio improvement of $n^{\frac{1}{2}}$, where n is the number of pulses averaged. For a fixed integration network this will be a function of the PRF, and since the PRF dropped as low as 2 pps, a long time constant was needed in this integration circuit. The time constant is chosen to achieve the maximum amount of signal to noise enhancement without at the same time so slowing down the meter response that inaccurate results are obtained when a slowly varying ion current is being observed. The circuits which were constructed for the sample and hold network are shown in Appendix I, and used field effect transistors to achieve hold times as long as 1 seconds with minimum sample pulse widths of 3 μsecs, which is more than enough accurate for determining delay times.

Further sources of noise include signals due to voltage breakdown during a pulse. These appear as very short, but high, spikes during the signal, and efforts to minimize them by reducing the number of sharp corners at high voltage and covering those that remained with insulating tape were unsuccessful in making very much improvement. These may well be the micro-discharges which are known to occur in high vacuum systems (28).

Having improved the Rogowski Belt and amplifier to achieve the sensitivity desired, the problem of capacitive charging the currents must be handled. As mentioned above, the Faraday cage has a 10 pf capacitance to earth. Additional wiring capacitance was minimized by putting the Rogowski Belt as close to the cage as possible, in spite of the undesired increase in magnetic coupling effects from the beam and magnet supply, but the net capacitance was found to be 20 pf. This capacitance must be charged to 17.5 KV during each pulse, and the charging currents are not negligible. Figure 16 shows the response to be expected. The initial charging current is 70 ma or more, and more importantly, a charging current flows during the pulse as well, due to the discharging which occurs from the pulse droop. The high initial transients may create problems in the amplifiers, and the negative current during the pulse would be difficult to subtract accurately from each ion current measurement. Thus it was essential to eliminate this problem and the Rogowski Belt offers a unique solution.

A cancelling loop connected to the same voltage source as the Faraday cage lead, but running through the Rogowski belt in the opposite direction, provides the solution (Figure 16c). The opposing lead was connected to a variable capacitor, and the system can be 'tuned' to null out capacitive effects. A variable capacitor which operates up to 20 KV and can be hand tuned while being pulsed, obviously posed a problem. The solution used was to put a length of high voltage cable into an earthed tube, and adjust the capacitance by inserting or withdrawing the cable. As was discovered by tedious error making, the cable characteristics on both leads must match and high quality cable must be used. Early experiments with so-called ignition cable gave very unpredictable and unsatisfactory results.

2.5 Overall Electrical Arrangement

Figure 17 shows the significant parts of the electrical layout of the experimental equipment, and shows the two inputs to the main pulser

a) Applied Pulse

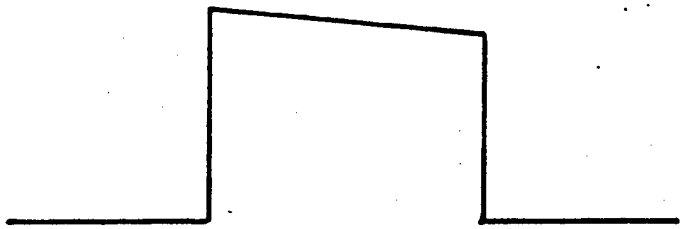

b) Faraday Cage Current

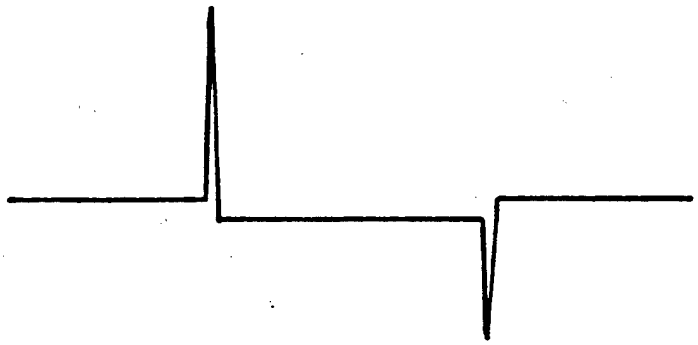

c) Equivalent Circuit

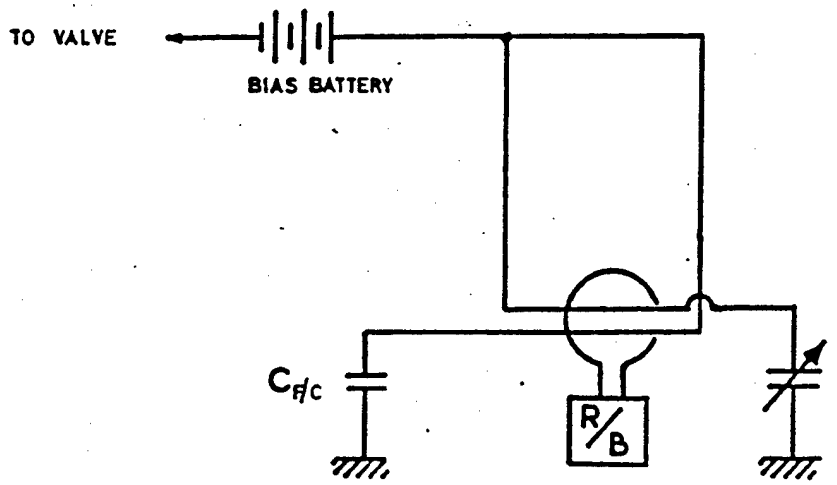

FIG. 16 CAPACITY CANCELLING CIRCUIT

discussed in Section 2.3: the pulse amplifier and the positive DC supply.

The overall time base for the system needs to be derived from the mains because of the Rogowski belt pick-up of mains fields present in the system. Furthermore, this synchronization needs to be adjustable with respect to the mains phase, and of variable PRF. The mains synchronization with adjustable delay is obtained using a comparator which produces a short rise time square wave. This triggers a Tetronix Model 585 oscilloscope, which has two time bases. One of these is used to be synchronized with the square wave, and then set at a sweep rate such that the sweep time is equal to or greater than the 50 Hz signal derived from the comparator. When the sweep time is greater than the time between synchronization signals, a sweep which is synchronized but not firing on every sync signal is obtained. The use of the 'gate' output of the oscilloscope then provides a mains synchronized signal which divides the mains frequency according to the sweep time. The sweep time thus becomes the adjustment of the PRF, which can, of course only be in submultiples of the mains frequency.

The variable PRF signal thus derived is used to operate the other time base and drive deflection circuits of the 585, and to provide a time reference for the Datapulse Model 109 pulse generator. This device produces 10 volt pulses of variable width and delay, ranging from 20 usecs to 1200 usecs, and .01 usecs to 10 msecs, respectively. This drives the pulse amplifier.

A synchronizing signal from the pulse generator drives a small pulse generator built specially for this experimentation. This unit provides a 9 volt pulse of separately variable width and delay to the sample and hold network. The pulse is also available for monitoring on the oscilloscope to determine the sample-and-hold position within the main pulse. Figure 63 of Appendix I gives the circuit diagram of this unit.

Figure 17 does not include the system of interlocks which was part

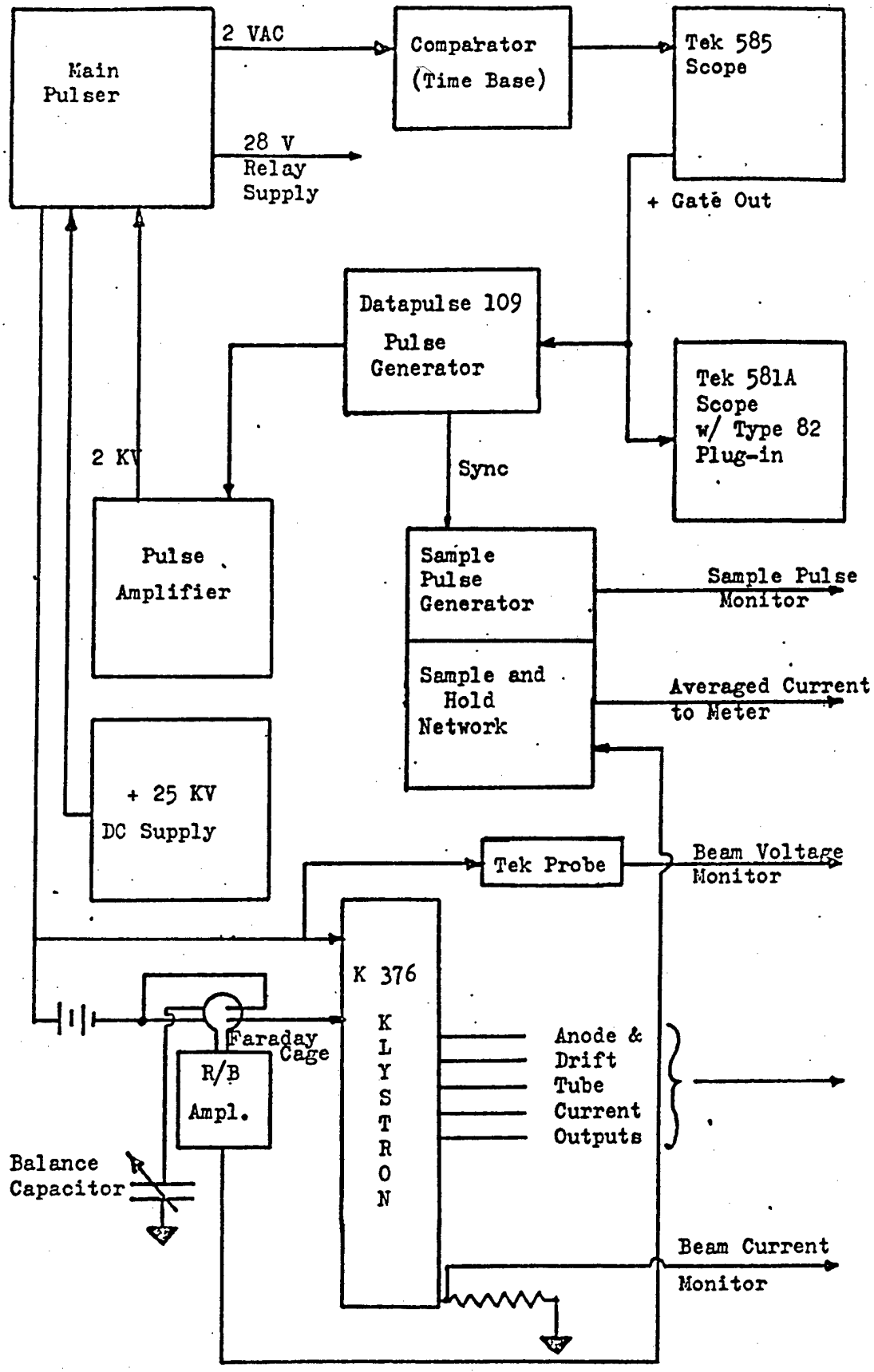

FIG 17 OVERALL BLOCK DIAGRAM

of the experimental set-up, nor does it show the more basic supplies.

It is with the final measurement system described above, the result of many changes and improvements, that measurements have been made, unless otherwise mentioned in the text that follows.

CHAPTER 3

ION FORMATION AND MOTION IN THE DRIFT TUBE

Before discussing the experimental data which was obtained in this study, it is important to extend the remarks made in Chapter 1 concerning the processes of ion formation and drainage in high power klystrons. In traversing the drift tube, beam electrons may make collisions with residual gas atoms and molecules which result in elastic rebound, excitation, or ionisation. At the gas pressures which are typical of high power valve operation the first two types of collisions have negligible effects upon the beam itself, but in the case of ionising collisions, they result in products which may have significant effects upon the beam, the valve components, and the RF operation. At the very least the products of ionising collisions are significant because of the cathode damage which is caused by their drainage. Furthermore, they may have effects upon the beam because of neutralisation of the negative space charge fields of the electron beam. Were it not for the drainage of these ions from the beam, they would quickly neutralise the space charge of the beam and create a plasma state along the drift tube.

This chapter deals first with the process of ion formation in the beam and then considers the forces which act upon the collision products and the trajectories which they typically follow. Because of the random nature of the collision phenomena, it is only possible to determine general characteristics of the ion and electron motions, but these will prove to be useful in understanding some of the experimental results.

Having determined the characteristics of the transverse motion of the collision products, possible causes of the loss of ions from the beam are considered. The main one of these losses, drainage to the cathode, is then discussed in greater detail.

3.1 Ion Formation by Collision

Collisions of beam electrons with the gas through which they travel

are generally discussed (29) in terms of the current still in the beam after the beam has travelled x' meters through the gas: $I(x) = I_o e^{-\alpha x}$. In association with this, the effective cross-section is defined $Q = \alpha/N$, where N is the number of gas molecules per cubic meter. From kinetic theory, $N = 9.70\ p/T$, where p is the pressure in Torr, and T the temperature in degrees Kelvin. The number α, which is measured in units of 1/m-Torr, is the total collision coefficient, and may divided into the constituent coefficients each describing one of the processes which is the result of collision. The coefficient relating to the production of a singly charged ion shall be denoted P_1, and its corresponding cross-section, Q_1. These coefficients are determined primarily by experiment, and several references give data (29,30,31).

The simple model which is thought to adequately describe the ionisation by beam electrons for this and similiar klystrons has been used byprevious authors (1,24,11,12, and others). This model assumes that the beam is a collision-producing cylinder of a radius that of the beam, and with a length that of the drift tube, l_D, at a uniform pressure, p.

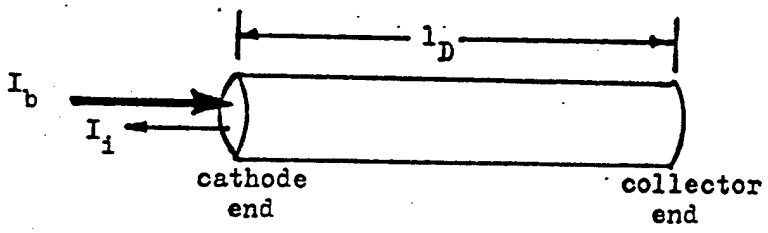

Figure 18 Model for Beam Ionisation

The amount of ion current produced in this cylinder will therefore be dependent upon the beam current, the collision probability for the gas which fills the space, beam length, and the residual gas pressure. If it is assumed that the only collisions of importance are those producing singly charged ions, then the total ion current originating in this length of beam will be:

$$I_i = I_b P_1 l_D p \qquad 3.1$$

where I_b is the beam current in Amps, and other symbols are defined as above.

The coefficient P_1 varies with both the residual gas species and the incident electron velocity. Figure 19 shows the variation of P_1 for a number of gases with respect to electron energy. The dependence of the ionization upon the velocity of the incident electron is highly non-linear. The coefficient increases rapidly from its low initial value near the ionisation energy of the target atom, and reaches a maximum value in the neighbourhood of 100 volts, and then decreases. An analytic expression for the cross-section which may be used with fairly good accuracy at higher energies in given in Mott and Massey (32):

$$Q_1 = \frac{2\pi e^4 c_{nl} Z_{nl}}{m v^2 |E_{nl}|} \ln\left(\frac{2mv^2}{c_{nl}}\right) \qquad 3.2$$

where Z_{nl}, c_{nl}, and E_{nl} are constants relating to the atom whose ionisation cross-section is being computed, v is the electron velocity and m the mass of the electron. Note the dominance of the $1/v^2$ term in the region of high beam energy, which is the usual experimental condition here.

Identification of the species of the gases which are present in the drift tube was not possible. It had originally been hoped that this equipment would be able to perform a mass analysis on ions draining to the cathode, but the spreading of the ions which occurs as they travel behind the cathode hole causes so many to be lost to the walls that not enough current to be measurable remains for analysis behind the cathode. Without this information the composition of the residual gases must be conjectured. Some information has been discovered for the case of cathode ray tubes (33), in which the main constituents were found to be H_2, N_2, C, O_2, and CO. The species of gas to be found in the valve will be determined not only by the materials used in the valve structure, but by processing techniques as well. The large amounts of CO_2 which are given off during cathode activation are probably the main constituent, and

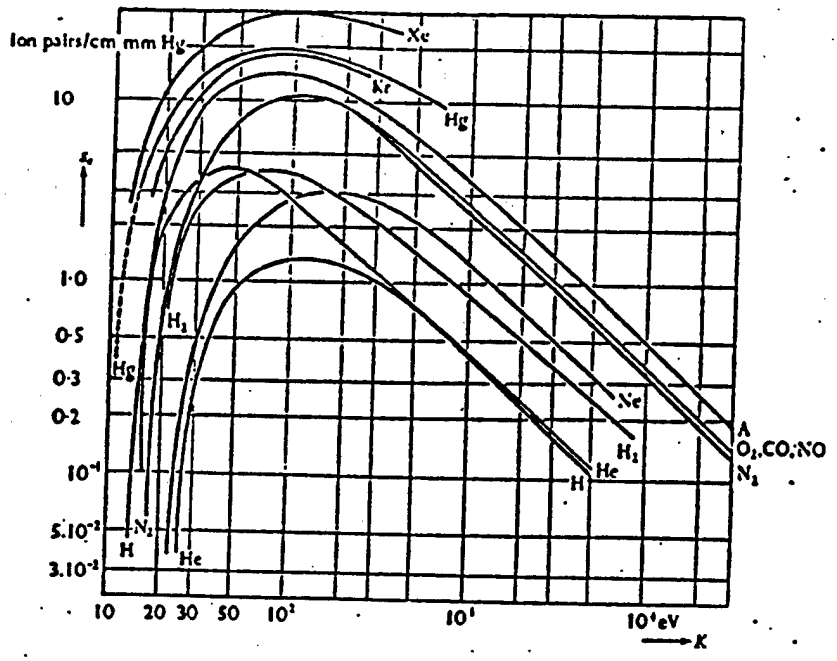

a) VARIOUS GASES

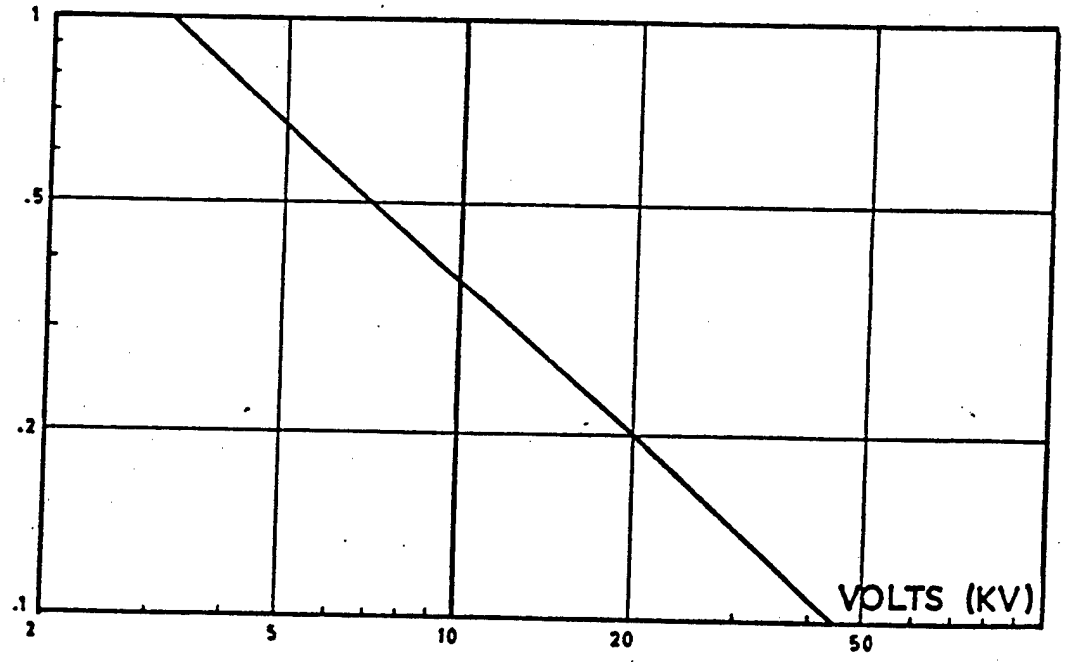

b) DETAIL FOR O_2, CO, NO

FIG. 19 IONISATION PROBABILITY

the ionisation cross-section for O_2 and N_2 is fortunately almost exactly equal to that of CO in the case of large potentials. It may be that copper atoms are also present due to the interaction between the beam and the collector. The equality of the coefficients for air and CO at high voltages suggest that this common line be used for making predictions of the amount of current generated by the beam. Figure 19b shows a blow-up of this part of the cross-section curve of Figure 19a. The mass of the gas is assumed to be 30 for the purpose of calculations.

It is relevant to note that the valve used in these experiments was not baked, although it was continuously pumped. This allowed a sufficient amount of gas to remain in the tube to allow the pressure to be changed over a fairly wide range. A controlled leak was not considered to be a safe addition to the valve in view of the risk which it would create. In spite of the lack of baking, pressures which are fairly typical of high power valve manufacture could be obtained, and it is not thought that the baking process would significantly change the relative abundancy of the gas species in the valve.

Using the data presented above, the expected steady state ion current for normal beam conditions can be calculated. Using $P_1 = 22.5$ for 17.5 KV beam voltage, $l_D = .8825$ m, and $I_b = 4.56$ A, Equation 3.1 yields the result that $I_i = 90.8p$ μamps, where p is in millimicrons (10^{-6} Torr).

Measurements which are discussed in Chapter 4 indicate that further considerations concerning the pressure distribution in this valve should be made before applying this formula.

3.2 Trajectories of Collision Products

Ionising collisions occur randomly thoughout the beam and result in a new ion and ejected electron, both of which may have some initial velocity. Because of the randomness, it is not the purpose of this section to trace each trajectory, but rather to characterise the motion which occurs after the collisions to a first approximation. Firstly,

the fields due to the electron beam are presented, and then the particle motion in these fields is analysed. In this work it is assumed that the beam is uniform and that only transverse motions are considered.

From first principles it may be shown that in a uniform electron beam passing through the drift tube a potential depression will be created due to the space charge of the beam. This potential exhibits a logarithmic form between the wall and theedge of the beam, and a parabolic form within the beam itself, as is shown in Figure 20a. If the beam has a circular cross-section, and is of radius r_b, the radial electric field inside the beam may be written:

$$E_r = \frac{-I_b r}{2\pi e_o u_o r_b^2} \qquad r < r_b \qquad 3.3$$

and the potential

$$V_i = -\int E_r dr = \frac{I_b r^2}{4\pi e_o u_o r_b^2} \qquad 3.4$$

Outside the beam,

$$E_r = \frac{-I_b}{2\pi e_o u_o r} \qquad r > r_b \qquad 3.5$$

$$V_o = -\int E_r dr = \left[\frac{I_b}{2\pi e_o u_o} \ln(r/r_b)\right] + V_i \qquad 3.6$$

where u_o is the electron velocity. Computer solutions provided by EEV, Chelmsford (Figure 21) indicate that the beam diameter varies between almost the full drift tube diameter, which is 1", and 0.75". The potential drop across the beam for normal beam conditions is 536 volts. For axial positions at which the beam diameter is almost that of the drift tube, there is only a small additional potential drop, but in the case of a 0.75" beam, the additional drop is 308 volts.

As is typical of high power valves, these potentials will be far more significant in determining the motions of collision products than the initial velocities acquired as a result of the collision or due to

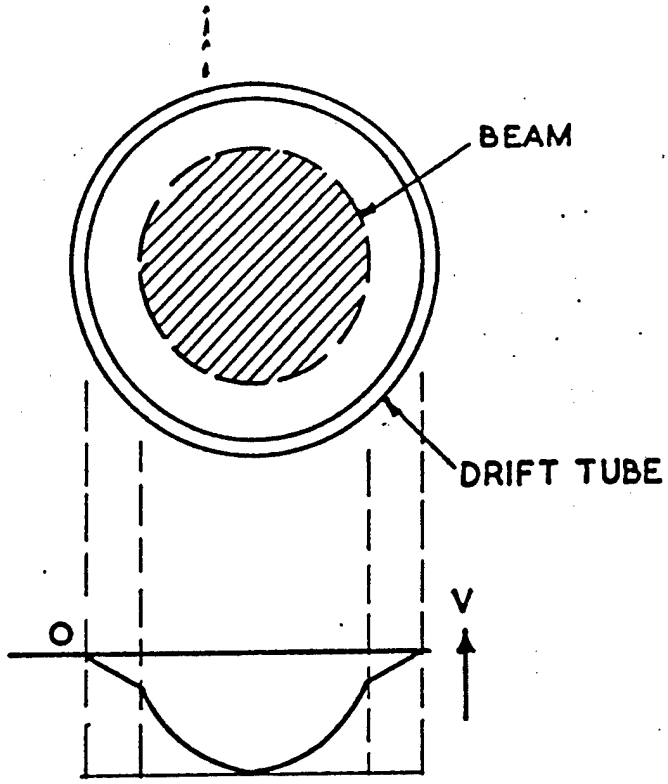

A) RADIAL POTENTIAL

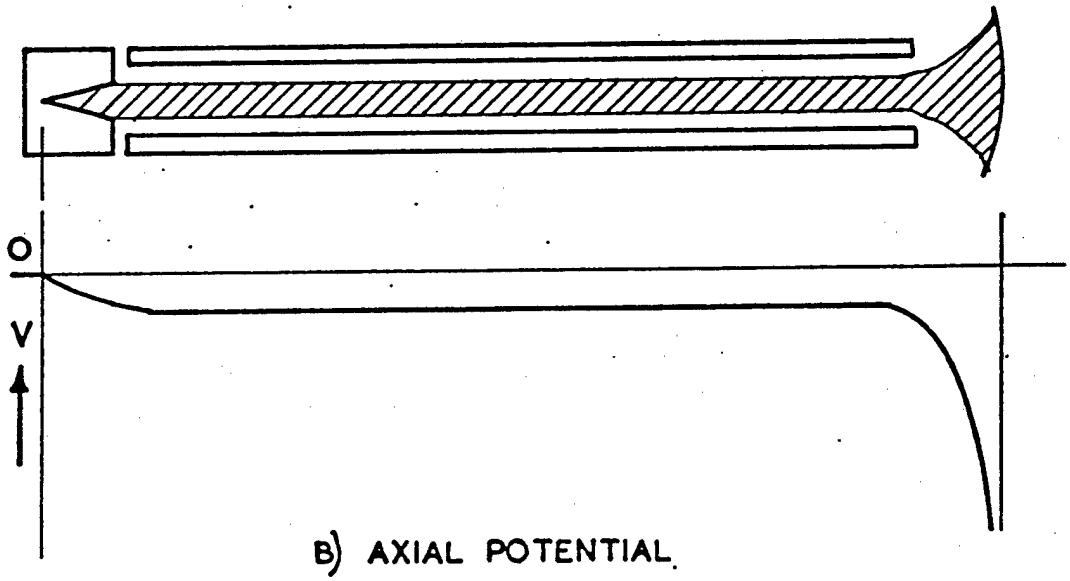

B) AXIAL POTENTIAL

FIG.20 POTENTIAL DEPRESSION

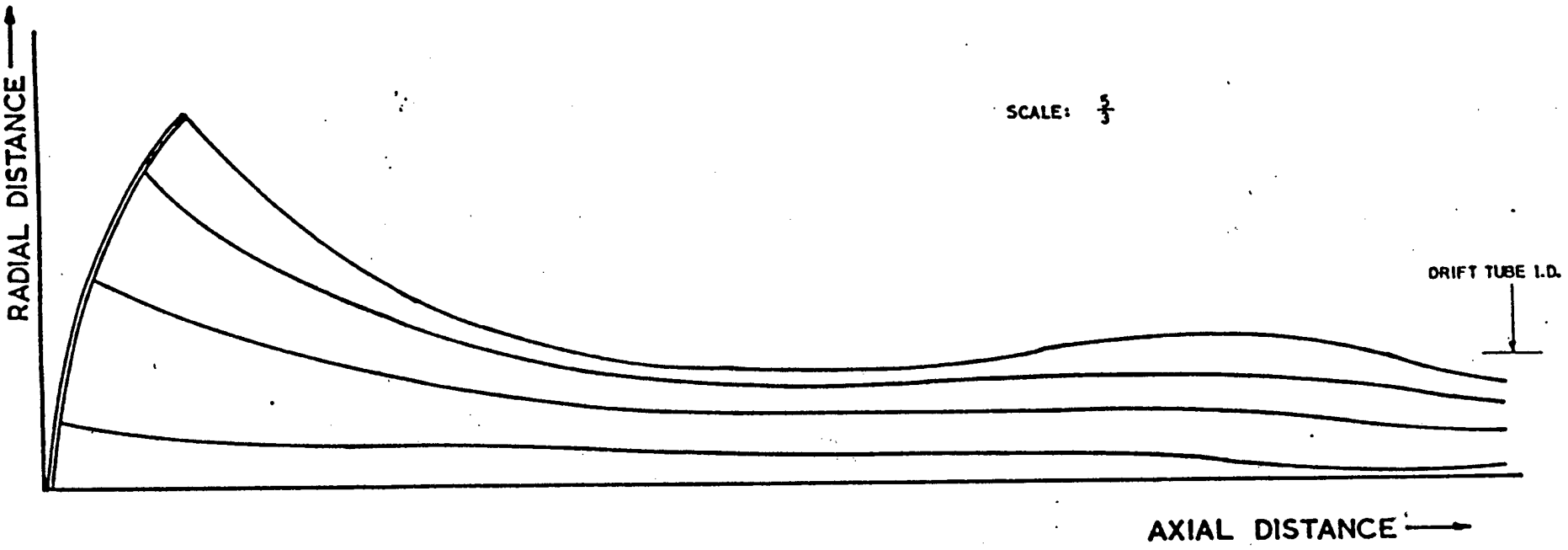

FIG. 21 EEV-COMPUTED TRAJECTORIES

thermal motion. This situation would change if a sufficient number of ions were present in the beam to significantly neutralise the negative space charge, but this is not typical of normal valve operation, and is only occasionally reached in the experiments described below. The neutralised beam has been dealt with by many authors (17,34,14), and will not receive further consideration here.

In the case of a single beam electron-molecule collision, three particles emerge from the interaction: an ion and two electrons. It has been found that in higher energy impacts, the probable energies of these two electrons can be used to distinquish between them (29). One, the secondary, will have an energy approximately equal to that of the incident electron, and the other, the ejected electron, will have a probable energy very much lower, between a few tenths of a volt and a few hundred volts. The secondary electron tends to be scattered in its original direction of motion, and will undoubtedly leave the beam at the collector end. The ejected electron, however, has an angular intensity distribution which reaches a maximum at 90 degrees to the incident electron's direction of motion, and emerges with a velocity which will usually be small when compared to the velocities which it will attain from acceleration by the fields which it encounters immediately upon formation. The initial energy varies with the target molecule and the incident electron energy, but it is generally less than 100 ev for this type of beam.

The ions which are formed by the collision also have a negligible initial energy, and are controlled by the large radial electric field caused by negative space charge in the electron beam.

Computations can now be made of the trajectories of hypothetical individual particles if appropriate initial conditions are assumed. These calculations cannot totally determine the motion of ejected electrons and ions, due to the random nature of the process of formation

and subsequent collisions, but are intended to serve to demonstrate the characteristics of the particle motion. In particular they may be used to demonstrate that both electrons and ions are prevented from escaping radially from the beam. As mentioned above, only transverse motions are considered, and particles with large initial longitudinal energy may well escape the beam at the ends without affecting the beam very much at all. Figure 22 shows the cylindrical coordinate system which shall be used for this discussion.

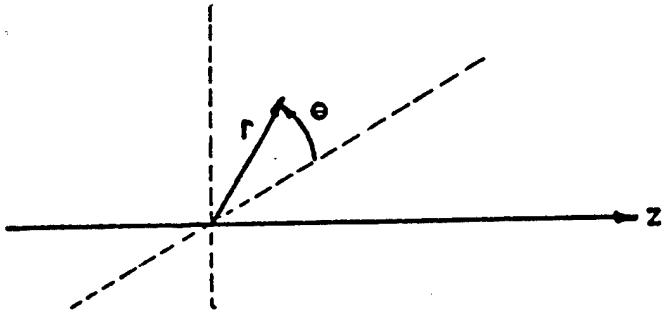

Figure 22 Coordinate System

Firstly the case of ion motion shall be considered. Let $w = \frac{d\theta}{dt}$, w_o its value at $t = 0$, and $w_L = \eta_i B_z/2$, where η_i is the charge to mass ratio for an ion, and B_z is the axial magnetic field, which is assumed to be uniform both axially and radially, and furthermore is the only significant magnetic field present. Then the rotational equation of motion for an ion with radial position r which was formed at r_o may be shown to be:

$$w = (w_o + w_L)\frac{r_o^2}{r^2} - w_L \qquad 3.7$$

The radial equation of motion may be shown to be:

$$\eta_i(rwB_z) + \eta_i E_r = \frac{d^2r}{dt^2} - rw^2 \qquad 3.8$$

where the radial electric field, E_r, is as defined in Equation 3.3 for a uniform solid beam.

These equations may be combined to obtain:

$$\frac{d^2r}{dt^2} = \eta_i E_r + r\left[\frac{w_B^2 r_o^2}{r^4} - w_L^2\right] \qquad 3.9$$

where the constant $w_B = w_o + w_L$, has been introduced for compactness of notation. Substituting for E_r,

$$\frac{d^2r}{dt^2} = r\left[\frac{-\eta_i I_b}{2\pi e_o u_o r_b^2} - w_L^2 + \frac{w_B^2 r_o^2}{r^4}\right] \qquad 3.10$$

If the first and second terms in the bracket are evaluated for the valve in question, with a 17.5 KV, 4.56 A beam of radius 0.4" in a magnetic field of 0.04 w/m, the first term is found to have a value of 3.176×10^{13} which is far greater then $w_L^2 = 4.074 \times 10^9$, and thus the second term may be neglected. Equation 3.10 obviously describes an oscillatory motion in which the ion moves nearly along lines of radius, each time passing close to the axis, and returning to approximately the radius at which it was formed. If the radial velocity is denoted $\dot{r}$, then

$$\frac{d^2r}{dt^2} = \frac{d\dot{r}}{dt} = \frac{d\dot{r}}{dt}\frac{dr}{dt} = \dot{r}\frac{d\dot{r}}{dr} \qquad 3.11$$

Equation 3.11 may then be integrated after substituting the results of Equation 3.10, and the following result is obtained after evaluation of the constant of integration by use of the initial condition that $\dot{r} = 0$ at $r = r_o$ (This is an acceptable approximation in view of the large fields which are present):

$$\dot{r}^2 = k^2(r_o^2 - r^2) - \frac{w_B^2 r_o^4}{r^2} + w_B^2 r_o^2 \qquad 3.12$$

where k^2 has been defined as $(\eta_i I_b)/2\pi e_o u_o r_b^2$. Solving Equation 3.12 for the derivative dt/dr, and then integrating:

$$t = \int \frac{r\,dr}{\left[k^2 r^2(r_o^2 - r^2) - w_B^2 r_o^4 + w_B^2 r_o^2 r^2\right]^{\frac{1}{2}}}$$

Using the change of variable $r = x^{\frac{1}{2}}$, this may simplified and integration is possible.

The result of the integration is:

$$t = \frac{1}{2k} \arcsin \frac{2k^2 r^2 - k^2 r_o^2 - w_B^2 r_o^2}{\left[\left(k^2 r_o^2 + w_B^2 r_o^2\right)^2 - 4 w_B^2 r_o^4 k^2\right]^{\frac{1}{2}}} \qquad 3.13$$

which may be solved for r to show that:

$$r = \left(\frac{(k^2 - w_B^2) r_o^2 \cos 2kt + r_o^2 (k^2 + w_B^2)}{2 k^2} \right)^{\frac{1}{2}} \qquad 3.14$$

in which the inital condition that $r = r_o$ at $t = 0$ has been used. Equation 3.14 reduces to the obvious solution of equation 3.10 when the magnetic effects are not considered, which is:

$$r = r_o \cos kt \qquad 3.15$$

Figure 23 illustrates the trajectories predicted by equations 3.7 and 3.14, and it is clear that although the ions cannot escape the beam radially, they oscillate, passing close to the axis and returning to a maximum excursion close to their formation radius. The magnetic field is seen to have little effect on the particle motion.

Because of their opposite electrical polarity and smaller mass, ejected electrons behave quite differently, although it will be demonstrated that they are also prevented from escaping radially and remain within a radius not much larger than that at which they were formed. In parallel with equations 3.7, 3.8, and 3.9, two equations describing rotational and radial motion may be combined in a third equation for radial acceleration:

$$w = (w_o - w_L) \frac{r_o^2}{r^2} + w_L \qquad 3.15$$

$$-\eta_e (r w B_z) - \eta_e E_r = \frac{d^2 r}{dt^2} - r w^2 \qquad 3.16$$

$$\frac{d^2 r}{dt^2} = -\eta_e E_r + r \left[w_E^2 \frac{r_o^4}{r^4} - w_L^2 \right] \qquad 3.17$$

where $w_E = w_o - w_L$, and w_L is the Larmor frequency for electrons, not

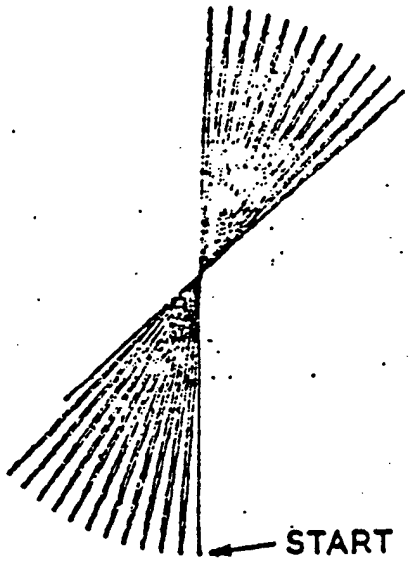

FIG. 23 TYPICAL ION TRAJECTORY

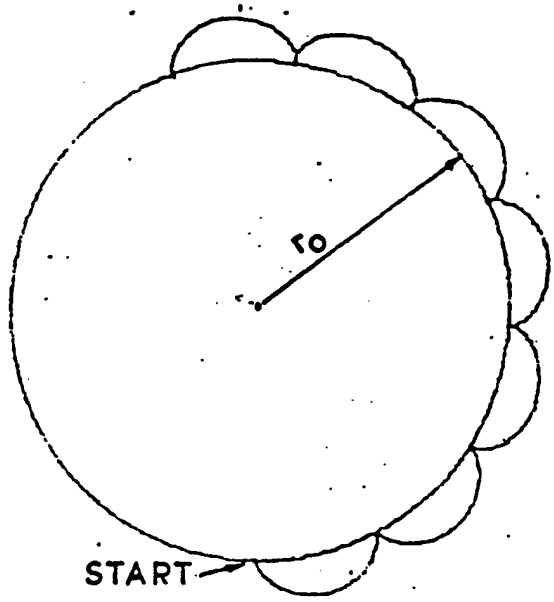

FIG. 24 TYPICAL ELECTRON TRAJECTORY

ions. Substitution of the value for electric field within the beam results in an equation for electrons parallel to 3.10:

$$\frac{d^2r}{dt^2} = r\left[\frac{\eta_e I_b}{2\pi\varepsilon_o u_o r_b^2} - w_L^2 + w_E^2\frac{r_o^4}{r^4}\right] \qquad 3.18$$

It is now informative to compare the magnitudes of the first and second terms within the bracket of Equation 3.18. For the beam current and voltage conditions assumed earlier, the values are 1.823×10^{18} and 1.237×10^{19}, respectively. It is obvious that the magnetic term dominates the solution, and it is convenient to define a constant k_e^2 which is the difference of the first two terms, $k_e^2 = 1.055 \times 10^{19}$. It is now possible to proceed as in the case for ion motion, and integrate to find:

$$t = \left[(r_o^2 - r^2)k_e^2 + w_E^2 r_o^2 - \frac{w_E^2 r_o^4}{r^2}\right]^{\frac{1}{2}} \qquad 3.19$$

This equation may be integrated to find t,

$$t = \int \frac{r\,dr}{\left[(k_e^2)(r_o^2 - r^2)r^2 + w_E^2 r_o^2 r^2 - w_E^2 r_o^4\right]^{\frac{1}{2}}} \qquad 3.20$$

Using C as an integration constant,

$$t + C = \frac{1}{2k_e}\arcsin\left(\frac{2k_e^2 r^2 - (w_E^2 + k_e^2)r_o^2}{r_o^2\left[(w_E^2 + k_e^2) - 4w_E^2 k_e^2\right]^{\frac{1}{2}}}\right)$$

$$\sin(2k_e t + C) = \frac{2k_e^2 r^2 - (w_E^2 + k_e^2)r_o^2}{r_o^2(w_E^2 - k_e^2)} \qquad 3.21$$

Since $t = 0$ at $r = r_o$, the right hand side of Equation 3.21 shows that $C = -\pi/2$, and the equation may be re-written:

$$r^2 = r_o^2(w_E^2 + k_e^2 - (w_E^2 - k_e^2)\cos 2k_e t)/2k_e^2 \qquad 3.22$$

This trajectory equation indicates that the ejected electron oscillates about an average radius which is somewhat greater than the radius at which it was formed, at least for the case of $w_o = 0$. For other cases, the average radius may be less or greater than the formation radius, but

solutions will be close to that indicated by Equation 3.22 since initial energies are not very important in determining the trajectory.

Ejected electrons escape the beam radially only if the maximum excursion which they make is greater than the diameter of the drift tube. In the case of zero initial angular momentum, Equation 3.22 shows that the maximum excursion of the ejected electron is 1.08 times the formation radius, which means that even an electron formed at the beam edge will not escape, at least on the basis of its trajectory after formation and before collision with any other particles. Furthermore, if it is assumed that all of an electron's initial energy due to the formation process is directed in the θ- direction so as to cause the largest excursion possible, 86 electron-volts of initial energy are required for escape even in the case of a beam edge-formed electron for this beam. Few ejected electrons would be expected to have this much energy. Thus, the vast majority of ejected electrons are trapped within the beam or between the beam and the drift tube wall, and may escape only by draining out longitudinally, or by having further collisions with residual gas molecules which result in a larger trapped radius. The results of a hypothetical trajectory calculation are shown in Figure 24, which is similiar, although not identical, to trajectory calculations for magnetrons.

No attempt has been made here to do more than to characterise the trajectories of ionisation collision products, but this characterisation has shown that both ions and ejected electrons are trapped within the beam or its immediate vicinity. The capture of ejected electrons differs from the work of previous experimenters, who dealt with beams not confined by magnetic field. Processes which would cause the loss of ions or electrons from the beam, but which were not accounted for by the above discussion are now considered.

3.3 Losses of Ions and Ejected Electrons from the Beam

The density of particles trapped by the processes described in the

above section would build very rapidly were it not for the loss processes which drain both types of particles out of the beam. The main cause of loss is longitudinal drainage, and this topic will be covered in detail in Section 3.4. This section will consider other possible losses of these collision products from the beam.

1) Loss from the beam radially. Section 3.2 has shown that this process can take place only if the beam space charge has been neutralised, or nearly neutralised, or in the rare case that the particles have very large initial energies. Thus radial loss is not a very significant loss in low pressure beams.

2) Recombination. Although this process is continuously taking place, the rate of recombination is negligible when compared to the production rate.

3) Loss to insulators. Wadia (12) mentions loss to insulators which become negatively charged because of beam interception and are thus able to draw ions from the beam. This process would seem to be important only in the case of beams near neutralisation, and is certainly not of importance in the valve used in these experiments, in which the insulators are well removed from the beam path.

4) Collector drainage. In all valves in which the collector is kept at a potential near or the same as that of the body, a longitudinal potential gradient will be created inside the collector and in the region between the collector and the drift tube (Figure 20b). This gradient will prevent ions from flowing into the collector in the same way that it prevents their radial escape, but will act to drain off ejected electrons. Valves which operate with collector depression for efficiency improvement will drain ions into the collector end of the valve, and this drainage may cause undesired modulation of the RF signal by collector power supply ripple. Such modulations would have deleterious effects in valve applications to doppler radars.

The main drainage path for ions is to the cathode, and this drainage is discussed in the next section. Because of their much smaller mass, the longitudinal fields which affect the ejected electrons and cause their drainage to the collector impart sufficient velocity to the particles to make their contribution to space charge negligible. Thus, unlike the draining ions, the draining electrons will have no major effect on the electron beam itself. Those which do not drain and are stored in the beam, however, may be important, and further discussion of these particles is deferred until Chapter 5.

3.4 Ion Drainage to the Cathode

This section will discuss the longitudinal potential gradient which causes ions to drain from the cathode end of the drift tube. The case of a smooth electron beam (i.e. without scallops) is first considered. In the absence of any gas in the drift tube, the beam will have only two regions of large axial potential gradient: at each end of the drift tube where fringing fields from the collector (due to space charge potential depression) and from the cathode (due to the accelerating potential) enter into the drift tube. In long, narrow drift tubes characteristic of this type of beam device, these fringing fields will become negligible not far from the drift tube ends, leaving a region within the tube which has potential gradients on the order of thermal energies or less.

The residual gases in a practical valve may change this condition in two ways. Firstly, the non-ionizing and ionizing collisions which beam electrons make with residual gas molecules cause an average loss of kinetic energy which is proportional to pressure. But at low pressures, such as 10^{-6} Torr, this loss can be shown to be equal to only a few tenths of a volt over the entire length of the beam for the beam under consideration. This is not enough to significantly affect the motion of ions along the drift tube. Secondly, the products of ionising collisions

may build-up in sufficient numbers to create a significant potential gradient in the drift tube. This is significant, even in small beams, as shall now be demonstrated.

The problem of ion drainage and the potentials which create it was dealt with by Field, et al (11), and adapted by Hines, et al (24) using more accurate values for ionisation probabilites than were used by Field, amd making slightly different assumptions concerning the boundary conditions. They also extended the work to magnetically focussed conditions. The following assumptions were made in the work:

1) Ions have the same mass and charge

2) Ion or plasma oscillations are not present.

3) Ejected electrons escape quickly and do not add to the space charge.

4) Initial velocities of the ions are negligible.

5) The potential over a cross-section of the beam is assumed constant at an average value which is directly proportional to the linear charge density (electronic plus ionic).

From the discussion of ejected electron motion in Section 3.2, it is obvious that the third assumption will be true only if the electrons are able to escape longitudinally to the collector end of the valve. This would be the case only if the scalloping of the electron beam had been eliminated by the drainage of ions to locations of potential minimums, and the drainage of the rotating ejected electrons to regions of potential maximums. As Figure 21 demonstrated, this beam does exhibit scalloping, which is typical of practical beams which use a confining magnetic field larger than the Brillouin value to obtain acceptable transmission. When a smooth beam is assumed, or a scalloped one which has reached a steady state and been smoothed by local neutralisation, the ejected electrons would be expected to drain to the collector under the influence of the same potential gradients which are responsible for

the ion drainage to the cathode. Although the magnitude of these gradients has not yet been determined, it is clear that because the electrons are affected by the same gradients as the ions, but have a charge-to-mass ratio which is much larger, any contribution which their space charge makes to the total space charge within the drift tube will be insignificant in contrast to that made by the slower-moving ions. Thus the third assumption is valid for smooth beams.

The fifth assumption is clearly not valid for the case of large beams such as the one dealt with here, which has a potential variation on the order of a few hundred volts across its radius in the absence of significant neutralisation. But the problem of accurately taking account of this variation across the beam is a difficult one to solve, and an approximation may be made by taking the average potential between the beam edge and the axis and using that as the 'constant' potential. Making such an approximation will allow a comparision between the work of Hines, et al on low power valves and the present work.

Ions are assumed to drain only from the cathode end of the drift tube and the smooth electron beam has a radius of r_b, and goes through a drift tube of radius r_D. If the drift tube is assumed to have earth potential, then the potential depression along the axis will be given:

$$V_{ax} = \frac{\sigma_T}{4\pi e_o}\left[1 + 2\ln\left(\frac{r_D}{r_b}\right)\right] \qquad 3.23$$

where σ_T is the total linear charge density due to beam electrons, ions, and ejected electrons. As mentioned above, the contribution due to ejected electrons can be neglected. σ_e, the charge density of the beam electrons is constant along the length of the beam, but the charge density of the ions, σ_i, will be a function of longitudinal position. The potential depression at the edge of the beam will be:

$$V_{ed} = \frac{\sigma_T}{4\pi e_o}\left[2\ln\left(\frac{r_D}{r_b}\right)\right] \qquad 3.24$$

The longitudinal gradients in these potentials are the forces which cause ion drainage from the drift tube. The average potential is a function of the longitudinal position as well, and will be denoted V(z):

$$V(z) = \left[\frac{\frac{1}{2} + 2\ln(r_D/r_b)}{4\pi e_o}\right]\sigma_T = K\left[\sigma_i(z) + \sigma_e\right] \qquad 3.25$$

K, defined by this equation, is a constant relating to the average potential. If the collector end of the drift tube is taken for z = 0, and only ions formed in the drift tube considered, then at position z the total ion space charge will be made up of contributions between the origin and the point z, since uni-directional flow of the ions is assumed. If the rate of ion formation per unit length is G_i, then the total ionic space charge density at z, $\sigma_i(z)$, will be given by:

$$\sigma_i(z) = \int \frac{G_i\, dx}{\left[2\frac{e}{m_i}\left[V(x) - V(z)\right]\right]^{\frac{1}{2}}} \qquad 3.26$$

Substituting the value of V(z) found in Equation 3.25,

$$\sigma_i(z) = \int \frac{G_i\, dx}{\left[2K\frac{e}{m_i}\left[\sigma_i(x) - \sigma_i(z)\right]\right]^{\frac{1}{2}}} \qquad 3.27$$

The solution for this integral equation was given by Field, et al (11):

$$\frac{3\pi G_i z}{2\left[\sigma_i(0)\right]^{3/2}\left(2K\frac{e}{m}\right)^{\frac{1}{2}}} = \left[1 + 2\frac{\sigma_i(z)}{\sigma_i(0)}\right]\left[1 - \frac{\sigma_i(z)}{\sigma_i(0)}\right]^{\frac{1}{2}} \qquad 3.28$$

The relative charge density, $\sigma_i(z)/\sigma_i(0)$, is plotted as a function of the left hand side of Equation 3.28 in Figure 25. This solution must be matched as well as possible to external potential gradients which are not accounted for in the derivation. These include the field at the cathode end, which is very large, and the field at the collector end due to space charge potential depression. If the collector field may be ignored on the grounds that it only affects ions created within the collector, and the high gradient at the cathode end is assumed to coin-

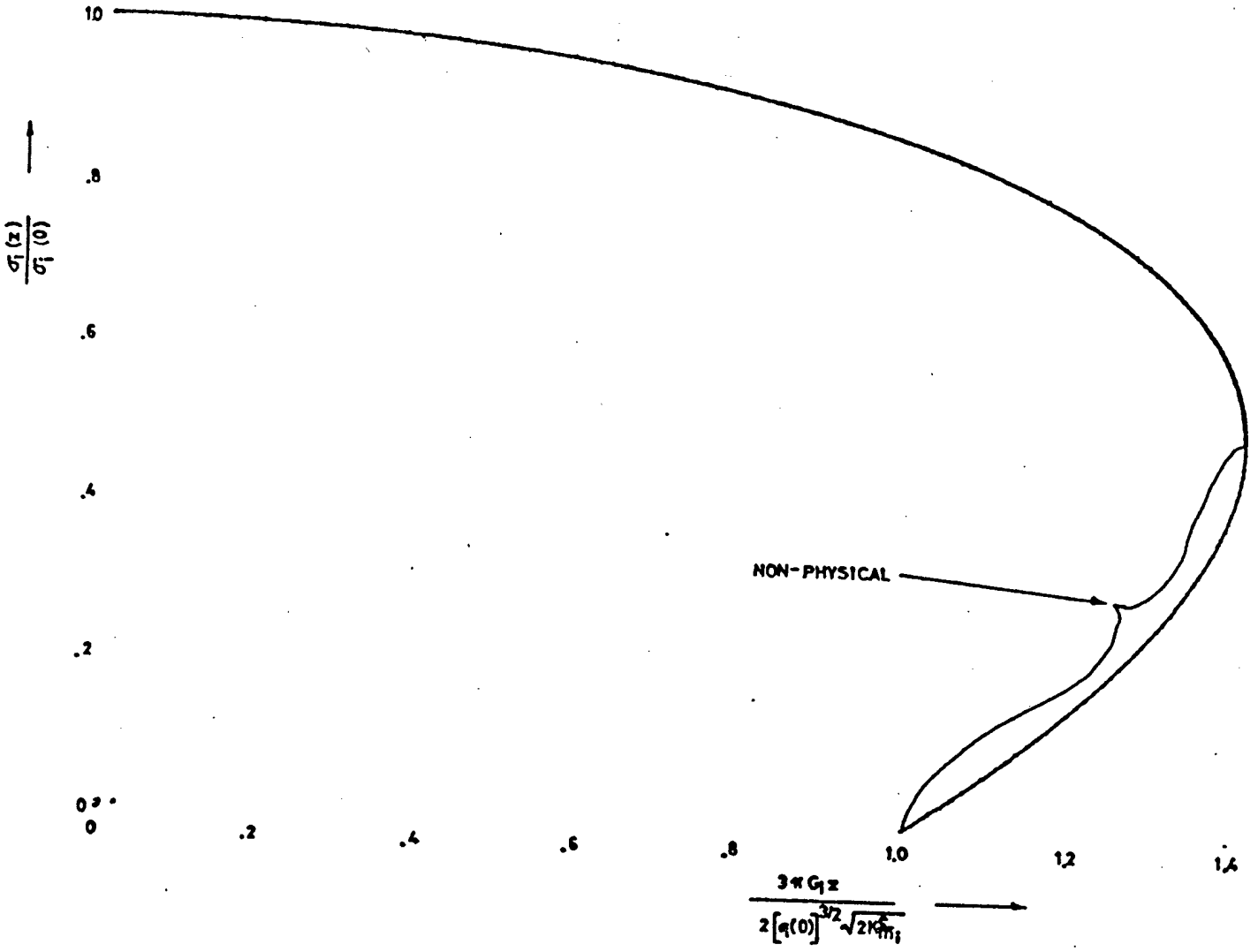

FIG.25 LONGITUDINAL IONIC CHARGE DENSITY VARIATION

oide with the infinite slope which occurs at the right hand side of Figure 25 where $z = l_D$, which must be approximately correct, then the maximum space charge density, $\sigma_i(0)$, may be calculated. Since the abscissa of Figure 25 then has a value of 1.414:

$$\sigma_i(0) = \sqrt[3]{\frac{9\pi^2 G_i^2 l_D^2}{16 \frac{e}{m_i} K}} \qquad 3.29$$

When this value of $\sigma_i(0)$ is used in Equation 3.28, the ionic space charge density can be calculated along the length of the drift tube. From this explanation of drainage three important measurable quantities relating to the ion drainage may be calculated:

1) The amount of space charge which is stored in the entire beam at various pressures.

2) The pressure at which total neutralisation should occur at the collector end of the valve.

3) The amount of neutralisation of the potential depression which occurs at a given pressure and given location in the drift tube.

3.4.1 Space Charge Storage in the Beam

The total ionic space charge stored in the beam can be computed by multiplying the drift tube length by the maximum value of space charge, and reducing the product by the integral of the area between the line of $\sigma_i(z)/\sigma_i(0) = 1$ and the curve $\sigma_i(z)$ in Figure 25. A computer integration of this quantity indicates that the total space charge within the beam, Q_i, is:

$$Q_i = .9052\, l_D \sqrt[3]{\frac{9\pi^2 G_i^2 l_D^2}{16 \frac{e}{m_i} K}} \qquad 3.30$$

Measurements of the rise time which are discussed in Section 4.3.3 and 5.2.2.4 allow a comparision of theoretical and measured values of the beam charge storage.

3.4.2 Neutralisation Pressure:

As the pressure rises, the ionic space charge will increase until it equals the electronic space charge due to the beam, at which point it can be said that the beam is neutralised. The neutralisation condition leads to oscillations in the beam and drainage current, and thus may be determined by experiment. The electronic space charge is given:

$$\sigma_e = \frac{I_b}{\left[2 \frac{e}{m_e} V_b\right]^{\frac{1}{2}}} \qquad 3.31$$

And this electronic charge will first be neutralised in the neighbourhood of the collector, when

$$\sigma_i(0) = \sigma_e(0)$$

3.4.3 Partial Neutralisation of the Beam Potential Depression

From Equation 3.25 it can be seen that the beam potential depression will be cancelled in varying amounts along the drift tube, dependent on the ionic space charge density. At the collector the average potential V(0) will be:

$$V(0) = K \left[\sigma_i(0) + \sigma_e\right] \qquad 3.32$$

3.4.4 Voltage Gradient in the Drift Tube

The longitudinal potential gradient which is created by the changing ionic charge density which is shown in Figure 25 can be calculated at a number of pressures. Table 3.1 shows the potentials at the center of the numbered DTS with respect to a zero potential at z = 0. The total drop between the two ends of the drift tubes is not easy to determine accurately because of the blending of the drift tube potential with the fringing fields of the cathode region. The pressures chosen for this table will be of interest in the measurements of ion current drainage to the cathode with a negatively biassed collector (Section 5.2.2.3). It is clear from Table 3.1 that the potentials created by the changing ionic space charge density will exceed both thermal velocities

and voltage gradients due to the kinetic energy loss from all types of collision.

Table 3.1 Potentials Drops due to Ionic Space Charge Variation

Pressure (Torr)	Radius	DTS 4	DTS 3	DTS 2	DTS 1
5.5×10^{-6}	Average	1.8	6.1	19.7	36.8 Volts
	Axis	6.2	20.7	67.5	125.7 Volts
2.6×10^{-6}	Average	1.1	3.8	12.5	23.4
	Axis	3.5	11.7	38.1	71.0
9.9×10^{-7}	Average	0.6	1.9	6.3	11.7
	Axis	1.8	6.2	20.0	37.3
2.4×10^{-7}	Average	0.2	0.7	2.4	4.5
	Axis	0.7	2.4	7.8	14.5

Table 3.1 shows the gradient both at the average radius, and at its maximum value, on the axis.

3.5 Summary

This chapter has discussed the ion formation process, the trajectories which the collision products follow, and the process of ion drainage. The theory of Hines, et al (24) which was used originally for low current beam experiments was discussed and the values of measurable phenomena which it predicts were calculated. The experimental values of these phenomena in high power valves are discussed in the next chapter.

CHAPTER 4

PRELIMINARY EXPERIMENTAL RESULTS

The K 376 valve and the basic operation of the measurement and power supply equipment have been described above. These experimental results are taken with the two guns which were modified as described above. Early plans had been to use a Faraday cage placed behind the modified header plate (Figure 5) and to collect ions after they had drained through the tube leading to the cathode surface. However, the spreading of the ion beam, which starts upon entry to the anode-cathode region, meant that the loss of ions to the walls of the tube was so great that only tens of nanoamperes could be measured with a 2 KV DC beam. Pulsed measurements at the normal operating voltages were not attempted since the current is so far below the measurement sensitivity for pulsed currents. Due to the non-linearities of the ionisation cross-section curves, not a great deal more ion current was to be expected at the higher voltages, in spite of the great increase in beam current.

To modify the Faraday cage and place it directly behind the cathode, rather than behind the header plate, necessitated opening the klystron and thus exposing the gun to the atmosphere. Although the gun was returned as soon as possible to the klystron, a good deal of de-activation had taken place, and only prolonged overheating and the drawing of some current began to restore the proper level of emission, and full emission was never achieved. ~~This lowered emissivity of~~ The first gun, with low emission, provided the first sets of readings of ion current drainage, which are characterised by not being above 2.9 Amperes. Some of this data is presented in this dissertation.

To improve the klystron performance to its normal levels, a new gun had to be made. Because of the construction of the cathode 'pot' the fitting of a new cathode surface alone was not possible, and thus construction of a whole new gun had to be undertaken to interchange guns.

The new gun was installed and showed much greater emission, thus allowing almost normal operation to be obtained. Although the measurements with the first cathode provide an occasionally useful contrast, the majority of the measurements discussed in what follows relate to the second gun, and thus to close-to-normal operating conditions.

From the physical description of the klystron, it can be seen that a great variety of biasing arrangements is possible, using the drift tube sections as electrodes, which would differ from the normal configuration. The use of these electrodes made the klystron a more useful piece of experimental equipment than would be immediately apparent from the initial description of 'operable klystron.' These many possibilities do at the same time pose the experimenter with a problem: what will be regarded as 'standard.' In the work that follows, unless otherwise stated as an experimental condition, all drift tubes, the modulating anode, and the collector were at or near earth potential, as would be the case in normal operation. The use of current measuring resistors on each of the valve electrodes, 100 ohms in the case of the anode and drift tube sections, and 1 ohm in the case of the collector, naturally caused these parts to be slightly negative during the pulse due to beam interception. However, subsequent experiments demonstrated that these small voltages in no way influenced the measurements of ion current. The No. 5 Drift Tube (Figure 4) was unfortunately in electrical contact with the magnet frame and thus prevented both biasing and body current measurements on that section. This condition could not be changed since the valve rests on this section, and movement would have meant the risk of damage to the valve. In view of its proximity to the collector, not much information was lost due to this abnormality.

As mentioned in the introduction, the majority of measurements in this research are based upon direct measurement of the ion current draining to the cathode. The other measurement occasionally used is the ob-

servation of drift tube interception current. Though only these two measurements may be made, they prove to be very versatile indeed.

The first goal of the experimentation is to determine the amount of ion current which normally drains to the cathode from the drift tube and collector. As has been noted above, measurements of this current have not been reported for high power electron beam devices.

To help to understand the results which are given below, it is instructive to consider a typical ion current response to an applied beam current pulse. As mentioned in Chapter 2, the beam voltage was always pulsed in these experiments to decrease the average power dissipation, and provide information about the build-up of ion phenomena. Figure 26 (p.24) shows a typical response, and is the ion current which flowed during a 550 μsec beam current pulse. The ion current rises from zero at the beginning of the pulse to a plateau value, but the observed rise time of about 200 μsecs is far greater than the 5 μsec rise time of the beam current pulse which causes the ion flow. The negative-going portion of the ion current trace is a transient due to capacitive pick-up from the main beam pulse and does not represent actual ion current. The plateau value represents the steady-state value of ion current which would be present in CW operation of the valve.

Three characteristics of this ion current trace are of interest in understanding the various mechanisms which determine ion drainage: the height of the plateau, the build-up time for the ion current to rise to this plateau, and any oscillations in the ion current which may take place once this plateau is reached (none are present in Figure 26). It is found that these characteristics of the ion drainage vary with beam current and residual gas pressure. The first part of the experimental work described below deals with the dependence of these characteristics of the ion flow upon these two parameters. Further experimental work discussed in Chapter 5 employed biasing of various electrodes in the

valve to study changes in the ion drainage caused by the biasing, and to determine the distribution of ion production within the valve.

4.1 Steady State Measurements

The measurements made of the steady state value of the ion current were made on both the low emission and near-normal emission cathodes. The use of a sample gate to determine ion current value at various time delays after the beginning of the pulse has been described in Chapter 2. The sample gate was positioned within the pulse so that it would measure the plateau level of the current, and the signal averaging described above was used. This resulted in a high degree of repeatability in the ion current measurements under identical beam current and pressure conditions. This repeatability was seen between measurements made after short and long turn-offs, and was within 5% at the higher pressures, where the signal to noise ratio is higher. It was reduced to 20% at the lower pressures in the neighbourhood of 2-3 x 10^{-7} Torr. The repeatability was demonstrated within courses of intensive experimentation lasting a couple of weeks. Because of the beam voltage droop during the pulse, which was discussed in Chapter 2, and may be observed in Figure 12, there is some ambiguity is assigning a beam voltage and beam current to relate to a given ion current measurement. This ambiguity occurs since the actual determination of the ion current is made well after the beginning of the pulse, and the beam voltage may have significantly declined. The difference in beam voltage between the beginning of the pulse and the time that a plateau has been reached in the ion current would be most significant in experiments conducted at the lowest pressures. The rise times to the steady state are longest at these low pressures. For the sake of consistency, therefore, any beam currents and voltages associated with data reported below are those which were present when the ion current sample was taken, rather than at the starting value of the applied pulse. When measurements are taken for purposes of com-

parision between different pressures, the sample point is the same for all. It should be pointed out that Figure 12 illustrates a pulse twice as long as that in normal usage, and the extreme droop observable between the beginning and end of that pulse are by no means typical of the experimental work reported. Most sampling was done at delays of 500 μsecs or less, at which point the beam voltage has dropped only 15% from its normal value. Although this indicates a corresponding decrease in the beam current, the ion production rate drops very little due to the increase in ionisation cross-section at the lower voltage. This problem did prevent measurements being made at the exact normal operating voltages of 17.5 KV. Starting the pulse at a higher voltage so that 17.5 KV would be achieved by the time the ion current plateau was reached, was not attempted again after a large discharge occured within the valve when the voltage was raised to 20 KV. The location of the discharge was not known, but the most likely place for such a discharge would be from the birdcage to the bellows along the main body. Since these are very thin wall bellows, it was feared that such discharges might make a leak in the bellows, and it was thought that the risk was not justified by the small differences to be expected in the results.

4.1.1 Dependence of the Ion Current upon Residual Gas Pressure

An important goal of this experimentation was to determine the amount of ion current drainage to the cathode as a function of residual gas pressure. This data was taken with much greater accuracy after the ion gauge had been placed in the valve. Pressure was varied by a number of techniques, but usually by reducing the voltage on the ion pump to low values to reduce the pumping speed. The slow variation of pressure obtainable using these methods proved very satisfactory for making the measurements which are now described.

Curve I of Figure 27 shows the readings of ion current made on the

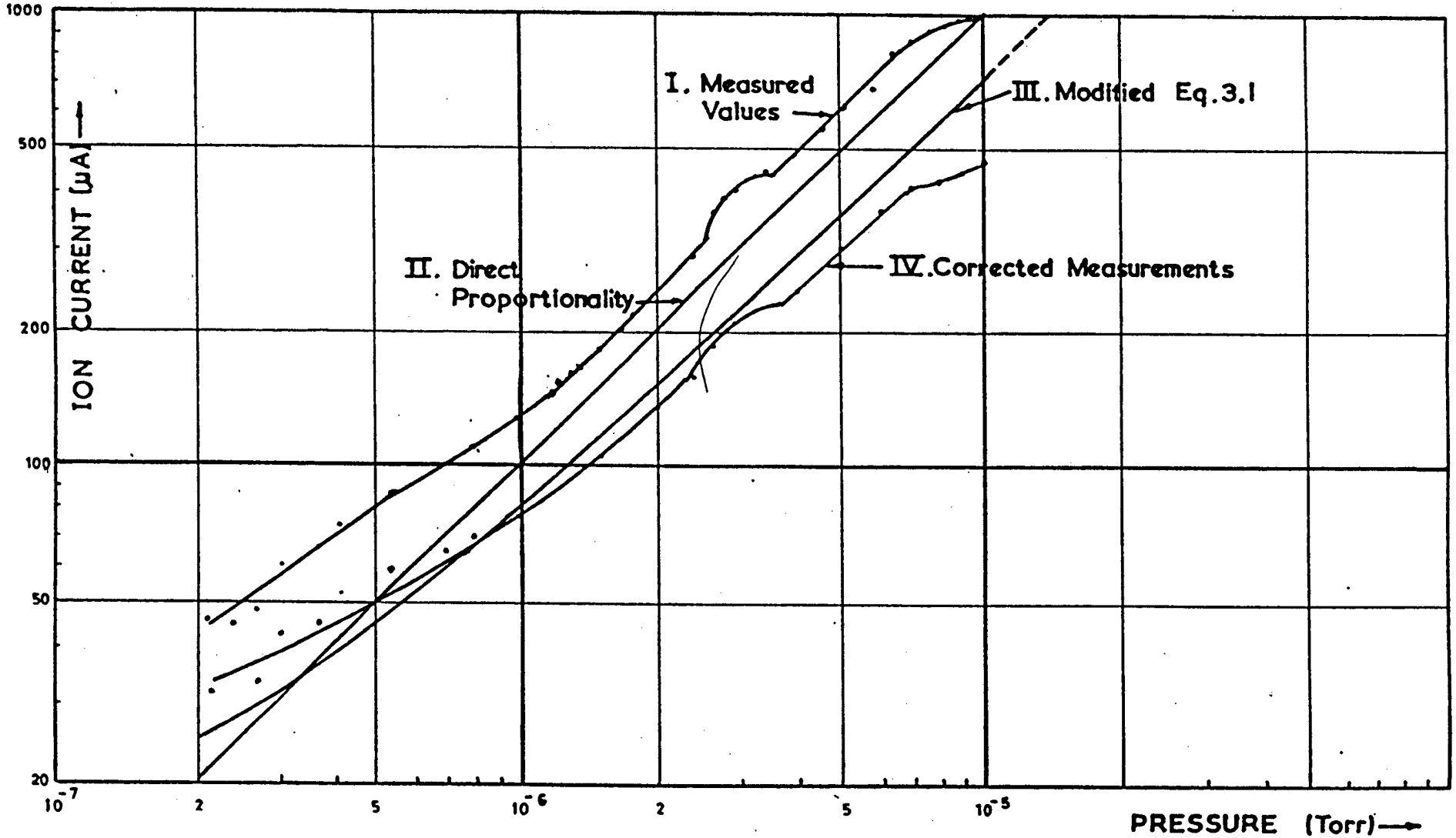

FIG. 27 ION CURRENT vs. PRESSURE

Faraday cage collector as the residual gas pressure was varied between 2×10^{-7} and 1×10^{-5} Torr. Although the pressure could have been reduced below the lower limit by continued pumping and heating of various valve parts, the increasing rise times which were observed as the pressure was reduced indicated that pulse lengths too great for the power supplies in use would be necessary to obtain stabilisation to the full ion current. Attempts to further reduce the pressure were therefore not made. Although the minimum pressure used in these experiments may thus perhaps be considered to be higher than that attained in many modern valves this size, it is felt that the results obtained apply with equal validity to a much lower pressure environment.

The data presented in Curve I was obtained by using an equal sample delay at all pressures so that the ion current relates to the same beam conditions, which are 14.5 KV and 3.2 Amps. The pulse started at 17.5 KV, as mentioned above. Curve I shows the ion current draining to the cathode to be proportional to the residual gas pressure, as would be expected from Equation 3.1. Three portions of the curve are of interest.

At pressures above 7×10^{-6} Torr the rate of increase of ion current with increasing pressure lessens until at 10^{-5} Torr, further increases in pressure do not cause a further increase in ion current. It is at this pressure that oscillations in the ion current are also seen. These phenomena can be associated with an increase in the ion production rate to the point that space charge neutralisation of the beam starts to take place and all the ions being created are no longer draining to the cathode, but rather being lost to the walls of the valve. Observations of the beam current intercepting various drift tube sections also shows this oscillation, as will be discussed later in the chapter in greater detail.

Between 2.5 and 3.5 x 10^{-6} Torr, a 'kink' may also be seen in Curve I. To assure that random experimental errors had not caused this irregularity, a recorder was used and the pressure was repeatedly plotted along with the ion current, and the 'kink' was found to be very repeatable. It is suspected that this kink has to do with variations in the focussing of the ion stream on the Faraday cage entrance which occur as the beam approaches neutralisation, but it was not possible to make measurements which could confirm or disprove this hypothesis. Total neutralisation does not occur until a pressure of 3 to 4 times as great is reached.

Comparison of Curve I with the slope of Curve II, which has a slope of direct proportionality between current and pressure, reveals that at pressures below 8 x 10^{-7} Torr there is again a departure from the proportional relationship. This is similar to the findings of Hines, et al (24) although their ion currents and pressure ranges are much different than those in use here. What is observed in the data of Figure 27 is that drops in the residual gas pressure as measured at the ionisation gauge do not cause proportional drops in the ion current at pressures below 1 x 10^{-6} Torr, although the ion current does continue to decrease as the pressure is dropped. Two possible explanations for this behavior are that 1) the change in the amount of partial ion neutralisation of the beam space charge depression which accompanies the lowering of the ion flow to the cathode has an effect of defocussing the ions from their collection at the Faraday cage; and 2) the ionisation gauge is not giving an accurate reading of pressure in the drift tube. The first explanation does not seem very reasonable in view of the normal behavior of the ion current in the pressure range directly above 1 x 10^{-6} Torr. The small ion current flow at these low pressures would be expected to have little effect on beam potentials in the area near the cathode. The finite conductance for gases of the drift tube,

however, suggests that the second explanation may be correct. Because of the impossibility of measuring the pressure at both ends of the drift tube, it is not possible to make a definite conclusion concerning this explanation. However, the available data is used to make a calculation, and this estimation is fully discussed in Appendix III.

From the results of Appendix III, one is led to conclude that there is a pressure differential of about 3×10^{-7} Torr along the length of the drift tube. The new information concerning this differential is then used to calculate the ion current predicted by a modified form of Equation 3.1. The results of this calculation are shown in Curve III in Figure 27, and it would seem that this pressure differential adequately explains the departure of the ion current measurements from a linear relationship with pressure at the lowest pressures.

Curve III represents the application of Equation 3.1 to the drift tube problem, and it is immediately observed that the measured values of ion current are 65-75% greater than the theory would predict. This is especially surprising since it is known that not all of the ions being created in the valve are draining to the cathode, as evidenced by the corona ring around the cathode hole. A value smaller than predicted by the theory would be expected because of that evidence.

4.1.2. Faraday Cage Effects

This large difference between the theory and the experimental data encouraged a close examination of the accuracy of the Faraday cage as a particle collector. Errors which arise in the current measured in the Faraday cage lead might arise due either to a loss of the original ions or loss of secondary electrons which are formed when the ions hit the cage material. Since a secondary electron leaving the cage would be measured as an ion arriving, it is important that the secondaries which are known to be generated when a high velocity ion hits the cage are kept within it. The number generated depends on the incident atom

species and velocity, and the angle of incidence. Although no researches on the bombardment of stainless steel by CO, O_2, and N_2 are known, from published data on single atoms (35) one might expect about three secondary electrons emitted per incident 17.5 KV ion. These are emitted with very low velocity, usually less than 5 ev. Higher numbers might be emitted from gas covered surfaces, but the high temperature of the Faraday cage would indicate that the surface is fairly clean, and certainly has no more than a monolayer. Part of the reason for the large number of electrons emitted is that a diatomic molecule behaves as two single atoms, each with half the energy of the original molecule.

If these secondaries are not prevented from escaping, a serious over-estimation of the ion current would occur. Ideally, a grid placed around the Faraday cage and appropriately biased would supress these secondaries. However, the very tight fit which the present Faraday cage makes excludes any such schemes at this one. The cone shape of the inside and the re-entrant mouth and grid are used instead of this shield. The grid in particular is very successful in acting to not only prevent fringing fields from draining ions or electrons out, but also acts as an electron trap in the same way as ion traps within the beam function. However, in order to determine as nearly as possible the number of electrons which were leaving the Faraday cage and therefore being incorrectly measured as ion current,measurements were made of the Faraday Cage characteristics. Ideally, it would be desirable to observe any changes in the measured ion current which take place as the bias on the Faraday cage is varied over a positive and negative range. Original goals of suppressing any ion escape from the cage led to a negative bias being applied, and it was found that positive biases did in fact mask the ion current, due to electron flows not related to the ion current at all. The details of these problems are now discussed,

and a method which allowed comparison of measured ion current with positive and negative biases explained.

Figure 28 indicates the measurements made of the pulse current flowing with a small (7 μamp) ion current actually hitting the cage. It is observed that the true current is reported for most of the negative bias, but that a great rise in current in the direction of positive ion current is seen when the Faraday Cage is positively biassed. The reason for this rise, which is in the opposite direction to what would be expected for positive biasing, is that when positive bias is applied, a large DC current due to electron flowing to the Faraday cage from the cathode is observed. When the pulse is applied for the beam current, the electric fields change in such a way that a large number of these electrons are drawn into the beam. Since an electron leaving the Faraday cage is measured as an ion arriving, it is clear that on an AC basis, this phenomenon will cause large currents in the direction of positive ion current to be measured.

But it is on an AC basis that the Rogowski belt measures the current which passes through it, and this means that there is no DC bassline which makes effects such as this one stand out clearly. DC meters were attached to the battery bias at high potential, and used to observe such DC currents as were present, but of course could not respond well at all to the pulsed signals, which have duty cycles no greater than .01 at low PRF's.

This large pulse with positive bias masks any ion current, and makes straightforward measurements of ion current with positive bias impossible. The negative bias measurements are very different, and the ion current measured is not a function of bias at all for biases greater than about -3 volts. The only currents flowing in this case are those due to electrons being emitted from the Faraday cage surface, and various leakage currents on the ceramics, which are all DC currents and thus not part of

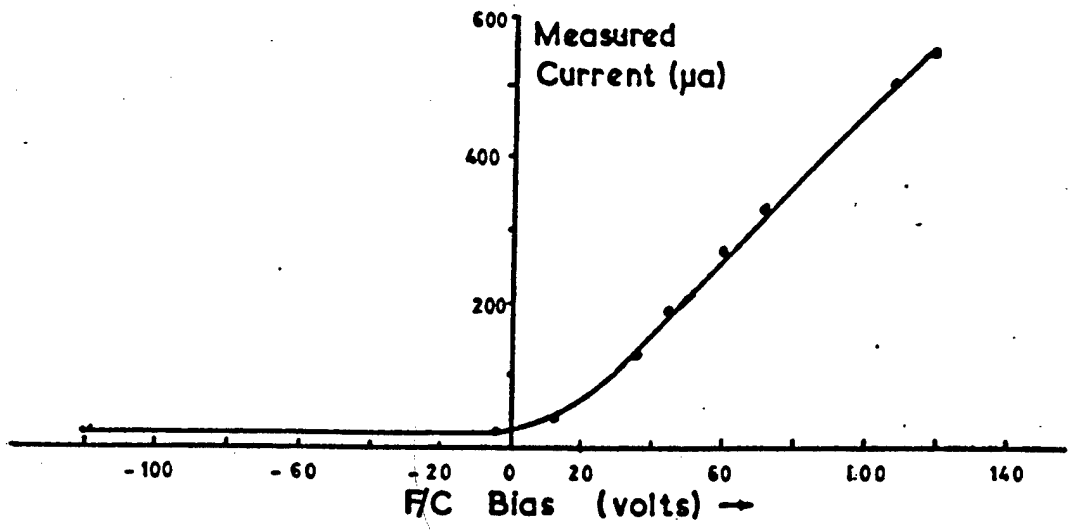

FIG.28 MEASURED CURRENT WITH A 7μa ION CURRENT

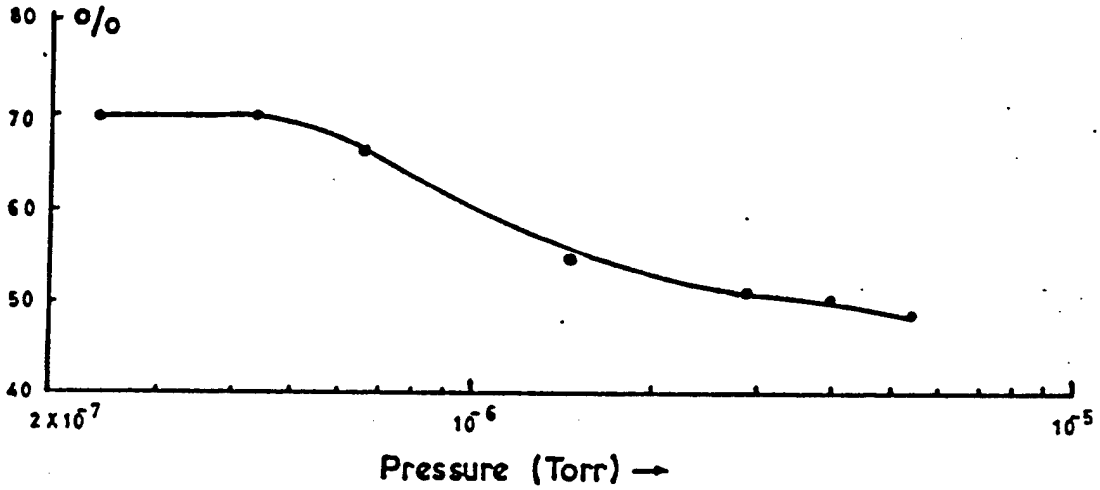

FIG.29 CORRECTION FACTOR vs. PRESSURE

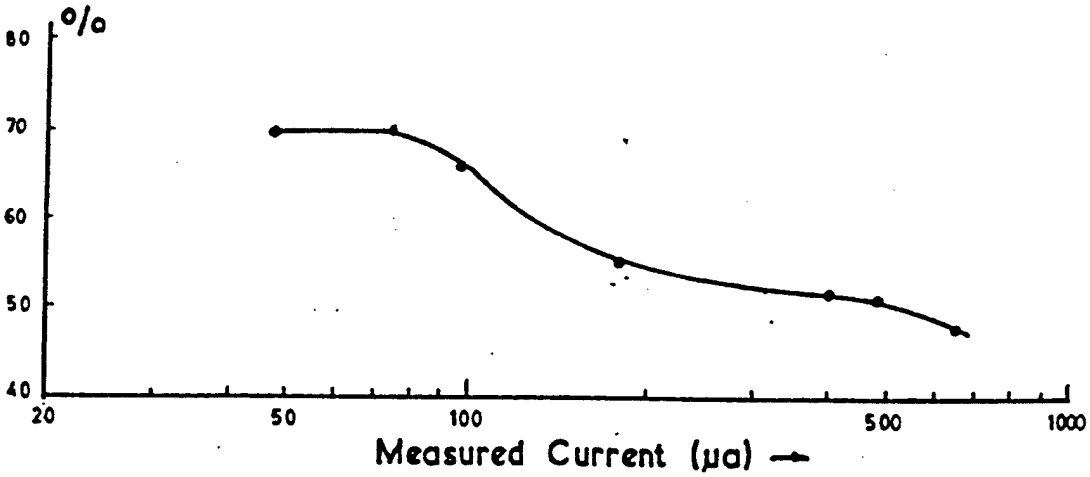

FIG.30 CORRECTION FACTOR vs ION CURRENT

the belt measurements. The advantages of using a pulsed measurement technique are obvious in this context. When the first Faraday cage was removed along with the first gun change, an inspection of it showed a white coating inside and out, which appeared to be BaO, as it was much the same colour as the cathode. From this, at least some DC current with negative bias would be expected. The Faraday cage used in the second gun was located much further behind the cathode to reduce this deposit, but a second examination of the Faraday cage has not taken place.

To determine the differences between ion current measurements with positive and negative bias, a technique of pulsing Drift Tube Section No.1. positively to cut off ion current in the middle of a pulse was used. Details of this technique are discussed in Chapter 5, and it will suffice to say here that the positive pulsing of the drift tube allowed the ion current coming from all but the near end of the valve to be shut off while the beam remained on. Thus the bias could be varied and differences taken between measurements with the ion current on and off. This allowed determination of the effects of bias on ion current. This method suffers only from the problem that taking small differences in large currents is difficult to do with great accuracy. Results indicated that the ion current dropped from its level with negative bias very sharply as positive bias was applied, to a level which remained roughly constant with increasing positive bias, the positive bias being varied over the range from zero to 120 volts. The value to which the ion current dropped can be expressed as a percentage of the negative bias levels. It was found that this percentage was a function of pressure, or alternatively, the total ion current (Figure 29). Two interpretations may be placed upon this behaviour: that the positive bias was causing ions to rebound out of the Faraday cage and escape; or that the positive bias was preventing secondary electrons from escaping and thus providing a more accurate measurement of ion current.

Definitive experiments which could resolve this problem are not possible because of the limitations imposed by the experimental equipment, but the information would seem to give the strongest support for the second hypothesis. There are two reasons for this. The first is the great number of electrons which are to be expected from ion-metal collisions, as mentioned above. The second relates to the pressure dependence of this percentage correction. Calculations show that the space charge potential elevation along the axis due to ions is on the order of a few volts for the level of currents present in this system. While this would have little effect behind the mesh, it would seem that a drain for electrons exists inside the Faraday cage on the drift-tube-side of the mesh (Figure 5) due to this potential elevation. This would increase as the ion current increases, and thus lead to greater errors in the case of larger ion currents. The change in percentage correction with pressure in Figure 29 can thus be explained. The mesh is not so fine that some fringing fields from this source would not exist, and the flatness with voltage of the ion current measurements with both positive and negative varying bias would indicate that fringing fields from external sources have little effect.

The correction curve found in the above experimental data may now be applied to the data reported in Figure 27, and Curve IV depicts the resultant corrected readings of the ion current. Comparison with Curve III, which used a modified form of equation 3.1 to predict ion current, shows that except at pressures below 10^{-6} Torr, the corrected ion current measurement lies below the theoretical line, by about 15%. At the lowest pressures Curve IV does exceed the theoretical prediction, and this may be due either to enhanced collection efficiency, or, as demonstrated in Appendix III, an underestimation of the amount of pressure differential which is present along the drift tube. It should be repeated at this point that Curve IV represents a correction made

to the original data which is based only upon certain assumptions which due to the limited space available in the valve construction, it was not possible to verify. The correction only represents one explanation which might partly explain the difference between the theoretical prediction of Equation 3.1 and the much larger amount of ion current actually measured.

A further consideration which would increase the amount of ion current predicted would be to take into account the electron path lengths travelled within the collector. Although the collector is re-entrant with an area ratio of 5:1 the potential gradients would make it reasonable to suspect that a fairly large number of the ions formed might escape down the drift tube and be collected at the Faraday cage. The path lengths of individual electrons would vary in length because of the expansion of the electron beam after it exits from the collector pole piece, but it would seem reasonable to assume that an additional length of the 20 cm would account for a large part of the additional current which the collector adds to the theoretical solution discussed in Appendix III. This would mean a 20% increase in the effective drift tube length, and thus a 20% increase in the solution shown in Curve III. This is shown in Figure 58 in Chapter 6.

The most important unknown concerning the accuracy of the measured data representing the ion drainage to the cathode is the ratio of the total ion current to that which is collected in the Faraday cage. As mentioned in Chapter I, damage in valves with long operating times consists of a darkened corona of about 1" diameter surrounding the central cathode hole. If it is assumed that ions are roughly equally distributed as a function of radius when they hit the cathode, then the percentage of the total ion current which is collected would be proportional to the ratio of areas of the collection hole to the darkened area, in which case it would be calculated that the true ion

current is approximately 6 times as great as that measured. Calculations of the trajectories of ions in the type of electric lens through which they pass after leaving the drift tube indicates that they would be diverging, but the amount of divergence requires knowledge of their initial axial velocities, which are not known. Although computer calculations were made of the trajectories which might be expected in the case of ions with zero initial radial velocity and a few hundred volts of longitudinal velocity entering the cathode region, the lack of sound knowledge of the initial conditions led to the abandonment of further work. The calculations made showed that a certain amount of focusing into the Faraday cage did take place for ions with initial velocities as indicated above. However, it was found that the use of drift tube biasing could provide information about the efficiency of collection of the Faraday cage. Since the technique involved requires some understanding of the experimental work which was done with drift tube biasing and furthermore the quantitative accuracy of the ion current measurement is not required for any work discussed in the remainder of this chapter, the results of these later measurements are discussed in Chapter 5. The work of this section indicates that a correction factor should be applied to ion current measurements to account for the Faraday cage release of secondary electrons. Further correction factors will be due to the collection efficiency of the 3/8" hole, rather than the cage itself. In conclusion, when the added length for the collector is assumed in the theoretical calculation, it is found that the Faraday cage corrected figures for measured ion current cannot be more than about 30% below the values predicted by Equation 3.1. The collection efficiency must be added to this figure.

4.1.3. Ion Current Dependence on the Magnetic Field

Because of the importance of the magnetic field in beam focusing, it was thought that the ion drainage to the cathode might be very

dependent upon the magnetic field. Because of the heavy mass of the ions, magnetic focusing effects are negligible for the ions themselves, but changes in the electron beam shape might in turn produce electric fields which would affect the ions. To evaluate the effect of magnetic field on the ion drainage, the solenoid supply was varied about the normal value of 9 Amps.

In measurements of the ion current at a pressure of 1.9×10^{-6} Torr, no change in either the steady state value or the shape of the ion drainage current response could be measured as the solenoid current was varied between 6.5.A and 12 A. At solenoid currents below 6.5A a very large change in the pulse shape took place, and gas pressure was observed to rise. It was concluded that the lowered magnetic field was allowing a large body interception to bombard the drift tube sections, and experiments were not continued below this field value. The ion drainage current was thus shown to have a great deal of insensitivity to the magnetic focusing field.

4.1.4. Ion Current Dependence on Beam Voltage and Current

Equation 3.1 shows a dependence of the ion current upon the beam current, and his dependence was next investigated. Because the ionisation coefficient depends upon the beam voltage, and the beam current of course is related to the beam voltage by $I = pV^{3/2}$ for space-charge-limited flow, it was not easy to separate the two effects. Three types of experiment were performed:

1) The beam current was varied by simply varying the applied beam voltage and comparison of experiment and theory is made by taking into account the dependence of ionisation coefficient on beam voltage (Figure 19).

2) The heater voltage was slowly raised from just below its normal level and raised to well above it. This resulted in a significant variation in beam current only to the extent that the gun was operating with an emission limit, which was particularly the case for the experiments

performed on the first gun. The problem with this method is that it provides a very limited range of current which it can produce. The variation of pressure with rising gun temperature made this a difficult experiment to perform.

3) The modulating anode (Figure 4) could be biased to reduce the current from the gun without affecting the electron velocity within the drift tube, if the cathode were kept at normal voltage. This was the best way to vary the beam current without changing anything else that affects ion formation. But it suffers from the disadvantage that at the same time as the current is varied by this method, a variable electric lens is created, which could affect the results both by causing defocusing of the ion current on the Faraday cage entrance and by increasing the body interception currents. Greater body interception would result in local bombardment and subsequent outgassing, which might lead to a greater ion current.

Figure 31 shows three of the results recorded by use of the first of these methods. Figures 31a and 31b show data recorded on the first gun at two different stages in the slowly increasing re-activation of its cathode. Both depict data recorded during cathode voltage variations between 4 and 18 KV in the first case and 4 and 16 KV in the second, and in both cases the recorded cathode voltage was used to determine the ionisation coefficient for the curve which shows the values predicted from Equation 3.1. In addition to these two curves, the correction factor determined for the Faraday cage and illustrated in Figure 30 has been applied to the experimental results to generate a third curve which represents the corrected ion current* Contrasting this corrected

* The use of this correction factor is certainly valid in the case of measurements made at high beam voltages near to those in which the correction factor was determined. Its application to data gathered at the much lower beam voltages in use here may need comment. It is known that the number of secondary electrons which are generated by an impacting

curve and the theoretical curve, it is observed that the measured data has a positive slope with respect to beam current, whereas the slope predicted by the theory is either negative or zero in the range of beam currents of interest. One possible explanation for this behaviour is that the reduced space charge fields at low beam currents cause the Faraday cage collection efficiency to be less as the beam current drops.

The data collected with the second gun and normal emission does not show this difference between the corrected measurement curve and the theoretical curve. Good agreement between the theory and experiment is shown in Figure 31c, for all but the highest beam currents. But, of course, because of the inefficiency in collection which was mentioned in the previous section of this chapter, this indicates that actual ion current is greater than that predicted by the theory over this range of measurement. The data presented in Figure 31c was taken at voltages between 3.2 and 15 KV.

Figure 32 illustrates the data obtained by use of the last two techniques, heater variation and anode biasing. Figure 32a shows the results of beam current variation over the range of 1.9 to 2.4 A, and was performed at beam voltage which was fixed at 15.5 KV. Three curves are again shown: the experimental data, the experimental data adjusted according to Figure 30 and the prediction made by Equation 3.1. Because no variation of the beam voltage takes place during the experiment, the theoretical prediction is a straight line. In contrast to the results shown in Figure 31, both the measured and corrected data are greater than the theory would predict over the entire range of the experiment.

ion is a function of the ion energy, and drops as the ion energy drops However, from the explanation which has been offered above for the existence of a correction factor, it is believed that the correction factor is most strongly a function of the ion current, not of the ion energy. For this reason, it is thought that it can be applied to these problems.

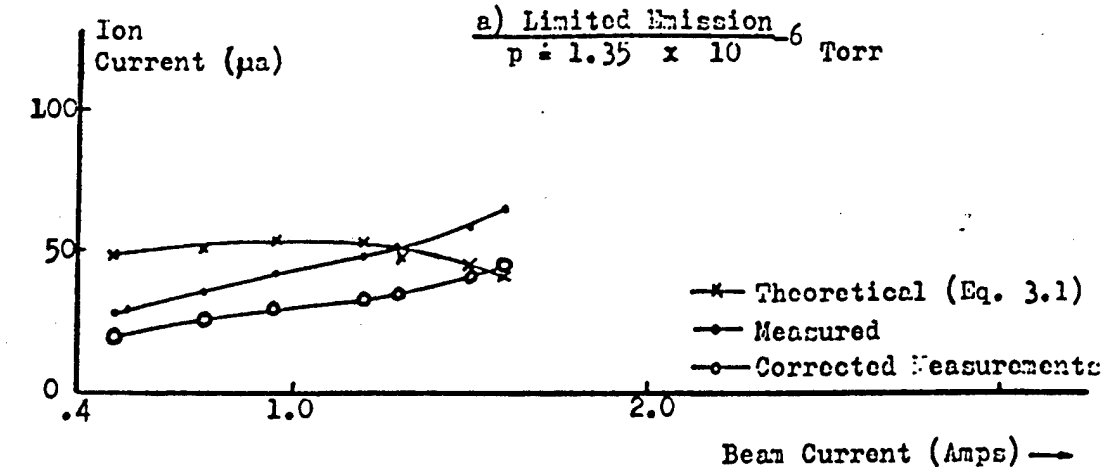

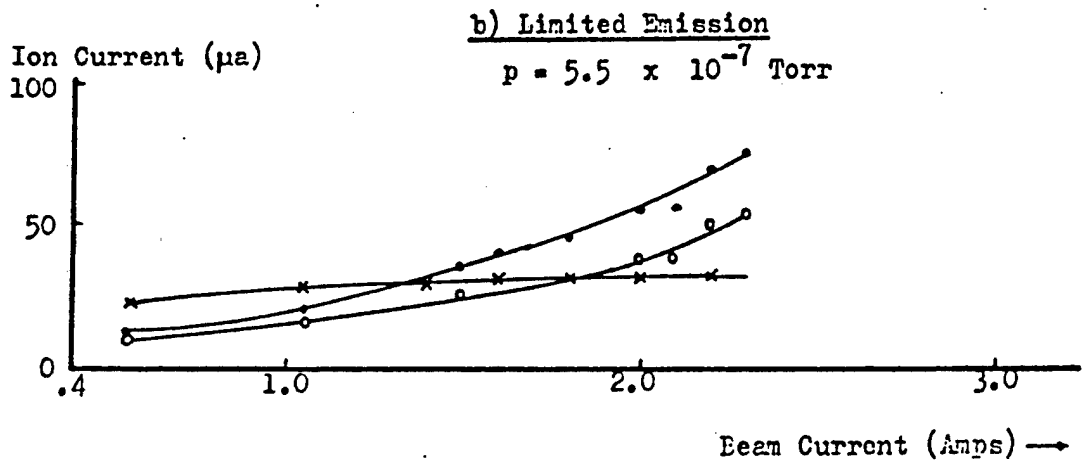

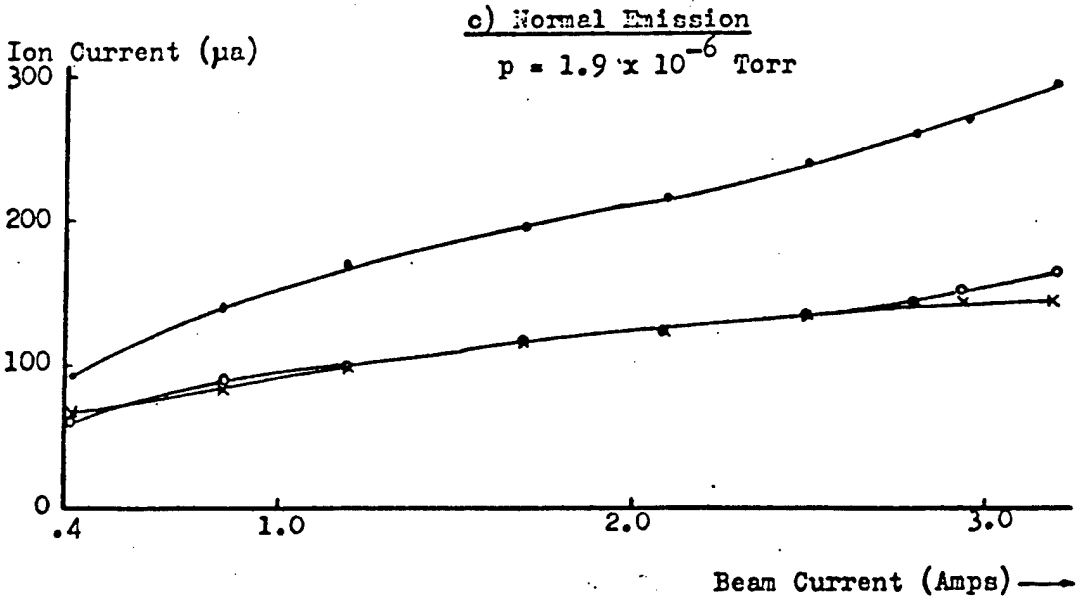

FIG. 31 ION CURRENT vs. BEAM CURRENT (METHOD I)

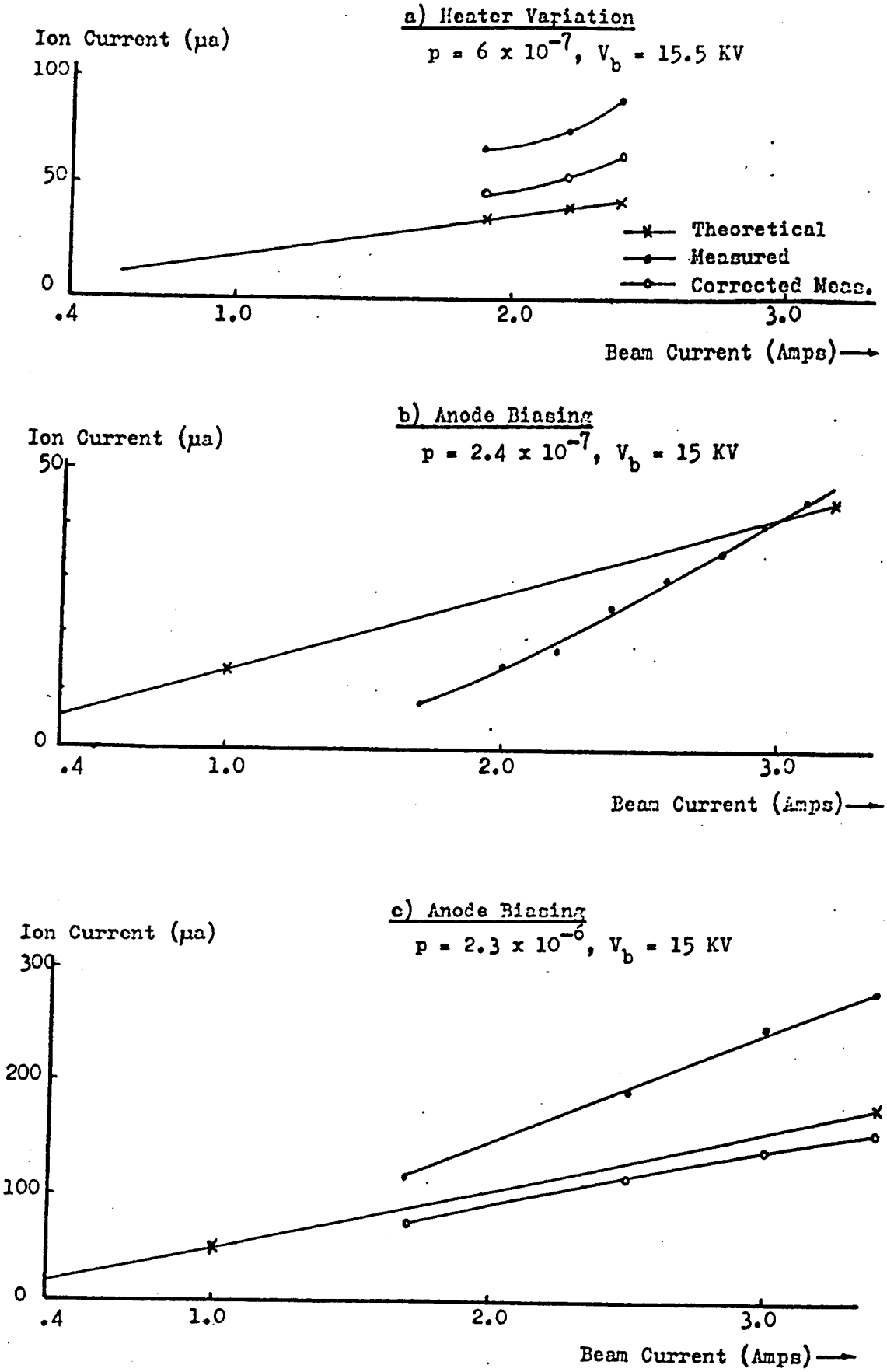

FIG. 32 ION CURRENT vs BEAM CURRENT (METHODS 2&3)

It is believed that this may represent an inaccuracy in the pressure measurements made on the ion pump current before the ion gauge was attached.

Figure 32b and 32c show the results of using the modulating anode to vary the beam current while at the same time maintaining the normal operating voltage between the drift tube and the cathode, and thus the same ionisation coefficients during varying beam currents. The first of the experiments described in these figures was performed at a very low pressure, 2.4×10^{-7} Torr, and a very poor agreement between theory and experiment was seen, particularly in that even the slope of the measured-data-curve does not agree with theory, but rather is greater than predicted. This characteristic is in agreement with the trend evidenced by experiments with the first two methods, that there is always a more positive slope for the experimental ion current vs. Beam current curve as compared to the theoretical curve. The experiment of Figure 32b was repeated at a higher pressure, 2.3×10^{-6} Torr, and the results shown in Figure 32c indicate that the experiment results in data which is very comparable to that which the theory predicts. The difference in the results at two different pressures for the same experiment suggests that the focusing effects caused by the electron lens created in this method may in fact cause changes in the ion collection and generation mechanisms.

The general conclusion which may be drawn from this series of experiments is that the rate of increase of ion current with beam current tends to be larger than that predicted in Equation 3.2, especially in the case of larger beam currents. Although the measured values tend to be fairly close to those which are predicted in magnitude, this is not so important since the collection efficiency of the Faraday cage is less than 100%, and when a correction is made for efficiency, the values will be farther apart. The greater slope of the measured data would be

an indication that the large beam currents which are encountered in high power valves may well cause a greater amount of ion current than would be expected from the simple approximation of Equation 3.1, although beam focussing effects which might decrease collection efficiency at lower beam currents cannot be ruled out as an explanation of these results.

4.2 Build-up Time to the Steady State

Thus far only the steady state values of the ion current drainage to the cathode have been discussed. A steady state value was possible to define because the behaviour of the ion current response to beam current pulses was such that a plateau of ion current was reached, as in Figure 26. Observations of ion current drainage under varying pressure and beam current indicated that the build-up time to this plateau was changed by these, and other, factors. One of the advantages of using a pulsed technique is that this build-up time may be observed and used to make further conclusions about the processes of ion formation and drainage. The length of the ion build-up time is important in two applications. Firstly it is of interest in the operation of pulsed valves, which for short pulse lengths may be unaffected by residual gas ions. Secondly, observations of this ion current build-up may be used to evaluate the applicability of the ion traps suggested by Hartnagel (2,22) to this valve.

Experiments were performed over a wide range of pressure with normal beam conditions and the results of this work are reported in the first sub-section. The effects of varying the beam current are next considered, and in section 4.2.3, the results of build-up time measurements are combined with those of the ion current production rate to calculate the amount of charge remaining in the beam as a function of pressure, and these results are compared with the theory of Chapter 3.

4.2.1. Build-up Time Dependence on Pressure

Figures 33 and 34 show some of the data collected during experiments with a 14.5 KV, 3.2 A beam (these values occuring at 400 μsecs after the start of a pulse of 17.5 KV). The beam rise time of 5 μsecs and the Rogowski Belt rise time of 4 μsecs are both negligible in comparison to the observed rise times. The start of all pulses is marked by a negative drop which interrupts the base line. The drop is not a function of ion current at all, but rather is due to undesired Rogowski Belt pick-up, and thus is the same amptitude at all pressures. Fortunately, it dies out after 20 to 40 μsecs, and does not seriously interfere with any of the measurements. Neglecting this negative-going-transient, it is seen that the ion current at all pressures in the range measured is observed to rise gradually from zero, and the time taken to reach a plateau value is dependent upon the pressure. In no case does there seem to be any delay in the start of flow of ions to the cathode. The rise time is seen to decrease with increasing pressure.

Exactly determining the rise time to the plateau level is difficult due to what in most cases is a gradual transition between the increasing ion current and the steady state level. By defining the rise time as the time required between the start of the beam pulse and the time that the ion current reached 90% of its plateau value, a consistent way of reporting build-up time as a function of pressure is defined. The result of making this analysis on data shown in Figure 33 and 34, and on other data which was collected, is illustrated in Curve I of Figure 35.

Ion current responses in the pressure range between about 3.4 and 4.0×10^{-6} Torr, however, were different in shape from the results reported at other pressures, and this method could not be applied to them. Figure 34a and 34b illustrate the difficulty, and these sorts of wave shape were observable in all measurements made in this pressure range. At the lower pressure a peaking is observed before a plateau is

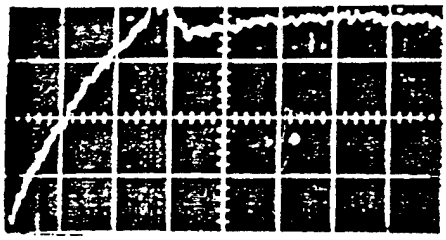

A) $p = 3.5 \times 10^{-6}$ TORR

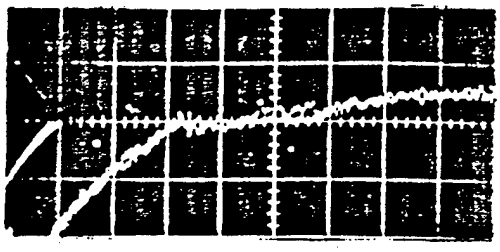

B) $p = 4.0 \times 10^{-6}$

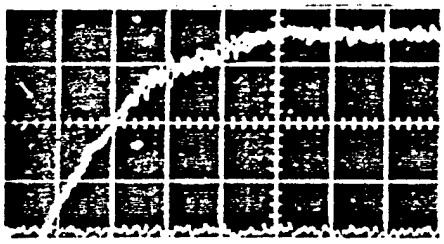

C) $p = 5.5 \times 10^{-6}$

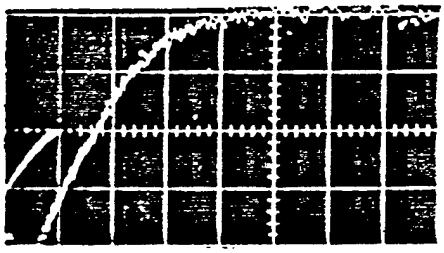

D) $p = 6.8 \times 10^{-6}$

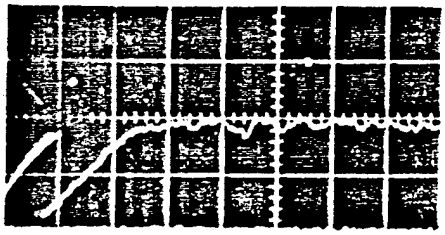

E) $p = 8.26 \times 10^{-6}$

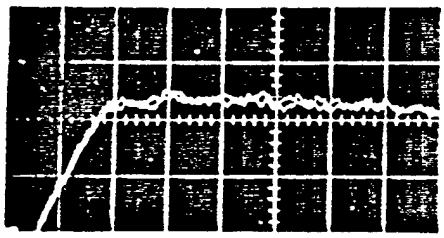

F) $p = 1.05 \times 10^{-5}$

Vertical Sensitivity

(a)	110 μa/div.	(d)	220 μa/div.
(b)	220 μa/div.	(e)	550 μa/div.
(c)	220 μa/div.	(f)	550 μa/div.

FIG. 34 ION CURRENT BUILD-UP TIME II

BEAM CURRENT: 3.2 A ; TIME SCALE: 40μS/DIV

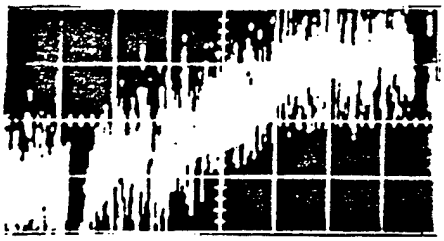

A) $p = 2.9 \times 10^{-7}$ TORR

100 μS/ DIV

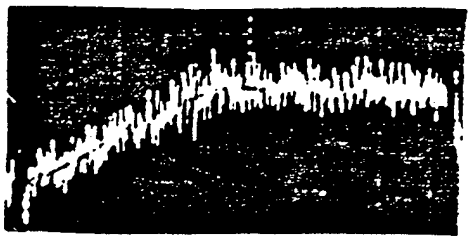

B) $p = 8 \times 10^{-7}$

100 μS / DIV

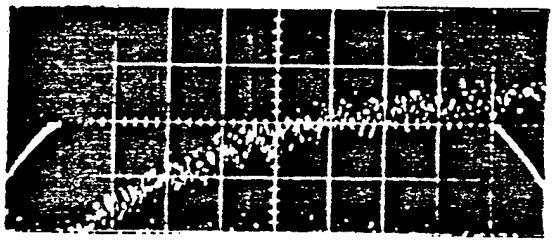

C) $p = 1.15 \times 10^{-6}$

40 μS/DIV

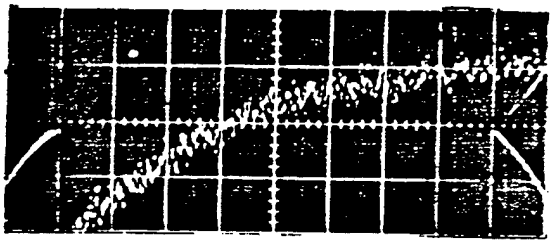

D) $p = 1.33 \times 10^{-6}$

40 μS/ DIV

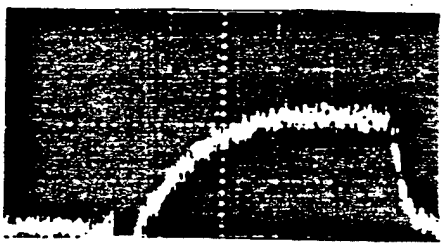

E) $p = 1.75 \times 10^{-6}$

100μS/ DIV

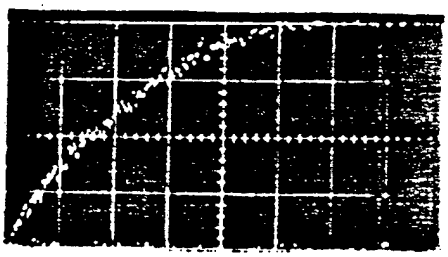

F) $p = 3.27 \times 10^{-6}$

40 μS/ DIV

Vertical Sensitivity

(a) 22 μa/div.
(b) 72 μa/div.
(c) 72 μa/div.
(d) 72 μa/div.
(e) 110 μa/div.
(f) 72 μa/div.

FIG. 33 ION CURRENT BUILD UP TIME

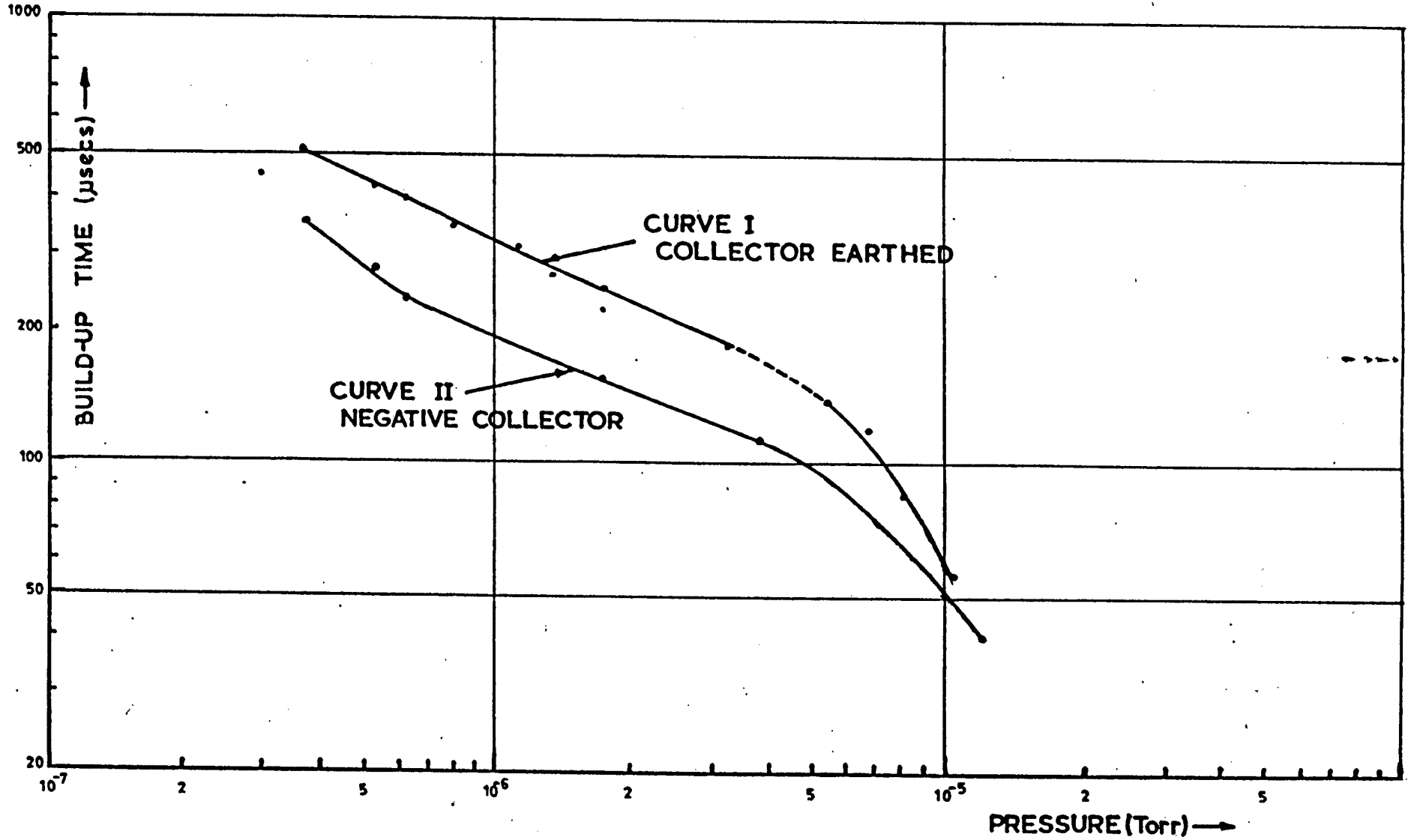

FIG. 35 ION CURRENT BUILD-UP TIME

reached, and in the example at the higher pressure, a two level plateau is observed. For this reason the curve showing rise time vs. pressure in Figure 35 is shown dashed in this region. This is roughly the same range of pressures at which the 'kink' in the curve of ion current vs. pressure (Figure 27)occurs, and this is further support for the suggestion that the beam is being neutralised enough at this pressure that unstable behaviour is present, and particular sensitivity to small changes in beam current may be present.

Curve I of Figure 35 indicates that the rise time of the ion current decreases with increasing pressure, as would be expdoted, and more particularly decreases inversely with the square root of the pressure in the range between 3×10^{-7} Torr and 5×10^{-6} Torr. At pressures higher than 5×10^{-6} Torr, a much more rapid decrease of build-up time with pressure is observed, but it is known that in this region the ion space charge has already started to neutralise large amounts of the negative space charge of the beam,as can be seen in Figure 27. It would seem to most likely be the case that the loss of some ion drainage to the cathode means that it requires less time to build-up to a steady state involving less ion drainage. The rise time measurements were not made above 10^{-5} Torr, at which pressure the ion current oscillates. The measurements made with a depressed collector are discussed in Section 5.2.2.4.

4.2.2. Build-up Time at Lowered Beam Currents

The beam current was lowered by biasing the modulating anode, as discussed in Section 4.1.4, and measurements of the rise time were made at pressures between $2\text{-}7 \times 10^{-6}$ Torr. These measurements were made at currents between 1 Amp and 4 Amps, and in no case was a significant change in the rise time observed. Due to the greatly reduced beam currents, it was particularly difficult to make accurate comparisons, however,

4.2.3 Charge Storage in the Beam

The theory which is discussed in Chapter 3 indicates that there is a significant amount of ionic charge storage even in a smooth beam. Further charge storage may be expected in real beams due to the existence of scallops which cause potential wells in the drift tube. These wells would trap ions with insufficient longitudinal velocity to escape them. Measurements of the rise time of the ion drainage current may be used to estimate the amount of ionic charge storage in the beam, as shall now be demonstrated.

Figure 36 depicts a typical ion current flow during a beam current pulse.

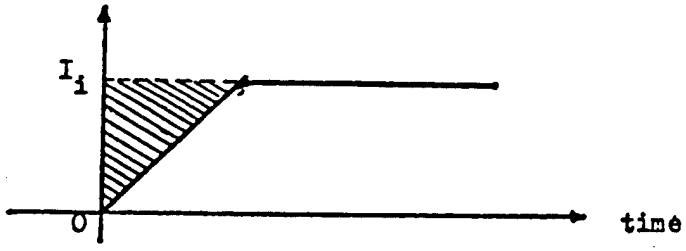

Figure 36 Integral of Ionic Charge in the Beam

If it is assumed that the ion production rate remains constant with time from the start of the beam pulse, then it may be concluded that the shaded area in Figure 36 represents the amount of charge still remaining in the beam. Mathematically, the total ionic charge remaining in the beam, Q_i, is given:

$$Q_i = \int I_i(\text{steady state}) - I_i(t)\, dt \qquad 4.1$$

This integral may be estimated with a fair degree of accuracy by using the values of corrected steady state ion current shown in Figure 27 and the values of build-up time in Curve I of Figure 35. The integral is approximately equal to half the product of these two numbers. What would seem to be more accurate graphical methods were shown not to be very repeatable due to ambiguities concerning the start of the steady state as discussed in Section 4.2.1. The results of the simple computation are

shown in Figure 37, as Curve I. There are three distinct portions to this curve: a section between 3×10^{-7} and 8×10^{-7} Torr, where it is relatively flat; a section at pressures between 8×10^{-7} and 7×10^{-6} Torr in which the total charge rises; and a region at the highest pressures in which the total charge decreases with increasing pressure. It must be remembered that these results include the charge storage in the collector as well as the drift tube. The measurement of the charge storage in the drift tube only can be accomplished by preventing any flow of ions from the collector to the cathode, and this measurement is discussed in Section 5.2.2.4. It shall be shown that the collector charge storage is large indeed. Furthermore, the calculations on which Curve I is based utilise only the measured ion current, and take no account of the ion current lost due to less than 100% efficiency in collection. Thus they will be lower than the actual value of charge storage. The shape characteristics of the curve, however, are of significance.

Equation 3.30 may be used to calculate the charge storage within the drift tube. Since the beginning of the beam pulse is the most important part of the pulse for these measurements, beam voltage and current which relate to the first 150 to 350 μsecs will be used in the calculation of the rate of ion formation, rather than the values at 400 μsecs, which are used for calculations relating to the steady state. In fact this change makes only a very small difference. The values of the coefficients used in Equation 3.30 for this calculation are: $G_i = 81.6$ p; $l_D = .8825$ meters; ion mass = 30; and $K = 8.509 \times 10^9$, which relates to a 0.4" beam radius. Equation 3.30 then predicts that

$$Q_i = 8.145 \times 10^{-5}\ p \quad \text{coul.} \qquad 8.1 \times 10^{-5}\ p^{2/3}$$

where p is in Torr. This calculation is shown in Figure 37 as Curve II. Curve II stops when it reaches the value of total ionic charge that equals the total negative charge, Qe, which is calculated by multiplying

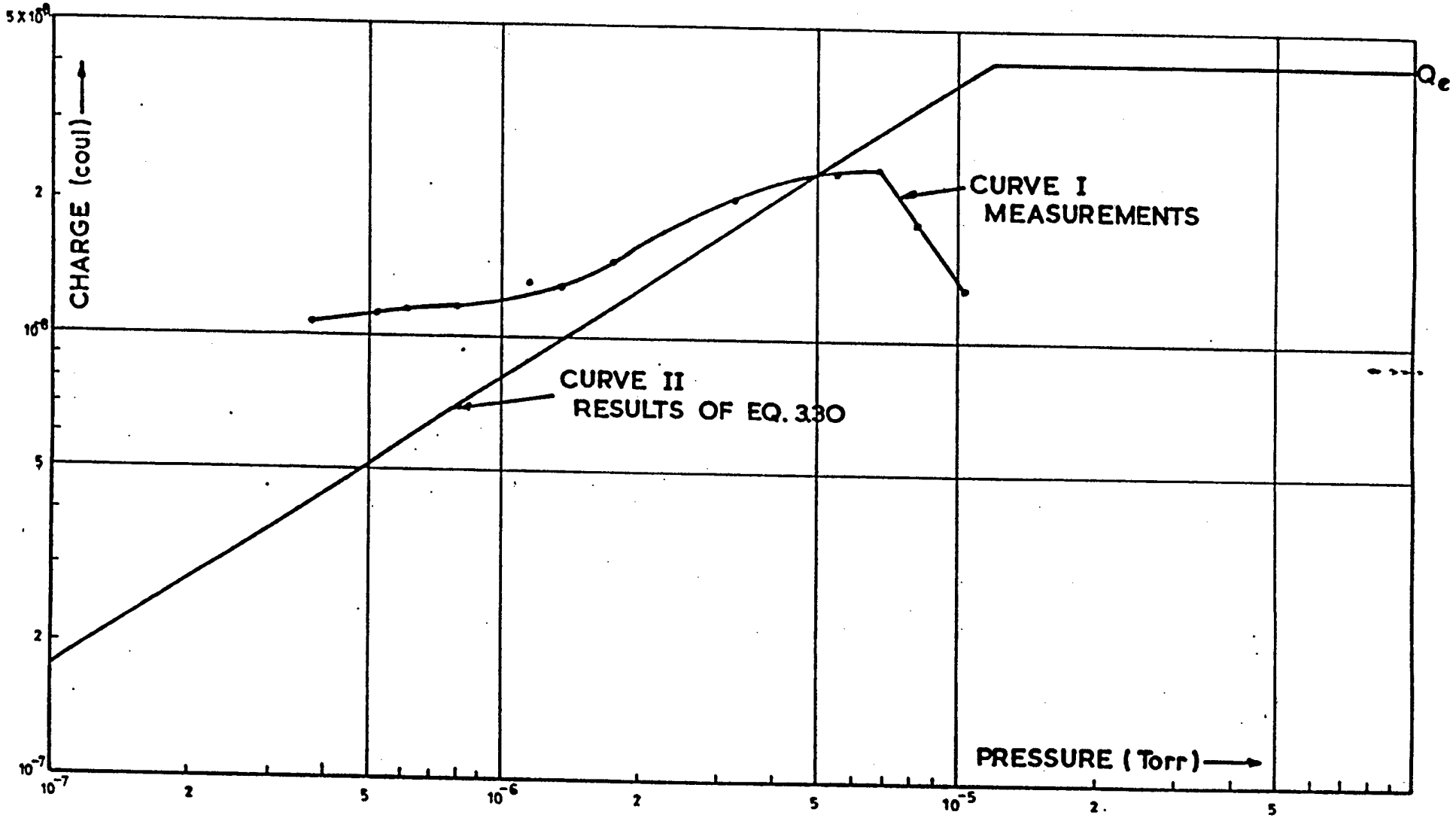

FIG. 37 TOTAL IONIC CHARGE STORAGE

the negative linear charge density of Equation 3.31 by the drift tube length. For the beam current at the beginning of the pulse this value is 4.19×10^{-8} coul. The curve of measured values of the total charge has the same shape as that which the theory predicts only in the middle section of Curve I. At the highest pressures the integral is suspect because the negative charge has become sufficiently neutralised to allow some ions to escape the beam potential depression, and thus impair collection efficiency. This would explain the measured drop in the integral. At the lowest pressures the total ionic space charge is seen to attain a minimum value which is 1.1×10^{-8} coul and therefore amounts to 28% of the electron beam total charge. This large storage of ionic space charge within the beam may be attributed to the flow of ions into the potential wells created by scalloping. A similar effect was found by Hines, et al (24) in their low power valve. Calculations as to whether this seems to be a reasonable figure cannot be made because of the unknown changes to beam size and shape which may occur due to this charge storage, and due to lack of knowledge concerning collector storage. From the knowledge which is available concerning the beam in the K 376 valve, potential wells as deep as 200-300 volts along the axis may be predicted in the absence of these residual gas ions. From this data it must be concluded that the charge storage in the beam will continue to have a significant influence on the beam potentials within the tube even as the pressure is reduced to the best vacuums. In the case of this particular valve, the reduction of pressure below about 7×10^{-7} Torr has little effect in changing the amount of charge stored within the beam (in usage with CW or very long pulses).

4.3. Oscillation in the Ion Drainage Current

As was mentioned in Section 4.1.1, the slope of the curve of ion current vs. pressure (Figure 27) shows a decrease below the expected linear slope. As the residual gas pressure is increased about 1×10^{-5}

Torr, oscillations in the ion drainage to the cathode are observable throughout the length of the ion current pulse. This section deals with a discussion of the observations of these oscillations as the pressure, collector bias, and beam current were varied. Oscillations of this sort have been observed in previous experiments (1), but the use of only the collector current as a measurement device meant a lack of sensitivity. The ion cyclotron oscillations reported by many past researchers would not be observed in the cathode drainage since the Rogowski belt has a rise time of 4 μsecs.

4.3.1. Oscillations during Low Beam Current Measurements

Oscillation phenomena were observed in experiments with the first gun, which had a lower emissivity than normal and thus provided lower beam currents at normal operating voltages. Because of the lack of an ion gauge for pressure measurements during these first experiments, and the necessity of turning off the ion pump in order to make the pressure rise to levels at which oscillations occured, the gas pressure could not be very accurately determined and only an abbreviated account of the experiments performed is mentioned here. Figure 38 (located in Section 5.2.2.) illustrates oscillation occuring at a pressure of about $9.\times 10^{-6}$ Torr, and oscillations are of the greatest amplitude at the end of the pulse, occuring at a frequency of approximately 40 KHz. Further increase in the pressure increases the frequency of oscillation to 70 KHz. The increase in pressure also leads first to oscillation throughout the entire length of the pulse and then to oscillations at the beginning of the pulse only. A further increase in the pressure causes the oscillation to stop. Measurement problems prevented determination of the pressure at which this occurs, but the cessation in oscillations did not prevent an ion current from flowing to the Faraday cage. The drop which occurs during the pulse is due both the loading of the pulsed power supply for the valve, and the use of a Rogowski

Belt with a faster decay than was used in later experiments.

4.3.2. Oscillations during Normal Beam Current Measurements

After installation of the second gun, measurements at normal beam currents could be made, and the pressure accurately controlled and measured. It was found that the behaviour with the normal beam current was somewhat similar to that observed at the low beam currents, but more careful observation showed that small oscillations occured at pressures as low as $3.\times 10^{-6}$ Torr. These oscillations were always associated with ion current responses which demonstrated a peaking of the ion current at the beginning of the pulse, as in Figure 34a. Furthermore, they were not stable oscillations of the sort seen in Figure 38, nor did they occupy as large a percentage of the total ion current. They appear instead as instabilities in the ion current level after the steady state plateau has been reached during the pulse, and amount to 5-6% of the ion current plateau level in peak amplitude. The frequency of these instabilities ranged between 33 KHz and 8 KHz.

As the pressure is increased these instabilities cease to be present, vanishing at a pressure of about 4×10^{-6} Torr, and would seem to be related to the unexpected phenomena discussed in Section 4.2.1 in relation to Figures 34a and b. At higher pressures, oscillations are first seen at the end of the pulse, as was observed in the low beam current observations. This may be seen in Figure 39a and 39b. During these experiments the valve was pulsed with an applied beam pulse starting at 17.5 KV and drooping as in Figure 12. This results in a current droop from 4.05 A at the beginning of the pulse to 3.0 A at the end of the pulse, which is 630 μsecs long.

The first sign of an oscillation is seen under these conditions at a pressure of 7.5×10^{-6} Torr. A definite oscillation pattern is discernable at a pressure of 8×10^{-6} Torr, as in Figure 39b, with a period of 58 μsecs, which corresponds to a frequency of 17KHz. This

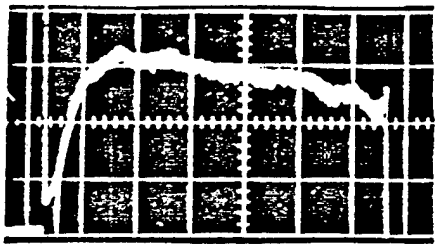

a) $p = 7.5 \times 10^{-6}$

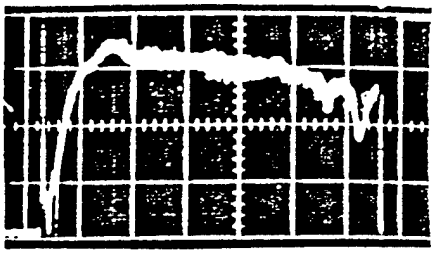

b) $p = 8.0 \times 10^{-6}$

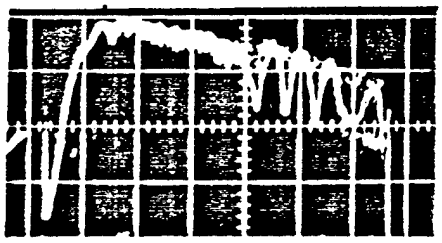

c) $p = 9.3 \times 10^{-6}$

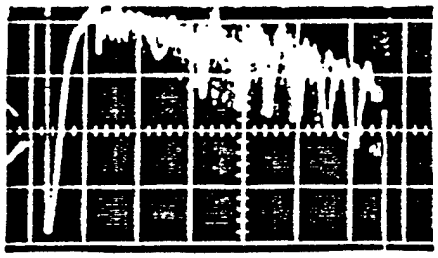

d) $p = 1.15 \times 10^{-5}$

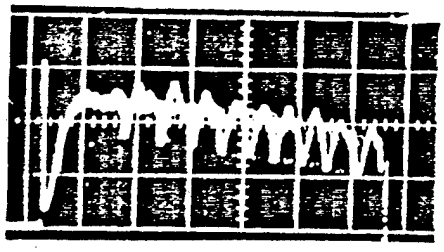

e) $p = 1.2 \times 10^{-5}$

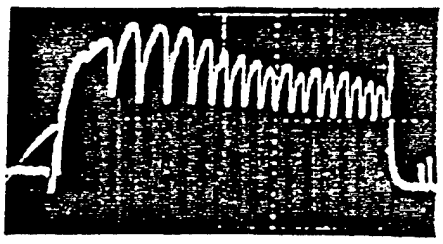

f) $p = 1.3 \times 10^{-5}$

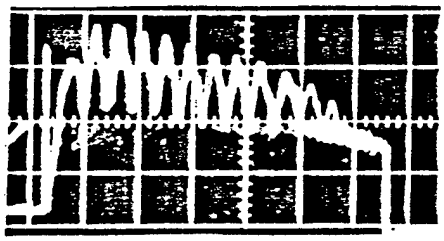

g) $p = 1.47 \times 10^{-5}$

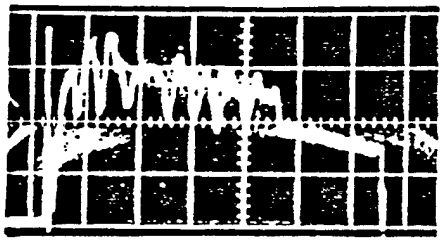

h) $p = 1.6 \times 10^{-5}$

FIG.39 ION CURRENT OSCILLATIONS
NORMAL BEAM CURRENT
COLLECTOR EARTHED
HORIZ.: 100μsec/div
VERT.: a-d 220 μa/div
e-h 550

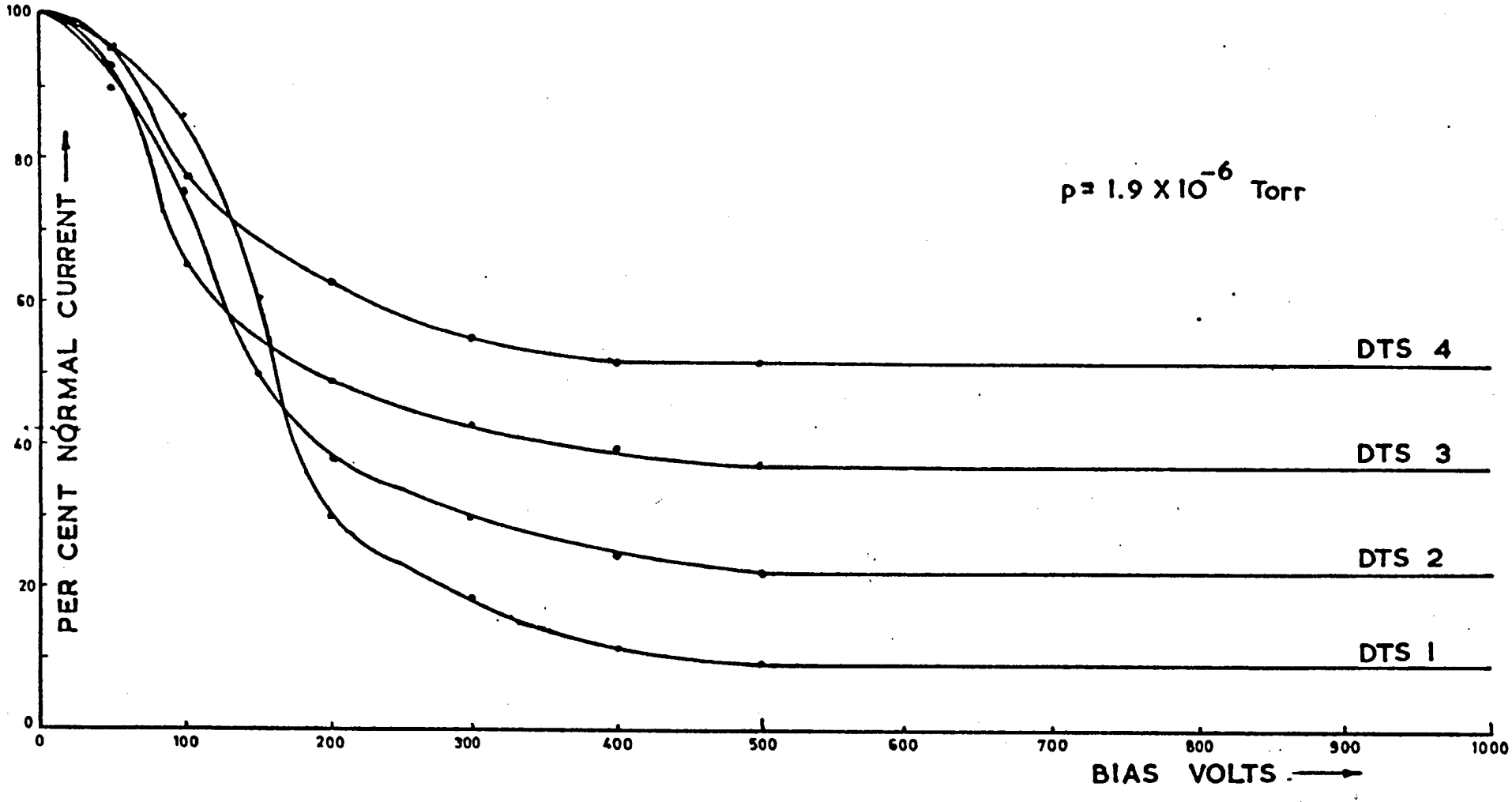

FIG. 55 ION CURRENT vs POSITIVE BIAS ON DTS 1–4

contrasts with the 52 KHz frequency in Figure 38, in which the current at the end of the pulse is 2.0 μa and the beam voltage is 16.5 KV. As the pressure increases to 9.3×10^{-6} oscillations are visible for a greater portion of the pulse (Figure 39c) and are of increasing frequency with smaller delay from the beginning of the pulse, with periods ranging between 66 μsecs and 50 μsecs. These large oscillations have an amplitude of about 130 μa peak, which corresponds to about 25% of the average ion current pulse height at the end of the pulse where they occur. Simultaneously to these larger scale oscillations at the end of the pulse, a smaller amplitude oscillation with a frequency of about 50 KHz and amplitude of 35 μa, or about 4% of the pulse amplitude, occurs between the beginning of the pulse and the point where the lower frequency oscillations begin. The transition between the two is abrupt. As the pressure is further increased, more and more of the pulse shows these large scale oscillations, and Figure 39d shows the ion current at 1.15×10^{-5} Torr. The higher frequency oscillations still exist at the beginning of the pulse and are of approximately the same frequency. The large scale oscillations have periods between 44 and 52 μsecs, with the trend to higher frequency with decreasing delay repeated.

As the pressure rises only a very small amount to 1.2×10^{-5} Torr, large oscillations are present throughout the length of the ion current pulse. They occur with periods ranging between 42 and 58 μsecs, with the highest frequencies(23 KHz)occuring at the centre of the pulse and lower frequencies, 17 KHz, at either end. The oscillations have a peak amplitude of 300 μa, which is again about 25% of the peak amplitude of the ion current. Figure 39e illustrates this condition, and Figure 39 f shows the same type of oscillations from a different course of experiments in which the beam current was somewhat higher. As the pressure is increased still further, oscillations continue throughout the length

of the pulse, and then start to vanish at the end of the pulse. This may be seen in Figure 39g. This photograph was made at 1.47×10^{-5} Torr, and the oscillations which are still present have periods between 42 and 48 usecs, with the usual trend of increasing frequency with decreasing rise time being present. The data collected thus indicates oscillations between 24 KHz and 21 KHz. No significant oscillations seem to be present in the last 100 μsecs of the pulse. Figure 39h shows the ion current at 1.6×10^{-5} Torr. At this pressure the last 200 μsecs of this 600 μsec pulse exhibit no oscillation, although there are oscillations between 20 and 25 KHz during the first part of the ion current pulse. It would not have been possible to further increase the pressure during these experiments without heating the walls of the valve, and thus the pressure did not rise so far as to cause oscillations to cease throughout the length of the pulse. However, it is believed that this would have occurred in these conditions of full beam current if the pressure had been high enough. In experiments with the first gun, the pressure would go higher than in the second case, and the cessation of oscillations throughout the entire length of the pulse was observed.

During the experiments in which oscillations were visible throughout the entire length of the pulse, at pressures of 1.2 to 1.3×10^{-5} Torr, the collector current was simultaneously monitored, and oscillations of amplitude 2 ma and less were observed. Since this represents only 1.05% of the collector current, in contrast to ion current measurements showing peak oscillation currents which were 25% of the average pulsed ion current, the difference in sensitivites of the two methods which was mentioned earlier is easily seen to be very significant.

At the same time as observations of the beam current were being made to look for oscillatory effects, the difference in beam current between the low and high pressure conditions was measured. These measurements were not able to produce a very accurate value because

of variations in the beam current due to mains regulation during the long time required to vary the pressure between the two conditions, but an increase of 250 to 300 ma was observed between low and high pressures. This would, of course, be due to partial space charge neutralisation caused by the increased flow of ions to the cathode during high pressure operation.

4.3.3. Oscillations with a Negative Collector

By biasing the collector negative, it is possible to produce a potential gradient which can drain some ions from the collector end of the drift tube. Since a gradient still exists at the cathode end, ions may also drain in that direction, and from the approximate symmetry of the situation, it would be expected that ions would drain from the half of the drift tube in which they were formed. Experiments approximately prove that this suggestion is correct (See Section 5.2.2.). Since the onset of oscillations is presumably connected with the increase of σ_i, the ionic linear charge density, until it reaches the point at which it equals the electronic charge density, any factor which reduces the ionic charge density should cause the onset of oscillation to be delayed until a higher pressure is reached. Since, from Equation 3.23, the ionic density of proportional to $l_D^{4/3}$, reducing the effective length of the drift tube by one half should cause a decrease in the ionic charge density by a factor of .63. In fact, if the same ratio of σ_i/σ_e is necessary for oscillation in both cases, the pressure at which oscillation starts with a negative collector should be twice that at which it starts with a normal bias arrangement.

To perform this experiment a large bias, -900 volts, was applied to the collector. It is shown in Chapter 5 that collector biases this large create drainage patterns which are fairly stable and not dependent on small changes in the bias. Figure 40 illustrates the results of these experiments.

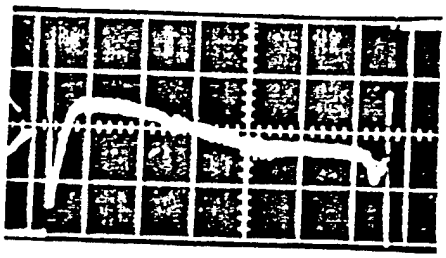

a) $p = 1.23 \times 10^{-5}$

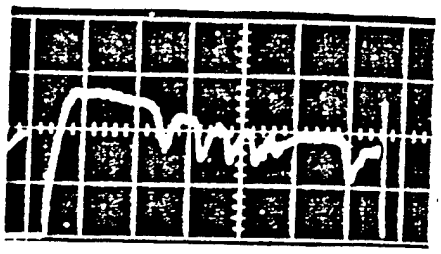

b) $p = 1.3 \times 10^{-5}$

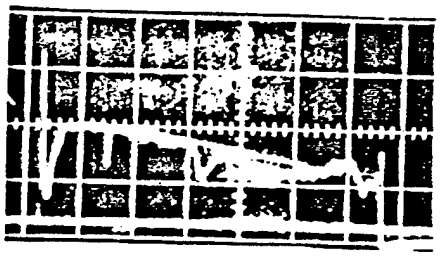

c) $p = 1.6 \times 10^{-5}$

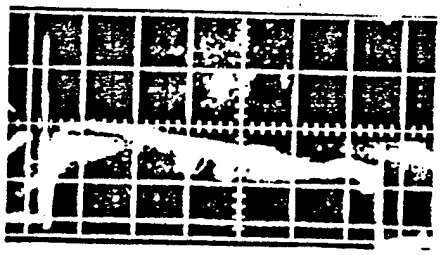

d) $p = 1.6 \times 10^{-5}$

FIG.40 ION CURRENT OSCILLATIONS, NEGATIVE COLL.
COLLECTOR VOLTS: a-c, -900 ; d, -700
HORIZ.: 100 μsec/div VERT.: 220 μa/div

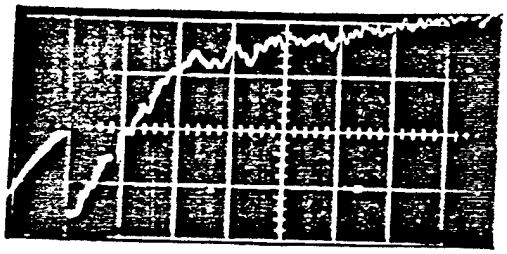

a) $I_b = 4$ A

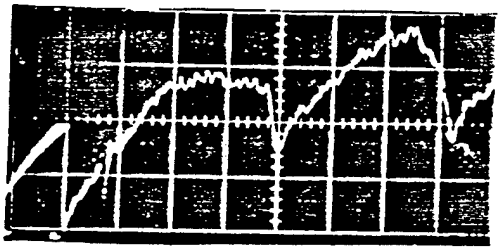

b) $I_b = 3$ A

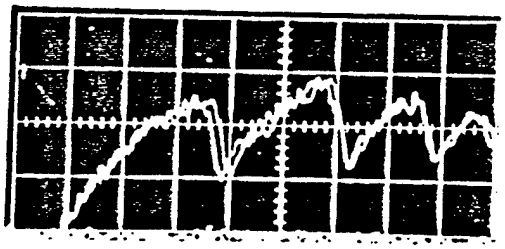

c) $I_b = 2$ A

FIG.41 ION OSCILLATION AT VARIOUS BEAM CURRENTS
HORIZ.: 20 μsec/div VERT.: 220 μa/div
Pressure: 7×10^{-6} Torr

Oscillations observed at pressures below 1.23×10^{-5} Torr with the collector earthed, vanished when the high negative bias was applied. As Figure 40a shows, oscillation with a negative collector first appears at this pressure. The 50 KHz oscillations observable in Figure 39c are also absent. Since the first oscillations with the collector earthed were observed at a pressure of 7.5×10^{-6}, the prediction of Equation 3.23 is not too far wrong in predicting the onset of these oscillations.

As the pressure is increased, large oscillations of the type seen under normal beam conditions appear, but the conditions for these oscillations seem to be far more critical than in the case of normal beam conditions. Figure 40b illustrates the oscillations occuring over a restricted portion of the pulse. The periods involved again are in the neighbourhood of 50 μsecs, which is the same as those present under earthed-collector conditions. When the pressure was increased to the maximum attainable, oscillations over small portions of the pulses continued to be present, but no pattern of oscillation throughout the pulse was observed. At 1.6×10^{-5} Torr, small oscillations at a frequency of about 60 KHz appear, as shown in Figure 40c, along with a single cycle of large scale oscillation at the centre of the pulse. The sensitivity of this oscillation to external conditions may be seen in Figure 40d, which shows the result of reducing the collector bias to -700 volts. From experiments which are described in Chapter 5, this is a surprising result since the change in ion flow between these two voltages could not be measured. The identical oscillation frequencies for depressed and normal operation also indicate that explanations for the oscillation frequency must not depend on the ion transit time between the collector and the cathode.

4.3.4 Oscillation at Different Beam Currents

The modulating anode was used to reduce the beam current as in Section 4.1.4, and the ion current was measured at the pressure of

7×10^{-6} Torr. With full beam current, in this case 4 A, measured 100 μsecs after the start of the pulse, there is no oscillation of the ion current, as was indicated in Figure 39. Figure 41a depicts the start of this pulse. However, when the beam current is reduced to 3 A, oscillations throughout the length of the pulse appear with a period of 64 μsecs, corresponding to a frequency of 15.6 KHz, as is shown in Figure 41 b. When the beam current is further reduced, to 2 A, oscillations with a period of about 40 μsecs appear, which corresponds to a frequency of 25 KHz, as is shown in Figure 41 c.

These observations may be used as a qualitative demonstration of some characteristics of the ion drainage which are predicted by the theory presented in Section 3.4. Since it can be assumed that oscillation will take place at or near the point when the positive and negative space charge within the beam are equal, the ratio σ_i/σ_e is clearly of interest in predicting the start of oscillation. Equations 3.30 and 3.31 may be used to calculate this ratio, and since G_i is proportional to the beam current, it is clear that at a constant pressure σ_i will be proportional to $I_b^{\frac{2}{3}}$, wheras σ_e is directly proportional to I_b. Thus as the beam current drops the ratio will rise, making neutralisation and oscillation possible at lower pressures when the beam current is lowered. This is exactly what is observed in the photographs of Figure 41.

4.3.5 Summary

From the data which was discussed above, the following conclusions can be reached about the ion drainage current oscillations which were observed at high pressures:

1) At pressures as low as 3×10^{-6} oscillations, or at least instabilities, in the ion current drainage are observed, with frequency content in the range between 8-33KHz. These oscillations are of such small amplitude that it is thought they would not have been measured

in experiments which only used the collector current as a method of investigation.

2) These oscillations cease above 4×10^{-6} Torr until at a pressure of 7.5×10^{-6} Torr, oscillations of the ion current which have peak amplitudes which are 25 % and more of the ion current appear. These first appear at the end of the long experimental pulse which was used, and with increasing pressure oscillation along the entire length of the pulse is observed. It is believed because of the experiments with oscillation at varying beam currents, that these oscillations occur first at the end of the pulse because of the lower beam current which is present there due to power supply voltage droop. Experiments with varying beam currents showed that the threshold pressure for the onset of these large oscillations decreased with decreasing beam current.

3) Further increases of pressure showed that the oscillations cease as the pressure was increased sufficiently, and that thus only a narrow 'window' of the correct beam current and pressure conditions exists for these oscillations. The frequency of oscillation rises as the beam current falls.

4) The oscillations appear to be some sort of relaxation oscillation, although in some cases the sudden drop in the ion current does not have a time constant very much shorter than that for the build-up time. Furthermore, these oscillations seem to have a constant amplitude throughout the pulse in spite of the differing beam current during the pulse. On the average they have a peak value which is only 25% of the ion current plateau level, and thus do not represent total collapses of the process of ion drainage to the cathode, but rather interfere with only a small part of the total current. The frequencies which were measured were between 15 KHz and 30 KHz.

5) With the collector biased highly negative, a cessation of

oscillations at pressures below 1.23×10^{-5} Torr was observed. Oscillations which finally were observed seemed to have a very narrow 'window' of necessary conditions, and oscillation throughout the entire length of the pulse was not observed. The oscillations which were observed had frequencies approximately the same as for the case in which drainage along the entire drift tube was used. This would indicate that whatever process is responsible for establishing these oscillations, it does not seem to depend on the length. A high sensitivity to the value of collector bias was observed, which was not shown in any other experiment which was performed with negative collector bias above 600 volts.

The mechanism for these oscillations could not be decided upon from these experiments. However, further information is obtained for this investigation in the experiments with body interception current.

4.4 Body Interception Current

Because of the construction of this valve it is possible not only to monitor the current to the body, but in fact to each drift tube separately. This was done by measuring the voltage across small resistors. In addition to showing the slower variations of the interception during the beam pulse, these interception currents could also be used to observe the high frequency oscillations mentioned in Chapter 1. These frequencies were well above the response time of the Rogowski belt.

The interception current of any drift tube section will be likely to be dependent on the beam current and voltage in a very complicated way. Therefore, body current which has the same pulse shape as Figure 12, the beam voltage pulse shape, cannot be expected. In spite of this problem, which causes peculiar pulse shapes such as are seen in the upper traces of Figure 42 c and d it was found there were changes in the body current which could be related to ion phenomena, in

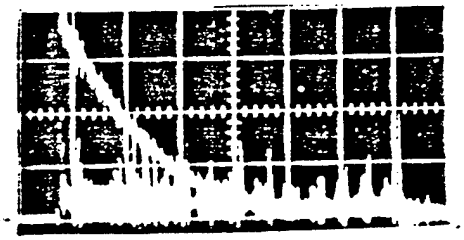

a) DTS 1, 2ma/div

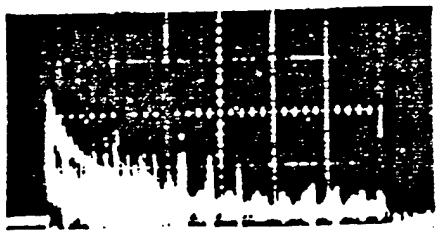

b) DTS 2, 10ma/div

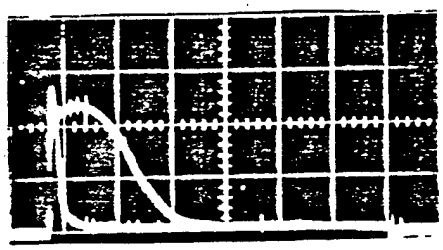

c) DTS 3, 20ma/div

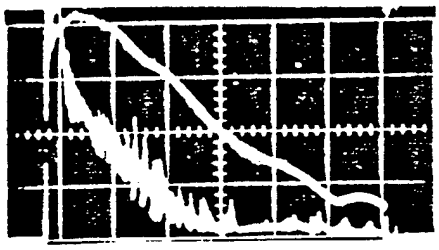

d) DTS 4, 20ma/div

FIG.42 DRIFT TUBE INTERCEPTION
UPPER TRACES: $p = 5 \times 10^{-7}$ Torr
LOWER TRACES: $p = 1.2 \times 10^{-5}$ Torr
HORIZ: 100 μsec/div

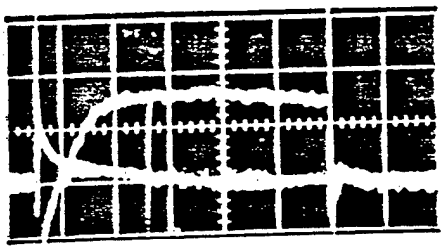

a) Upper: DTS 1, 5ma/div
Lower: I_i, 110μa/div

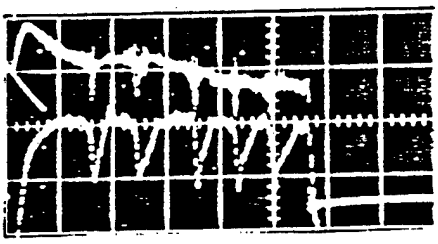

b) Upper: DTS 4, 2ma/div
Lower: I_i, 550μa/div

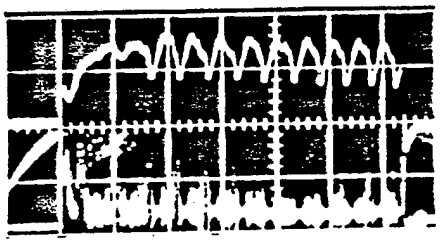

c) Upper: I_i, 1.1ma/div
Lower: DTS 1, 1ma/div

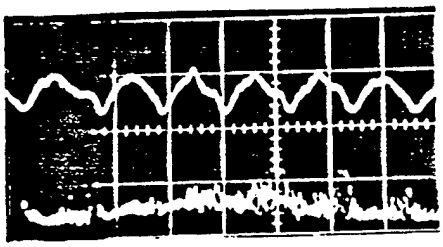

d) Upper: I_i, 1.1ma/div
Lower: DTS 4, 5ma/div

FIG.43 DRIFT TUBE CURRENT AND ION CURRENT
HORIZ: a-c 100μsec/div; d, 40μsec/div
Pressure: a, 1.8×10^{-6}; b-d, 1.1×10^{-5} Torr

particular the build-up time and oscillations. The drift tube sections referred here are numbered as those in Figure 4, 'DTS' again being the abbreviation for drift tube section.

Figure 42 depicts the interception currents of the four drift tube sections for long pulses at high and low pressures. DTS 5 is earthed due to a fault, and measurements with this section could not be made.

4.4.1 Body Current at High and Low Pressures

Data supplied with the valve indicates that the body interception should not exceed 150 ma. It is obvious from the photographs in Figure 42 that is is difficult to determine at what point the current should be measured to see if the specification is being met. The very beginning of each current response is the point closest to normal beam conditions, and if this value is taken on the upper traces of Figure 42 a sum of 141 ma is arrived at, with the current to DTS 5 not included. The upper traces of Figure 42 are data taken at 5×10^{-7} Torr, which would be near the pressure which might be reached in normal operation. No change in the levels of body interception was noticed in experiments when the pressure was reduced below this level.

From the data recorded in the lower traces of Figure 42, it is obvious that operation at high pressure has the effect of improving the focusing of the electron beam, as would be expected. Also visible in the lower traces are bursts of a high frequency oscillation, which are discussed in greater detail in the next section. But it is important to observe that the interception current to all drift tubes, and especially Nos. 1-3, is a decreasing function of time, and that this decrease occurs at different rates at high and low pressures. So in addition to some decrease which might be expected due to the decrease of beam current with time, there is a decrease with time constants which seem to be related to the time constants which are associated with the ion current drainage to the cathode. This is most

clearly seen in Figure 43 a, which compares simultaneous ion current and DTS 1 current at 1.8×10^{-6} Torr. Fall times on the order of 30 - 40 μsecs from initial conditions are seen in the lower traces of Figure 42 c and d, and this is the rise time which appears in ion current measurements at this pressure. From this it may be concluded that even at low pressures, the ions which remain in the beam have a considerable effect upon the beam focussing, and that in the case of pulsed valves may mean that stable operation during short pulses will be interfered with if the pulse lengths are comparable with the ion current build-up times for the beam and pressure range in question.

B-4

4.4.2 Drift Tube Interception and Ion Current Oscillations

It was found that the bursts of high frequency oscillation which were seen as part of the drift tube interception mentioned in the previous section had the same period as ion drainage current oscillations observed at the same pressures. This is most clearly seen in Figure 43 b, which depicts simultaneously the interception current on DTS 4 and the ion current measured at the cathode. A synchronism between the bursts of oscillation on the interception current and the relaxation-type of oscillation in the ion current may clearly be seen.

The interception current on the drift tubes alternates between a quiescent condition in which no oscillations are seen, and bursts of high frequency oscillation. These bursts have fairly sharply defined starts and finishes, and rise to a sharp peak of amplitude in the middle of the burst. Thus two characteristics may be defined for these bursts: burst length and the delay in time of the central maximum. In contrast, the characteristics which are best defined for the ion oscillation are the length of time required for the ion current to fall from its highest to lowest level, and the time delay at which this fall starts. It is assumed that the periods for both ion current and body current phenomena are the same. Attempts to measure the frequency

of the high frequency oscillation with the oscilloscope were not very accurate, and the oscillation is very random, and ranges between 1 and 2 MHz.

The ion current oscillations in Figure 43 b and 43 c are of quite different shape, 43 b having a fall time which is very short compared to the period of repetition. From a comparison of the two it is obvious that the burst length is proportional to the fall time, but not equal to it. In Figure 43 c the burst lengths are between 32 and 38 usecs, whereas the fall time is between 24 and 30 μsecs for the second half of the pulse. This is evidence that the oscillations in ion drainage occur at the same time as changes in the beam diameter.

DTS 1 and 4 were measured because it was thought that any phase difference between interception currents on each and the ion drainage oscillation might be of interest in examining the nature of the oscillation. It is clear from the photographs of Figure 43 c and d that no large difference exists, but measurements do indicate that the start of the high frequency oscillation burst on DTS 1 precedes the ion current peak value by 9 - 12 μsecs, whereas the burst of DTS 4 precedes it by only 6 μsecs. The peak value of the burst current appears in approximately the middle of the fall of the ion drainage current, and in both DTS 1 and DTS 4, the burst ends at approximately the same time as the ion current reaches its minimum. This data would indicate that the change in beam diameter occurs first at the gun end of the valve, and that the reduction in ion drainage current is only very slightly delayed from this broadening of the beam.

CHAPTER 5

EXPERIMENTAL RESULTS WITH DRIFT TUBE AND COLLECTOR BIAS

5.1 Introduction

Chapter 4 has indicated the experimental results which may be expected during measurement of the ion drainage with all valve electrodes at their normal electrical bias. However, these measurements were not able to supply such important information as the ion formation distribution, the ionic charge storage distribution, the efficiency of the Faraday cage collector, and information concerning the ion velocity distribution during drainage. In addition, because of the collector current generation and charge storage, it is not easy to apply the theories developed in Chapter 3. These problems can be alleviated by the use of electrode biasing.

The experimental work discussed in this chapter first covers experiments done with negati e and positive biases on the collector, and then covers experiments with bias applied to DTS 1 - 4. A number of interesting results which increase the range and accuracy of measurements made in Chapter 4 are discovered.

5.2 Experimental Results with Variable Collector Bias

The axial potential gradient which is to be expected in a valve with an earthed collector, the normal operating-condition for this valve, is shown in Figure 20b. The potential gradient at the collector end acts both to drain ions from the collector end and to provide a boundary which forces the ions generated in the drift tube to drain to the cathode. If the potential on the collector is reduced, the gradient will first drop to zero and then reverse itself. Thus, introducing a negative bias on the collector will cause two important changes in the ion drainage: reduction in the drainage to the cathode of collector-formed ions, and the creation of gradients which would allow ions to drain from both ends of the drift tube. This second change is of particular importance because it matches

the boundary conditions which are assumed for the theoretical treatment of ion drainage which was mentioned in Chapter 3.

The effect of negative collector bias on the observation of oscillations in the ion current was reported in Chapter 4. This section will deal with measurements made of the steady state ion current which flows with various amounts of positive and negative collector bias. The steady state current is determined by the same methods as were outlined in Chapter 4.

5.2.1 Positive Collector Bias

It is obvious from Figure 20 b that only small changes would be expected in the ion current drainage to the cathode if the bias present on the collector were to be raised. A drainage pattern is established with the collector at earth which positive bias on the collector would only tend to reinforce.

The collector was biassed positively from 0 to 300 volts by using a variable positive supply with large capacitors to maintain a fairly constant voltage during the pulses. Positive biases between 0 to 100 volts had the effect of reducing the ion current by about 5 %, and further increase appeared to have no further effect.

An increase in the ion current caused by positive bias on the collector would have suggested the possibility that not all the ions being created in the collector and drift tube were being drained to the cathode, but the above-mentioned results indicate that total drainage is being achieved. The small decrease in the ion current is not easily explained but is discussed further in Section 5.2.2.3.

5.2.2 Negative Collector Bias

A resistor box put in the collector lead of the klystron was used to obtain negative biases on the collector. This was used in preference to a continuously variable DC supply since the supply would have required very large capacitors, as it was required to work at voltages up to

1000 volts. The box was designed so that switching bias levels without turning off the valve was possible, which avoided problems of stabilisation after turn-on. The range of collector depression which was employed was not intended to be typical of the depressions which occur in valves which are biassed for efficiency improvement. It was chosen as the range which included the voltage at which further bias increases had no further effect upon the ion drainage.

Figure 44 shows the results of ion current measurement with negative collector bias at pressures between 2×10^{-7} and 5×10^{-6} Torr. All results are normalised to the collector-earthed value of ion current for the purpose of comparison. In each case a small negative bias has no effect upon the ion current flowing to the cathode. As the bias increases, an increase in the ion current is observed, generally on the order of 10 to 15 % above the zero-bias value. This increase changes to an abrupt decrease as the collector depression is further deepened, but the biases for the maximum and the start of the decrease vary with the pressure. As the negative bias is further increased, the ion current continues decreasing until a minimum value is gradually approached. Once this minimum has been reached, increasing bias has no effect in further reducing the ion current drainage. The relative values of ion current are approximately that same at all pressures.

Refering to Figure 20 b, the ion current drainage to the cathode would be expected to remain constant as long as the axial potential provided a gradient which directed all ions in the neighbourhood of the collector toward the cathode. This would be the case not only for an earthed collector, but for a collector with a bias which is less than the calculated potential depression of the beam due to net space charge. When the bias does exceed the potential depression, the gradient reverses and the axial potential is changed to one like that shown in Figure 45.

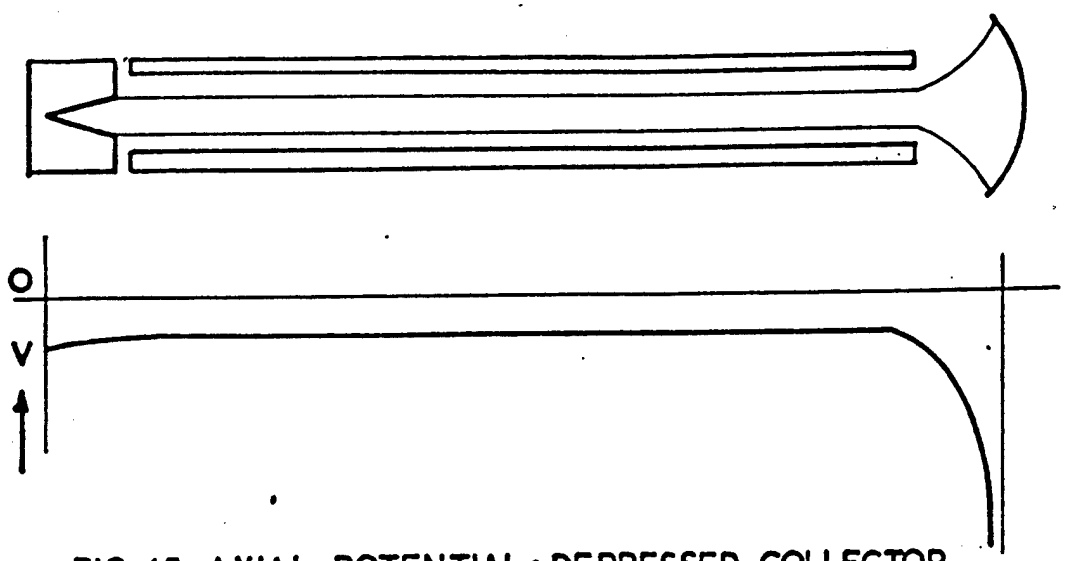

FIG.45 AXIAL POTENTIAL; DEPRESSED COLLECTOR

Because the bias at which this decline in the ion current flow to the cathode starts depends on the net space charge potential depression, it will be a measure of the amount of positive space charge to be found in the beam.

The minimum value of ion current reached, as a percentage of the ion current at zero bias, is the portion of the total ion current formed in the cathode half of the drift tube. The amount of ion current not reaching the cathode flows toward the collector. That this amount is the ion current which is formed in the collector and the collector half of the drift tube, may be seen as follows: A drift tube from which symmetric drainage would occur, i.e. one in which the ion current created in the cathode half drained toward the cathode, and that created in the collector half drained to the collector, could be created by applying equal potential gradients to both ends of the tube. Such a tube would have a maximum of potential at the center of the tube, and ions would flow away from this maximum in either direction. It is clear that this exact symmetric situation can never occur in practical

valves. but with the narrow, long drift tube such as is used in this valve, potential gradients applied to the end do not extend very far into the valve. Thus some imbalance in the amount of potential gradient applied to each end of the drift tube may still result in drainage which is very close to the symmetric case. The levelling-off of the decrease of ion current with increasing negative bias is evidence that this explanation is correct, since it implies that the affects of fringing fields at the end of the drift tube are of less significance that the fields due to the ions themselves. This situation of symmetric drainage to both ends of the drift tube is of great interest since it most closely matches the theoretical models introduced in Chapter 3. In addition, it will serve to experimentally determine the proportion of ions formed in the collector and collector half of the drift tube, as compared to the proportion formed in the cathode half.

5.2.2.1. Spatial Distribution of Ion Formation

From the assumption of symmetric drainage, it is concluded that ions flow left and right from the centre of the drift tube when a large negative bias has been applied to the collector end of the drift tube. Therefore, the proportion of the ions which are formed in the cathode half of the drift tube is the percentage of ion current reached at biases in which the decline in ion current has levelled off in Figure 44. This level is almost the same at all pressures in Figure 44, about 32%. The model of ion formation discussed in Chapter 3 predicts that the amount of ion current formed will be directly proportional to the length of electron beam path, Equation 3.1. Thus a simple approximation would be made by assuming that the collector half of the drift tube creates an amount of current equal to the cathode half, and that the remaining 36% of the total ion current is produced in the collector itself. However, two modifications must be made, the first

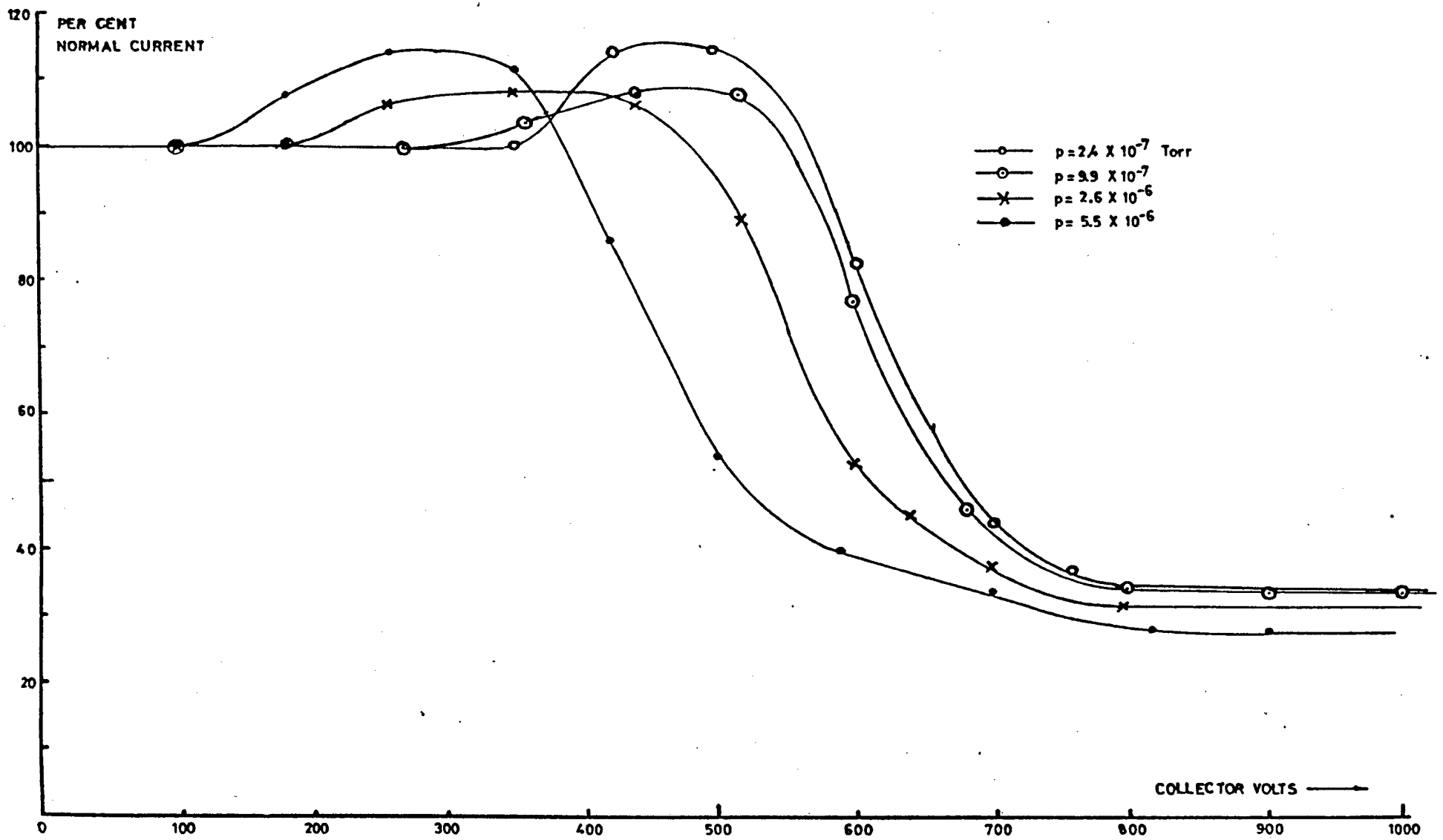

FIG. 44 ION CURRENT WITH NEGATIVE COLLECTOR

to t e experimental data, and the second to the application of Equation 3.1. to this problem. Because there is such a large difference between the ion currents flowing with and without the collector bias, the experimental results of Figure 44 must be modified to account for the Faraday Cage correction presented in Figure 30. The corrected values of the current measured to be originating in the cathode half of the drift tube are presented in the second column of Table 5.1.

In addition to this experimental correction, the pressure gradient which was found along the drift tube length must be taken into account. This is done by splitting the drift tube into halves and assuming that the effective path length of the beam within the collector is 20 cm. Then the current generated in the cathode half of the drift tube is (from Equation III.3)

$$\text{per cent} = \frac{(l_D/2)\,(p_a + \Delta p/4)}{(l_D/2)\,(p_a + \Delta p/4) + (l_D/2)(p_a + .75\Delta p) + (.2)(p_a + \Delta p)}$$

where Δp is the pressure differential, and p_a the pressure at the anode. For the value of Δp of 3×10^{-7} Torr, which was found in Appendix III, the third column of Table 5.1 may be calculated. The reasonably good agreement means that no more current is produced in the collector than would be expected on a simple model which measured the beam path within the collector and used Equation 3.1 to predict the ion current which would be produced. This shows the same trend as the work of Hines, et al (24), the only other experimenters to measure this characteristic. Their study indicated that the ion current generated in the collector would be a larger part of the total current as the pressure dropped, and that is also the conclusion of this experiment. From Equation 5.1 it can be seen that as p_a becomes negligible, the collector will finally contribute 33% of the total current. In contrast, Hines et al (24), found that it contributed 50% in their valve.

TABLE 5.1

Corrected Relative Ion Current Measurements at Zero and High Collector Depression

Pressure (Torr)	Measured Percentage	Theoretical Percentage
5.5×10^{-6}	35	39
2.6×10^{-6}	39.8	39
9.9×10^{-7}	39.9	36
2.4×10^{-7}	32	31

TABLE 5.2

Collector Depression for Collector-Drift Tube Potential Gradient Reversal

Pressure (Torr)	Collector Bias	Computed Depression(edge)	Computed Depression(axis)
5.5×10^{-6}	360	49	161
2.6×10^{-6}	460	100	323
9.9×10^{-7}	540	136	441
2.4×10^{-7}	545	161	521

The demonstration that ion production rate has the expected proportional relationship to the length of beam path is an important result because it indicates that any gas which might be evolved from the electron beam hitting the collector does not significantly disturb the experimental results.

5.2.2.2. Potential Gradient Reversal

The point of gradient reversal is marked by a decrease in the ion current measured at the cathode, but as can be seen in Figure 44. no sharp transition is present, due to both the spread in velocities which the ions have, and the increase which occurs before the point of gradient reversal. The point at which the ion current has dropped 5% below its maximum value is chosen to provide data for Table 5.2, which indicates the voltage at which gradient reversal takes place in each of the curves of Figure 44.

The computed depressions are arrived at by taking Equation 3.32 and substituting the values of positive and negative charge density which are predicted by Equation 3.29 and 3.31.

The experimental results clearly show the anticipated reduction in the net potential depression as the pressure rises. It would appear that only very small changes in the potential depression occur after a pressure of 1×10^{-6} Torr has been reached and the pressure is further reduced.

The theory, on the other hand, predicts a continuing increase in the potential depression as the pressure drops below 1×10^{-6} Torr. At the same time it predicts values of potential both at the beam edge and axis which are far less than those measured. From measurements of the body interception at low and high pressures, it is known that the beam becomes smaller at high pressures, but the change in diameter does not appear to be overwhelming. Thus, the disparity between theory and experiment cannot be fully explained by a reduction in beam diameter, which would cause the potential to increase. Thus it must be concluded that the theory

of Chapter 3 does not provide a very accurate estimate of the ionic space charge neutralisation in the neighbourhood of the collector. The large voltage required to reverse the ion flow at pressures close to neutralisation (ie.5.5. x 10^{-6}) is especially surprising in view of the large amount of ionic space charge which is found to be in the beam at high pressures.

From these experiments it is clear that the larger potential depression exists near the collector at high pressures than would be expected, which may indicate that the ions are draining with high axial velocity in that region. Furthermore, it is found that the pressure has only a small effect on changing the potential depression in the neighbourhood of the collector at pressures below 1 x 10^{-6} Torr. This is only in very rough agreement with the finding in Chapter 4 that the amount of charge storage in the beam remained constant at pressures below 7 x 10^{-7} Torr.

5.2.2.3. Increase in the Ion Current at Small Depression

The model of ion drainage which was discussed in Chapter 3 does not predict the rise or hump in ion current which is observed in Figure 44 as the collector negative bias is increased from zero. The rise occurs at a different voltage for each pressure, with the voltage required being greater in the case of lower pressures. Nor does the theory predict the drop in ion current which occurs with positive bias, as was mentioned in Section 5.2.1.

The following observations may be made about the 'hump' which is seen in Figure 44 :

1) The height of the 'hump' is roughly the same percentage of the reference ion current at all pressures over the measured range.

2) Over this same range of pressure it is observed that the rise always occurs directly before the point of potential gradient reversal, which causes the decrease in ion current measured at the cathode.

Two explanations may be suggested to explain this increase in ion

current at the cathode with collector depression:

1) This is a focusing effect which enhances the Faraday Cage efficiency. Since the only ions which could be affected by the new potential gradients caused by collector depression are those formed in the collector and in the drift tube very near to the collector, any rise in efficiency must relate only to ions formed in these regions. Previous experiment has shown that only about 20-25% of the total current is formed in this region, and thus the observed 'hump' height of up to 15% of the total current, would mean almost a doubling of the efficiency of collection for ions in this region. Not enough is known about the beam scalloping to make any analysis of the trajectories of ions which are formed in the collector, but it does seem that because of the large distance involved between the collector and cathode it would be very unlikely that any collector focusing effects could be important enough at the cathode to cause a doubling of the efficiency.

2) Although the trajectories of secondary particles have been discussed in Section 3.2., their possible influence in increasing the ion formation rate has not been discussed. From the discussions which follow it will be seen that these secondary particles could generate enough ion current to create the 'hump' of Figure 44. Both the ejected electrons and the ions themselves must be considered in the role of producers of added ion current, and although detailed knowledge of the trajectories of these particles is not possible, enough is known to make a rough approximation of the ionizing collisions made by these particles.

Firstly, the ions are treated. The Chapter 4 analysis of the rise times observed for the ion drainage current shows that a significant number of ions remain in the beam, trapped by the scallops. These ions will oscillate radially and have ionizing collisions with residual gas molecules present. The collision cross section for ionisation of molecules by ions of the same gas increases with increasing energy

in the region of interest in this case, in which ion energies must be less than the potential depression within the beam. The ionisation effeciency would not exceed 10 ion-electron pairs/cm-Torr.(30). By taking a maximum value for all parameters influencing the rate of ion production, it will now be shown that the ions oscillating within the beam make only a negligible contribution to the total ion current at a given pressure.

To find a maximum value of ion current produced by these trapped ions, it is assumed that there are as many ions present as electrons, or that Q_i, the total ionic charge in the entire beam is given by $\sigma_e l_D$, where σ_e is found by Equation 3.24. It is further assumed that these ions travel at their maximum velocity all of the time, thus maximizing the probability of making an ionising collission. The ion current arising from these collisions will be

$$I_{ii} = \text{(ionisation efficiency)} \times \text{(ion velocity)} \times \text{(number of ions)} \times e$$
$$= (10\ p) \times (2eV_i/m_i)^{\frac{1}{2}} \times (\sigma_e l_D/e) \times e$$

For a 17.5 KV, 4.6 A beam this is

$$I_{ii} = 2.07p$$

where p is the pressure in Torr. The ion current calculated from Equation 3.1. is

$$I_i = 97.2\ p$$

Thus at the very maximum, the ion current from this source is negligible, and realistic considerations concerning the amount of stored charge and the time at maximum voltage would probably reduce this figure by much more than an order of magnitude.

The ion current which ejected electrons in the beam could create is now considered. The calculations of Section 3.2. indicate that ejected electrons are forced by the confining magnetic field to rotate in orbits of radius somewhat greater than the radius which they were formed until they are drained away longitudinally. In the same way

that the scallops trap ions in the beam, it would seem reasonable to suppose that some of these ejected electrons are also trapped in the drift tube. These electrons can escape radially only as a result of further collissions with residual gas molecules, and from the assumption that some trapping is necessary to provide a stable condition for the removal of ions, those electrons which did escape would be replaced by others. These electrons will have energies in the neighbourhood of 50 to 100 volts, which is close to the value at which the ionisation cross-section reaches a maximum for gases such as CO, O_2 and N_2 (30). Making a conservative estimate, it may be assumed that ionisation efficiencies of 5 electron-ion pairs/cm-Torr, may be applied to these particles. If it is assumed that there is as much negative charge in the scallops as the amount of positive charge which was found to be present in Section 4.2.3., then a calculation of the ion current created by this source may be made in the same manner as was done for ions. The number of electrons may be taken to be $(.28)\ \sigma_e l_D/e$, corresponding to the 28% ion storage found in Section 4.2.3. The ion current due to this source is then =

$$I_{ie} = (5p)\ (\ 2\ e\ V_e/m_e)^{\frac{1}{2}}\ \ (.28\ \sigma_e l_D/e)\ (e)$$

$$= 21\ p\ \text{Amps}$$

This compares with an ion current of 72 p amps at the beam current and voltage at which this measurement was made, and may thus be a significant proportion.

Negatively biasing the collector disturbs the drainage patterns of both ejected electrons and ions by changing the gradient at the collector end of the drift tube. Since ejected electrons are identified as a possible cause of significant ion formation, the rise in ion current at the cathode with a small amount of negative bias may be explained by a trapping of more ejected electrons in the beam, and the consequent production of more ion current.

5.2.2.4. Build-up Time and Charge Storage Measurements with Negative Collector

The model which is used for the theory of ion drainage explained in Section 3.4. assumes a maximum of ionic charge at the collector end of the drift tube. This maximum does not occur in practice because the potential depression due to the beam space charge causes a gradient at the collector end which reduces space charge density at that point. (Figure 20b). However, by biasing the collector negative enough so that ions which are formed in the drift tube may also drain out the collector end, a maximum of ionic space charge will be created at the centre of the drift tube, and ions from the collector half of the drift tube will drain toward the collector, with the cathode only receiving those created in the first half of the drift tube. The results explained in Section 5.2.2.1. indicate that this is an accurate explanation, and that the dividing point for ion flow is indeed somewhere near the middle of the drift tube. Figure 25 is applied to this situation by imagining the symmetric half of its solution on the negative side of the horizontal axis, and applying it to the collector half of the drift tube. Thus the formulas which were developed in Chapter 3 will be applicable to the results of ion drainage from the first half of the drift tube if the drift tube length, l_D, is reduced to half the full drift tube length.

Figure 46 provides a demonstration of the effects of negative collector bias on the build-up time of the ion drainage current. Figure 46 a - c shows ion drainage at a pressure of 3.7×10^{-7} Torr, with variable collector bias. The first significant change is seen at a bias of 480 volts and is illustrated at Figure 46b. In the first half of the pulse a lowering of the drainage current is observed, but by the end of the pulse it has increased to the same value which occured at zero collector bias. By the time that the collector depression has been increased to 580 volts, a lowered ion current is observable throughout the entire

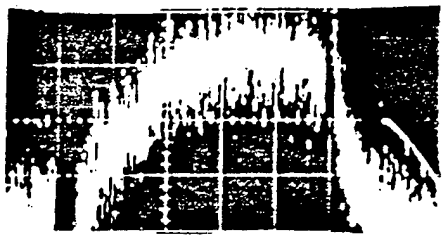

A) $p = 3.7 \times 10^{-7}$ TORR

COLL: 0 VOLTS

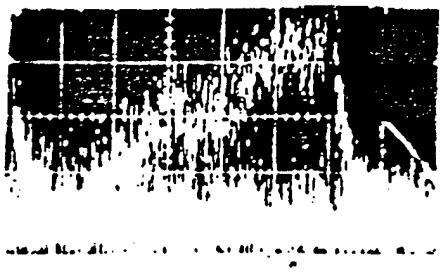

B) $p = 3.7 \times 10^{-7}$

COLL: -480 VOLTS

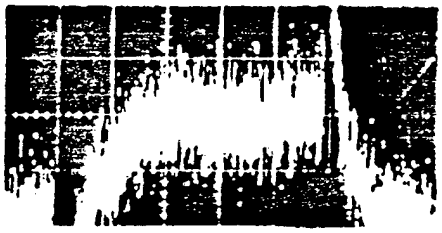

C) $p = 3.7 \times 10^{-7}$

COLL: -580 VOLTS

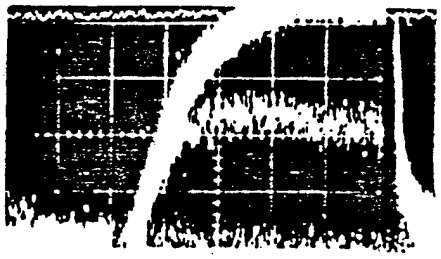

D) $p = 1.75 \times 10^{-6}$

UPPER: 0 VOLTS

LOWER: -800

FIG. 46 RISE TIME: COLLECTOR NEGATIVE

A-C: 200μS/DIV ; D: 100μS/DIV

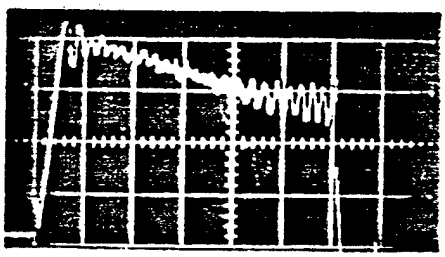

ION CURRENT OSCILLATION

16.5 KV, 2.8 A BEAM

VERT: 170 μa/DIV

HORIZ: 100 μs/DIV

FIG. 38

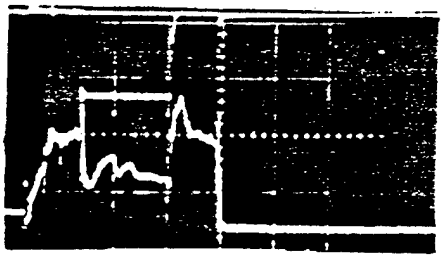

TYPICAL RESPONSE TO POSITIVE PULSE ON DTS No 1

UPPER: INV. BIAS ; 200 V/DIV

LOWER: ION CURRENT ; 220μA

FIG. 49

pulse length. Further increase of collector bias causes no change in the pulse shape, and corresponds to the lack of change in steady state ion current with increasing bias that was described in Figure 44. In these experiments a decrease in the rise time is also observed as the collector is depressed. Figure 46d shows the results of collector depression at a higher pressure, and a decrease in the rise time is again observed. This change in the rise time is surprising, for although there is less ion current available to fill the scallops, it is also true that there are proportionately fewer scallops to fill, and thus the rise time would have been expected not to change. The results of rise time measurements with depressed collector are shown in Curve II, Figure 35. The collector was fully depressed in these experiments and no effects occuring during the transition between full drainage to the cathode and partial drainage are included.

Curve II of Figure 35 shows that the build-up time with negative collector is less than with earthed collector, but shows the same decrease in build-up time with increasing pressure as is observed in Curve I.

By using the results obtained in Section 5.2.2.1. which indicate the corrected ion current which flows with a depressed collector, and this data on build-up time, an integral representing charge storage in beam may be calculated as in Section 4.2.3. This charge storage in the half-beam is shown in Figure 47, along with the charge storage for the half-beam calculated from Equation 3.23. As in Figure 37, the theoretical curve is again stopped when the predicted charge storage equals the total electronic charge in the half beam.

A region of fairly close agreement in shape and magnitude between the theoretical and measured curves is seen in the central region of the graph, between pressures of 1.5 and 4 x 10^{-6} Torr, At higher pressures, the loss of collection efficiency due to the neutralisation

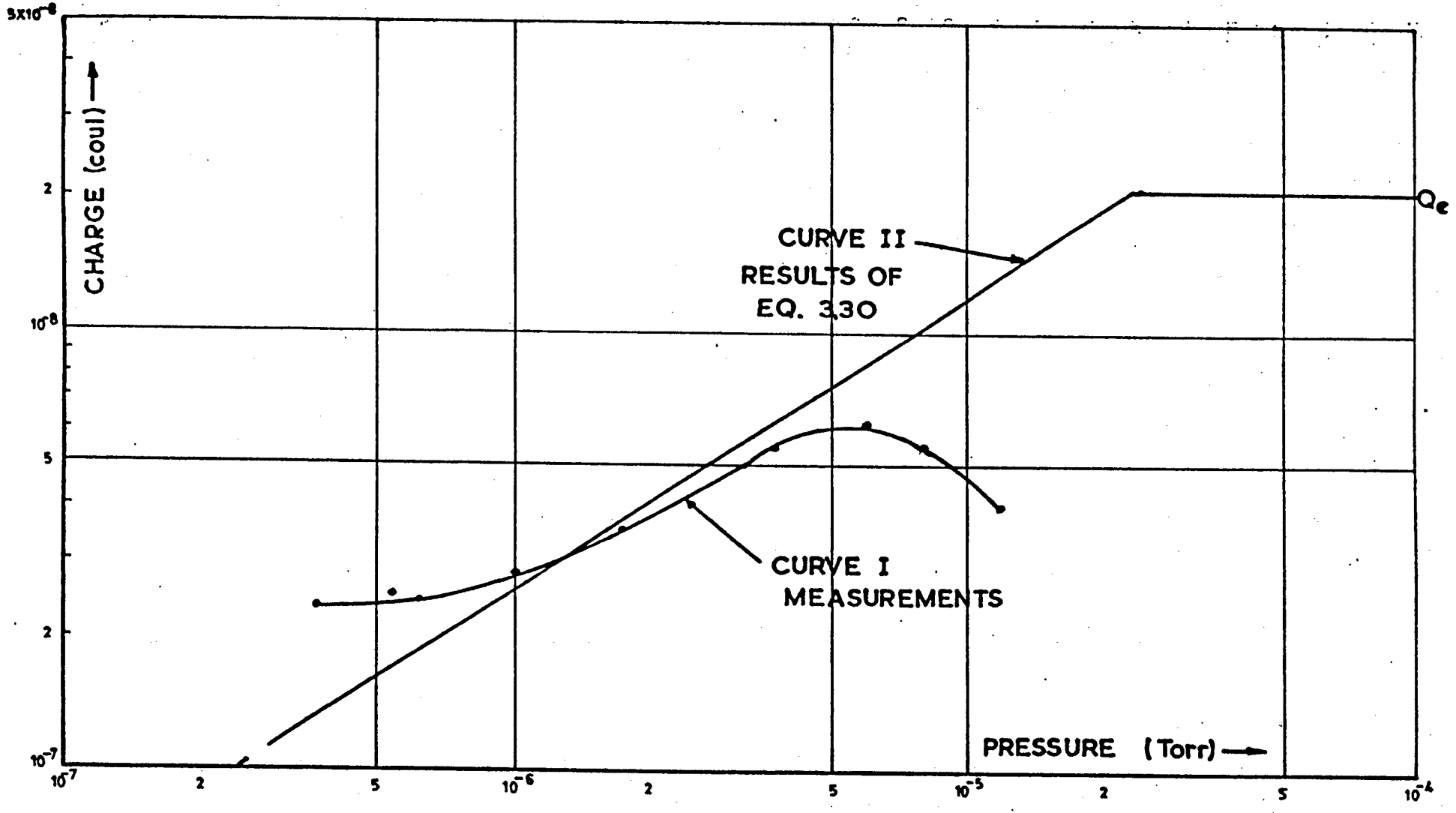

FIG.47 IONIC CHARGE STORAGE WITH NEGATIVE COLLECTOR

of the beam is most probably responsible for the drop in measured charge storage, but at the same time there is seen to be a lack of consistency between the highest amount of charge storage recorded and the amount necessary to produce total neutralisation. If, as suggested, neutralisation is causing a drop in collection efficiency, and thus in the measured charge storage, it seems strange that the measured total charge storage is not a fairly large proportion of the electronic charge for half beam, Q_e. The disparity revealed may be explained by the fact that the measurements presented in Figure 47 do not include any ion current which escapes collection in the Faraday cage. Thus, Figure 47 is an indication that the collection efficiency of the Faraday cage is on the order of 30 - 60%. This same reasoning cannot be applied to Figure 37 since measurements on the whole beam include such effects as collector charge storage, which is significant.

Data collected to measure the efficiency in Section 5.3.2.3. indicates that there is in fact a low efficiency, and Figure 47 shall be re-plotted in Chapter 6 in light of the data obtained in those measurements.

At a pressure of about 7×10^{-7} Torr, the charge storage is found to reach a minimum of 2.4×10^{-9} coul., and this is thought to be due to charge storage in the beam scallops. This is the same effect observed in experiments with the earthed collector and was discussed in Section 4.2.3. However, since it would be thought that the amount of charge storage of this type would be proportional to the length of path, it is of interest to make a comparison between data obtained with collector earthed and collector negative. It is found, from Figure 37 and 47 that the earthed value is 4.6 times that measured with negative collector. If it is assumed that the half of the drift tube near the collector stores the same amount of charge as the half measured in Figure 47, then the amount of charge stored in the collector

itself may be calculated. This calculation indicates that although the collector itself has been shown to have an electron beam path length of about $\frac{1}{4}$ that of the whole drift tube from the point of view of ion production, it stores 1.3 times the amount of ionic charge that the whole drift tube stores, at these lowest pressures. This proportion may change as the pressure increases, as the theory of Chapter 3 would indicate when ion drainage is considered, but for the case of minimum charge storage, the collector is seen to store a very significant number of ions.

It is thought that this phenomena is due to a large potential well within the collector which would be due to the increased wall diameter. It also indicates that it is likely that the ions drain in the direction of the collector at the beginning of the pulse in order to fill this very large well, which would be of significance in the operation of pulsed tubes since it would reduce cathode damage.

5.3. Drift Tube Biasing

Because the cavities are removed from the K 376 valve, it is possible to bias individual drift tube sections above and below earth potential. 'Humps' and wells can be produced in the drift tube axial potential by doing this, as is shown in Figure 48.

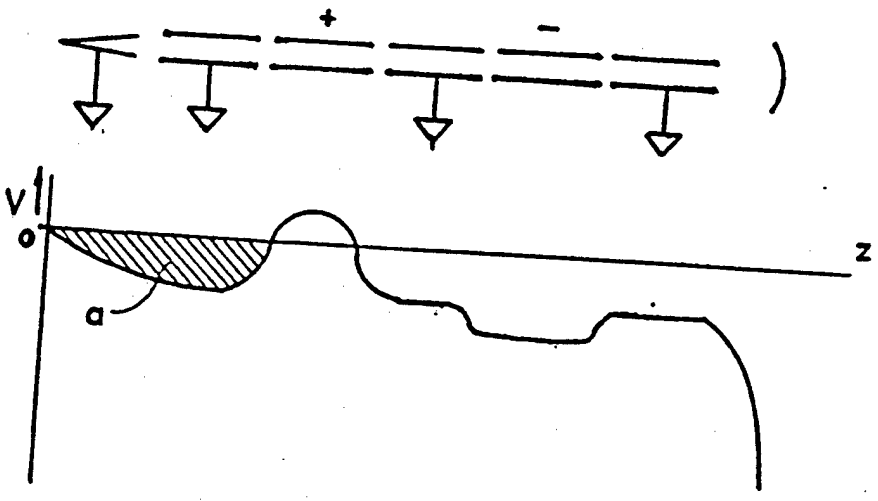

Figure 48 Axial Potential with Drift Tube Biasing

The humps can be expected to create ion traps, and ions originating between the collector and the positively biased electrode would be trapped in that region, eventually causing beam neutralisation. Region A is such a region. Ions originating on the cathode side of the hump would drain in the normal manner, as if the collector had been moved forward and the drift tube shortened.

In the experiments described below the drift tubes were biased by both DC and pulsed voltages. The effects of fringing fields from adjoining tubes tend to lessen the actual voltage which is seen on the axis in a biased drift tube, but from the geometry of these tubes it can be shown that the potential at the centre of the drift tubes was within 97% of the applied voltage (Appendix IV). It was the primary intention of these experiments to investigate the changes in ion current which would come about as the result of such biasing, and to determine the spatial distribution of ion current formation. In addition these results of the first experiments led to the use of drift tube biasing to determine the collection efficiency of the Faraday cage collector in a unique way, and also to make crude determination of the axial velocity of the ions draining to the cathode. The abbreviation 'DTS', introduced in Chapter 2, shall again be used for Drift Tube Section.

5.3.1. DC Positive Bias

A variable DC supply was arranged to individually bias any of the drift tubes. Since the number of ions draining to the cathode will be roughly proportional to the length of the drift tube which it drains, it was predicted that if a positive bias larger than the potential depression was applied to the first drift tube, only a small proportion of the normal ion current would be measured during the beam pulse. It was found, however, that this was not case in experiments, although a small reduction in the ion drainage current was observed. Large positive biasing with a DC voltage on any of the drift tubes near the cathode

(DTS 1,2,3) apparently has a great effect upon the beam flow in the region between the biased electrode and the collector and also may cause a DC current to flow. Small changes in such parameters as the pressure and beam current, as well as the bias voltage, produced very great effects in the measured ion current. These changes, furthermore, were eratic. The ion current did not return to its normal value when the bias was removed, but was found to be higher. In some cases when bias was applied to DTS 1, ion current actually increased with increasing bias. It is suggested that the application of DC bias causes sufficient localised heating of the body to evolve enough gas to significantly affect the residual gas pressure, and thus the ion drainage. Thus experiments performed with positive DC biasing of the drift tubes did not give accurate results concerning steady state operation, and were abandoned. Fortunately, it was possible to use large positive pulses for biasing which could be timed to occur within the beam pulse and thus remove the problems which were encountered with DC biasing.

5.3.2. Positive Pulsing of the Drift Tube Sections

5.3.2.1. Methods and Typical Reponses

A pulse amplifier similar to that which was used to drive the main pulser was found, and pulses of height variable to 1000 volts could be applied to each of the drift tubes. A separate pulse generator, a Cintel Model 3352, was synchronised to the system and used to drive the amplifier. The pulses applied could be varied in width and delay from the start of the beam pulse, and a description of the effects which this pulsed biasing had on the ion drainage current is now discussed.

Figure 49 illustrates a typical ion current response to a pulse on any of the drift tubes. In the photograph shown, DTS 1 is pulsed by 290 volts, which is shown, inverted at the top of the picture. The lower trace is the ion current response, on the same time reference

as the drift tube pulse. Three important characteristics of the ion current response are to be noted: a short positive-going spike which occurs just after the pulse is applied; a lowered ion current following this spike and lasting the length of the applied pulse, in this case accompanied by oscillations; and finally a temporary increase in the ion current following the applied pulse to DTS 1. In the example chosen, 100 usecs after the end of the applied pulse the ion current has returned to the level it would have been without the pulse. These regions are more clearly shown in Figure 50.

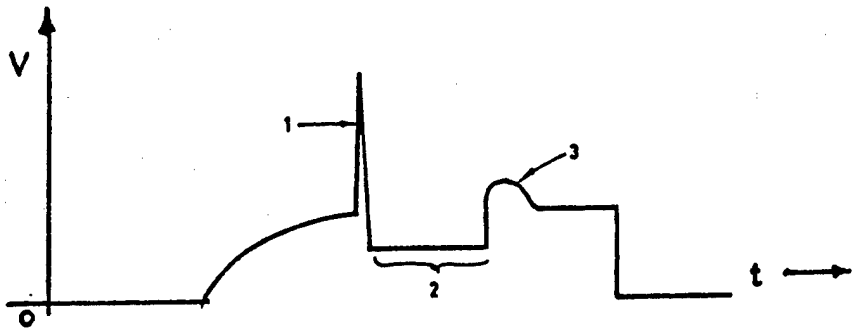

Figure 50 Ion Current Response to Pulse

This response is typical of what would be observed in the case of measurements made when any of the drift tubes are pulsed. Each of the three aspects of this response is now discussed.

The initial spike, 1 in Figure 50, which becomes smaller in size relative to the steady state ion current at higher pressures, is difficult to interpret. Tests were made to check that this was not a capacitive effect. It is suggested that this surge of current represents a sudden partial drainage of ion space charge storage which has accumulated within the beam. The ability of thebeam to store charge is reduced in the area of the high potential gradients set up by the biased drift tube section. Since the amount of spaoe charge stored in the beam builds up gradually after the start of the beam pulse

until it has reached its steady state value, this spike should be smaller the earlier in the beam current pulse that the bias pulse is applied. Figure 51 a is a multiple exposure showing a 200 μsec positive pulse applied to DTS 1 with various delays. The pulse height is 600 volts, which is sufficient to form a total ion trap. It is seen that as the bias pulse is delayed more and more from the beam pulse start, and therefore acts on more and more charge stored in the beam, that the spike amplitude rises. The shape of the ion current without the bias applied may be seen in this figure by the integrating effect of the multiple exposure. Once the ion current pulse has reached its plateau, and thus the ionic space charge storage within the beam has reached a steady state, the delay does not alter the spike amplitude. Thus the suggested explanation of this positive spike seems a good one.

The region denoted by 2 in Figure 50 is the ion current response during the bias pulse after the initial transients have settled to negligible values. During this part of the response a barrier to the flow of at least some of the ions which originate between the biased drift tube and the collector (region a in Figure 48) has been established. Whether or not this acts as a barrier to all ions will depend upon the amplitude of the applied pulse and the axial velocities of the ions which approach the biased drift tube. At values of bias greater than the potential depression, it is clear that it will act as a total barrier, and the only ions which flow to the cathode will be those which are formed between the center of the biased DTS and the cathode itself. Bias values as high as this are characterised in their ion current response by a flat region, as shown in Figure 50, and as may be seen in Figure 52 d. Values of bias less that one forming a perfect trap have various responses, which are now discussed.

Figure 52 illustrates the result of applying various biases to

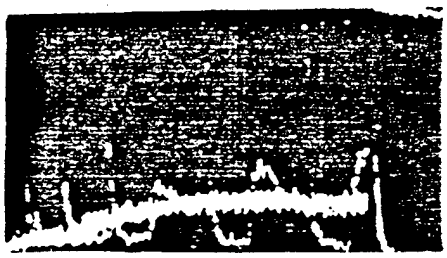

A) MULTIPLE EXPOSURE

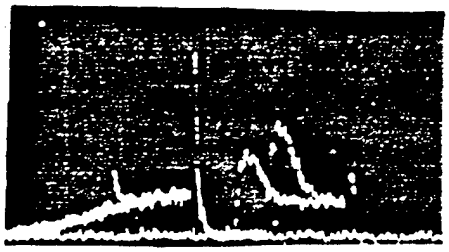

B) MULTIPLE EXPOSURE
VARIABLE PULSE DELAY

FIG.51 POSITIVE PULSING ON DTS No.1
$p = 5 \times 10^{-7}$ TORR ; 100μS/DIV

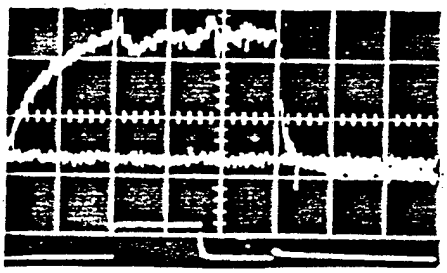

A

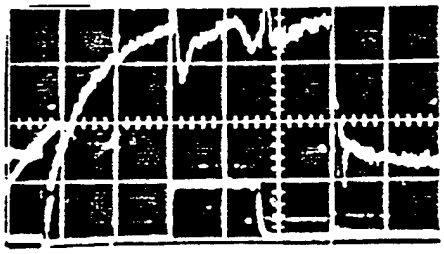

B

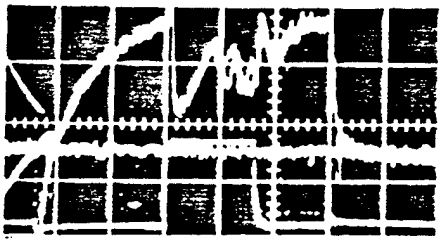

C

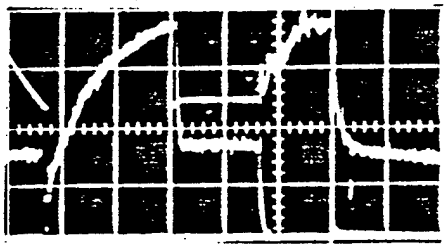

D

FIG.52 POSITIVE PULSING ON DTS No 1
$p = 3.3 \times 10^{-6}$ 100μS / DIV

UPPER TRACES : ION CURRENT, 220 μA/DIV
LOWER TRACES: BIAS VOLTS, 200/DIV

DTS 1 at a pressure of 3.3×10^{-6} Torr, and with normal beam operating voltages. The high pressure was chosen because of the greater clarity with which signals may be seen, and to take advantage of the shorter build-up times to the steady state, which was necessary for these experiments. The changes which occur as the pulsed bias were changed are typical of the results observed on all drift tube sections, except as noted below. Figure 52 a-d shows both the applied pulse and the ion current response. In Figure 52 a a bias of 90 volts is seen to have little effect on the ion current, but a small drop just after the beginning of the pulse may be seen. The ion current then rises during the pulse, back to the level which it had before the pulse. This is caused by the ion current produced between DTS 1 and the collector, the trapped ion current, building up enough space charge neutralisation to raise the beam potential between DTS 1 and the collector sufficiently to overcome the barrier, and allow the normal drainage of the ion current from the whole drift tube. Thus the measured ion current rises to the steady state value which it had before the pulse. This situation is shown in Figure 53.

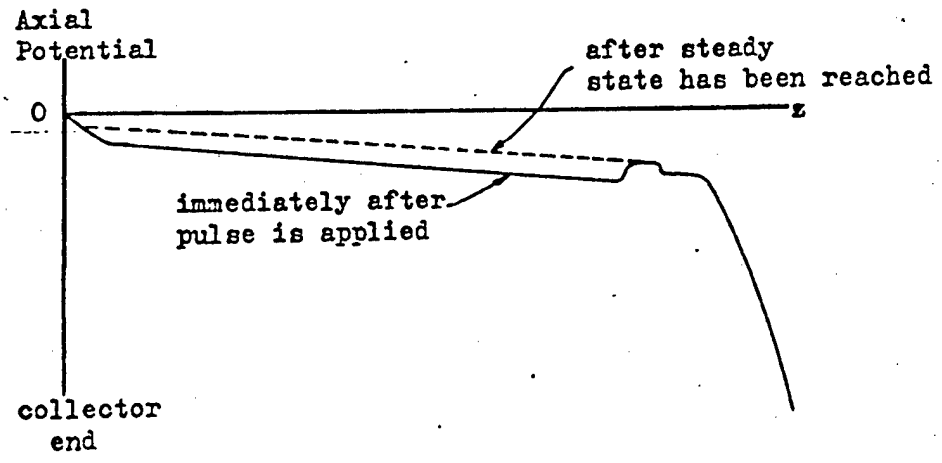

Figure 53 Axial Potential with Pulsed Bias on DTS 1

Figure 52 b illustrates the next stage which occurs as the bias is increased. The photograph shows the response to a 165 volt pulse. The ion current again drops and recovers, but toward the end of the pulse, the beginning of an oscillation is seen. This condition occurs when the ion trap has risen to a sufficient height that neutralisation of the beam between DTS 1 and the collector has occurred. This neutralisation will occur at all biases greater than 165 volts, for this case, although the oscillations will only be seen at the cathode when some of the oscillating ions have sufficient energy to get over the potential barrier. Once neutralisation is reached, further increase in the potential between DTS 1 and the collector due to ionic space charge accumulation is impossible because the ions escape radially. The oscillations are still visible on Figure 52 c, which is the response to a 280 volt pulse, but from the lowered average value of ion current during the pulse, it is obvious that not all ions being formed in the trap attain sufficient energy to get over the barrier. By the time that the bias is increased to 460 volts, as in Figure 52 d, no ions at all from the trapped section get past it, and the reduced ion current now measured is that which originates from the drift tube between the center of DTS 1 and the cathode. Further increase of the bias on the DTS caused no changes in this response. From this discussion it is apparent that use of drift tube biasing will make it possible to determine the distribution of ion formation in the drift tube, and confirm and expand the results of the negative collector measurements. The measurements made of this phenomena are discussed in the next section.

Figure 50 shows a third region of the response to positive pulses, the ion drainage current immediately after the bias pulse is finished, denoted 3 in the drawing. This response takes two forms; a sharp rise in the ion current to above normal values, as shown in Figures 49, 50, and 52 a and b; or a gradual return to the normal value requiring 50 to

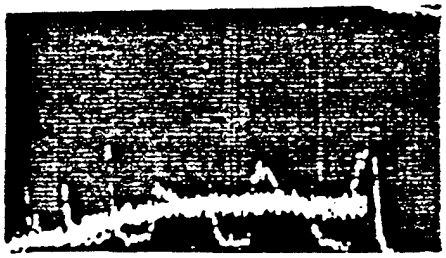

A) MULTIPLE EXPOSURE

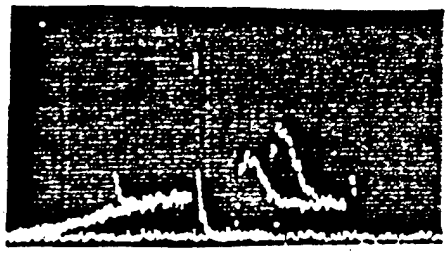

B) MULTIPLE EXPOSURE
VARIABLE PULSE DELAY

FIG.51 POSITIVE PULSING ON DTS No.1
$p = 5 \times 10^{-7}$ TORR ; 100μS/DIV

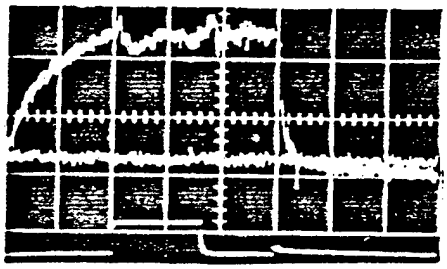

A

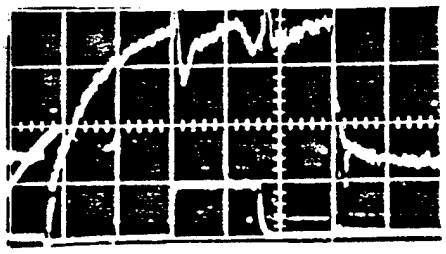

B

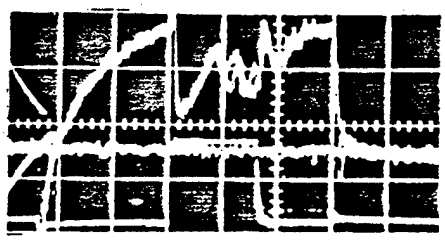

C

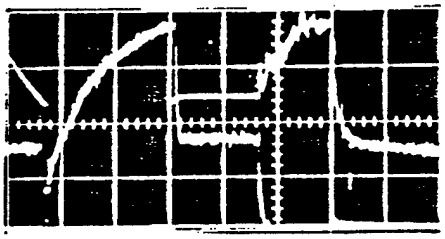

D

FIG.52 POSITIVE PULSING ON DTS No 1
$p = 3.3 \times 10^{-6}$ 100μS/DIV

UPPER TRACES: ION CURRENT, 220 μA/DIV
LOWER TRACES: BIAS VOLTS, 200/DIV

100 μsecs, as is seen in Figures 52 c and d, and 54 a-c. The peaking of ion current following the pulse occurs at low pressures for all biases, and at high pressures for the lower biases. It is suggested that this peak represents a drainage of the ionic space charge which has been trapped in the region between the biased DTS and the collector.

Figure 51 b is a multiple exposure photograph to demonstrate this idea, and shows two pulses applied at different times. The earlier pulse was started before the ion current had reached a steady state, and thus had less charge to drain back into the beam when the pulse was removed than the second one, which exhibits a large peak after the pulse. In the case of high pressures and high bias voltages, it is thought that the charge which must drain away when the bias pulse is removed is so great that it neutralises the beam and drains off radially. The slow rise time to reach the steady state value of the ion current is caused by the time required to again store enough charge for the proper equilibrium state.

The results of applying bias pulses to the other drift tube sections are exactly the same as for DTS 1, except of course that the ion current does not drop as much since the trapping volume is reduced. The exception to this similar behavior is seen in the behavior of DTS 3 and 4 at high pressures and large bias. As Figure 54 b and c show, oscillations take place long after the bias pulse is removed, although regular oscillations of the type seen here have not been observed without the bias pulse being applied. It is not clear what mechanism is responsible for this effect.

The application of drift tube pulsing to the determination of ion formation distribution, Faraday cage collection efficiency, and ion velocity filtering is now discussed.

5.3.2.2 Determination of Ion Formation Distribution

It is clear from the above section that if sufficient positive

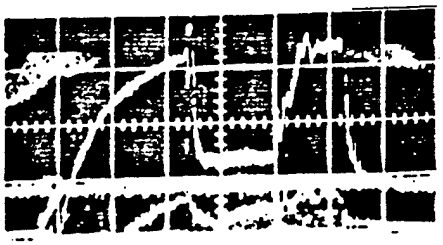

a) DTS 2

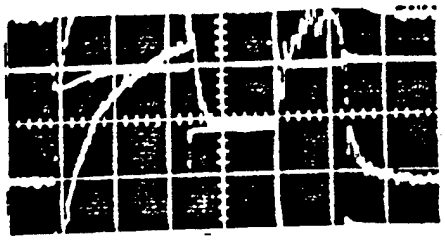

b) DTS 3

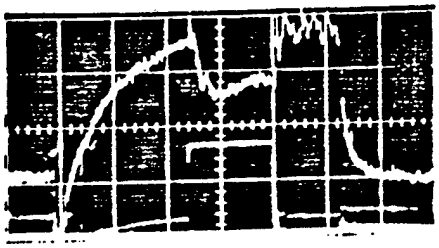

c) DTS 4

FIG.54 POSITIVE PULSE ON DTS 2-4
UPPER TRACES: ION CURRENT, 220 μa/div
LOWER TRACES: BIAS, 200 V/div
HORIZ: 100 μsec/div ; PRESSURE: 3×10^{-6} Torr

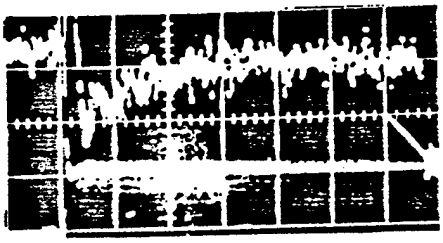

a) 80 V

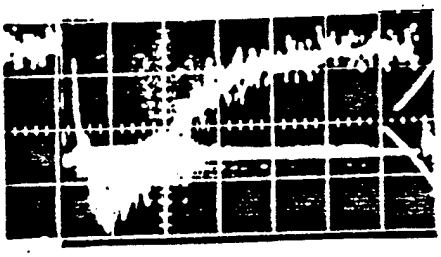

b) 130 V

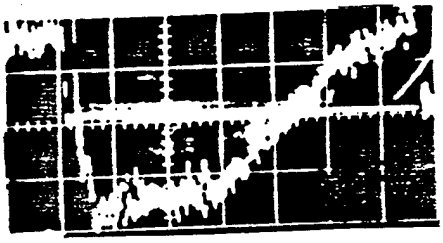

c) 200 V

FIG.57 EXPANDED TRACES OF PULSE ON DTS 1
UPPER TRACES: ION CURRENT, 18 μa/div
LOWER TRACES: BIAS, 100 V/div
HORIZ.: 40 μsec/div ; PRESSURE: 6.4×10^{-7} Torr

bias is applied to a drift tube section, the only ion current which will reach the cathode will be that originating between the centre of the biased drift tube and the cathode. Measurements of the ion current originating in each portion of the drift tube were made, and since it is also of interest to measure the voltage required to obtain the total barrier to ion flow, measurements were made of the ion current draining to the cathode as the bias voltage was increased. The results of these measurements are shown in Figure 55. Although there is no ambiguity in measuring the ion current which flows during a very high pulsed bias and results in responses such as are shown in Figure 50, the changing ion current which is present at lesser biases, such as is seen in Figure 52 b, makes measurement difficult. To make measurements as accurate as possible, the accurate positioning properties of the sample and hold circuitry were used, and the measurement made at the exact point of lowest ion current. Due to the large positive transient spike at the start of the response, these measurements may still be somewhat inaccurate. No correction was possible for the effect of the spike.

Figure 55 shows that, as expected, sufficiently large bias on any of the drift tubes sections is capable of creating a total barrier to the flow of ions originating between the biases DTS and the collector. After the results have been corrected for the Faraday cage effects, according to Figure 29, the ion formation distribution is found to be as listed in Table 5.3.

TABLE 5.3 Ion Formation Distribution

Location	Measured	Predicted
Cathode to Centre DTS 1	11 %	10%
Centre DTS 1 to Centre DTS 2	15 %	17%
" DTS 2 to "	18 %	18%
" DTS 3 to "	12 %	16%
" DTS 4 to collector	44 %	39%

These measured values may be compared with the information concerning ion formation distribution which was obtained from the measurements made with a negative collector (Section 5.2.2.1). At the same pressure, 1.5×10^{-6} Torr, these experiments with a negative collector show that 39.9% of the ions were formed in the cathode half of the drift tube. Although none of the DTS centre lines coincide exactly with the centre of the whole drift tube, the ion formation within the cathode half may be determined by summing the measured current between the cathode and DTS 2, and adding 84.3% of the current generated between DTS 2 and 3. This amounts to 41.2%, which is well within measurement accuracy of the above value. Thus the two experiments agree.

The third column of Table 5.3 is the prediction that Equation 3.1 would make for a beam in this drift tube including a collector with .2 m path length and a .05 m path length of significance between the drift tube and the cathode. The pressure differential discussed in Appendix III is also included in these calculations, which were made in the same way as those done in Section 5.2.2.1. It is seen that a significant amount less current is observed to form between DTS 3 and DTS 4 than would be expected, but otherwise the ion formation is fairly close to the predicted values, which indicates that the model for ion formation and drainage which has been used is at least approximately correct insofar as predicting spatial distribution of ion formation is concerned.

5.3.2.3 Experiments with Integration to Determine Faraday Cage Efficiency

It was mentioned in Section 5.3.2.1 that pulsed biases of only one or two hundred volts caused a temporary drop in the ion current just after the start of the bias pulse. During the pulse, the ion current returns to roughly the level which had been established before the pulse. An example of this behavior was shown in Figure 52 a, and the

behavior was explained with the help of Figure 53, which shows how the ions formed between the biased DTS and the collector act to fill the potential well which is created by the positive bias on the drift tube. Since oscilloscope photographs show the amount of time required for this to occur, and furthermore the way in which the ion current returns to its normal value, they may be used to determine the amount of ionic charge which is trapped between the biased DTS and the collector as the potential well is filled. The time integral of this ion current will be equal to the total charge stored in the trap. This integral is the shaded area in Figure 56.

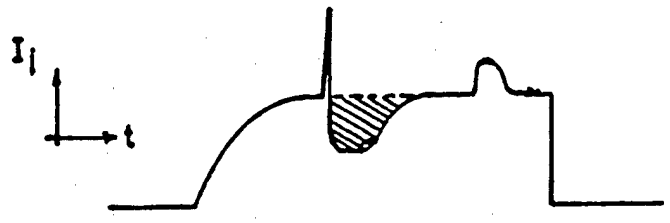

Figure 56 Ion Current with Low Pulsed Bias on DTS

Expanded oscilloscope photographs of this portion of the ion current response to pulses of various amplitudes which were made at 6.4×10^{-7} Torr are shown in Figure 57. The lower traces show the pulsed bias voltage applied to DTS 1 with a scale of 100 volts/division. The results of using graphical techniques to determine the integral for the cases shown here, and for measurements at other pressures are shown in Table 5.4. Figure 57 shows that any change in focus of the ions on the Faraday Cage due to the electric fields created by the biased DTS is insignificant, since the ion current returns to roughly the same level as it had before the pulse was applied.

Figure 53 illustrates how a theoretical value of this integral may be calculated with only the knowledge of the bias voltage. Without knowing the amount of charge which is stored in the beam before the

pulse is applied to the DTS, and thus without knowing the exact shape of the solid line in Figure 53, it can be said that at least to a first approximation, the dotted line which represents the potential distribution after the potential hump is overcome will be parallel to the first line and separated from it by the bias voltage. This is because Equation 3.26 shows that the potential gradient due to the ionic space charge is independent of the beam current except insofar as it relates to the rate of ion formation. Thus, if a drift tube is positively biased and causes a partial neutralisation of the beam potential depression along the section of the drift tube in which the ions are trapped, there should be no change in the gradients in the ionic space charge distribution, which are a function of only the ion formation rates and electron beam geometry. Thus if a potential barrier is erected by biasing a drift tube, the amount of charge which will be required to fill the ion trap so that normal current can be reached again should not be a function of the pressure at which the experiment is performed. This seems to be demonstrated by Table 5.4 in the case of the lower biases. Exceptions will be made to this rule to the extent that the stored ionic charge starts to neutralise the beam sufficiently to cause changes in beam geometry, and thus in the solution to Equation 3.28, and the overall space charge potential depression.

Because the potential along the axis after an equilibrium has been reached and the ion trap filled, is seen to be parallel to the original potential, the amount of ionic space charge which is necessary to accomplish this may be calculated from Equation 3.32. This equation relates the linear charge density to the potential rise it causes. If it is assumed that the bias causes the potential all along the drift tube to increase to the bias level, then a total charge storage may be calculated by multiplying by the length over which this change

takes place, which will be the portion of the drift tube included in the trap. Because of the potential gradient already present in the collector, it is not thought that additional charge is stored in that portion of the beam. Thus a theoretical calculation of the trapped charge can be made in which only the bias voltage is involved, but which relates to ions formed in the whole beam, not just those collected in the Faraday Cage. The integral which was measured using the Faraday Cage will be equal to the theoretical trapped charge only if the Faraday collection is 100 % efficient, and thus the difference between these two numbers will be a measure of the collection efficiency. This efficiency should be the same for all values of the bias voltage which are not so large as to cause escape of any of the trapped ions. The theoretical values of trapped charge are shown in Table 5.4, and the ratio of measured to theoretical storage, which is the efficiency, has also been calculated and is included in the table.

TABLE 5.4 Trapped Ionic Charge

Pressure (Torr)	Bias Volts	Measured Integral	Calculated Storage	Efficiency
6.4×10^{-7}	80	1.46×10^{-9} coul	4.97×10^{-9} coul	34 %
	130	3.66	8.06	45 %
	200	6.40	12.4	51 %
1×10^{-6}	120	2.75	7.44	37 %
	185	4.74	11.49	41 %
2.7×10^{-6}	120	3.50	7.44	47 %
	150	4.51	9.30	48 %
	205	5.98	12.7	47 %

No very large changes in the efficiency are observed as either pressure or voltage are varied, and the variations which are observed are partly explained by the inaccuracy of the graphical integration which was done on oscilloscope photographs. In addition, an unknown amount of beam diameter reduction may take place as the large amount of positive

charge is accumulated between the biased DTS and the collector. The change of beam diameter would have the effect of increasing the potential depression of the trapped portion of the beam, and thus even more positive charge than is calculated in Table 5.4 would be required to overcome the potential hump. This would cause measurements of efficiency made by this method to be higher than the actual value, especially at higher bias voltages. There is a small trend in this direction to be observed in the measured data of Table 5.4, but it is not possible to take account of the effect with any accuracy with the measurements which is possible to make on this valve.

The recorded data shows the efficiency of the Faraday cage to be between 40 and 50%, which is a great deal more than can be assumed from the simple comparison of collector area and beam diameter. This indicates that the true ion current is about 1/.45 = 2.2 times greater than that which is recorded, and from the comments above, this is seen to be a conservative estimate.

Figure 47, which showed the calculated ionic charge storage within the beam, should now be re-considered briefly, because it adds support to the efficiency determined in this experiment. If the value of ion current were to be increased by X2 or X3, the charge storage measured for the cathode half of the beam would not follow the prediction of the theory of Chapter 3, but the value which it has at the point where neutralisation effects are becoming apparent (pressure = 6×10^{-6} Torr) would be realistically close to the total electronic charge, and this is a most basic agreement which strongly supports the evidence gathered in this section.

5.3.2.4 Potential Gradients due to Ionic Charge

Because of the potential difference which exists across any diameter of the beam, the method of biasing the drift tubes is not very accurate for determining the velocity distribution of ions draining from the

drift tube. However, the data gathered may be used to compare the voltage required to first attain a total barrier to ion flow as the pressure is varied. This barrier voltage is defined as the minimum bias voltage required to cause the ion current to drop to its minimum value. This point is first reached in the case of DTS 1 at a pressure of 6.4×10^{-7} Torr at a voltage of 130 volts, as can be seen in Figure 57 b. Table 5.5 shows the results of measurements made on DTS 1.

Table 5.5 Barrier Voltage for DTS 1

Pressure (Torr)	Voltage
6.4×10^{-7}	130
1.0×10^{-6}	190
2.7×10^{-6}	200
3.3×10^{-6}	350

The voltage values determined by this experiment are far greater than those predicted in Section 3.4.4, which predicts voltage gradients of 125 volts along the entire beam at pressures of 5.5×10^{-6}, which is just below neutralisation, and gradients far less at lower pressures. The existence of these larger gradients would seem to indicate that further study of the boundary conditions and assumptions of the theory presented in Section 3.4 is warranted. Further experiment with equipment designed to measure this gradient would also be of great interest.

CHAPTER 6

Summary and Conclusions

By placing a Faraday cage behind the cathode of a high power valve, measurements of the ion current drainage to the cathode have been made, and data collected on the magnitude, build-up time, and spatial distribution of formation of this ion current. In addition, observations have been made of the changes in ion current drainage which occur with residual gas pressure, magnetic field, beam current, and bias applied to various electrodes of the high power klystron with which these investigations were made. Because of the direct measurement of the ion drainage a great deal of sensitivity was possible, while at the same time the experimental arrangement did not interfere with the normal operation of the valve. This chapter will review the findings which were made, and make comparisons between this new data and the investigations of previous authors. In addition, the further study which is necessary to relate these findings to the RF performance of these valves will be outlined.

In reviewing the experimental findings, results which were obtained in later experiments utilizing the biasing of valve drift tube sections shall be combined with the first experimental findings to indicate the full steady-state ion drainage current to the cathode. The variation of this steady state current with pressure, beam current, and magnetic field is first discussed, and explanations presented which may account for the large magnitude which was observed. The observations of the build-up time of this ion current are then discussed, and these are used to determine the charge storage within the beam. Some behavior which would have been expected from the experimental work and explanations of other authors but was not observed in this work is discussed.

The various electrodes of the valve, the collector in particular,

were biased in experiments to determine the spatial distribution of the ion current formation, and to measure the effects of collector depression. The results of this work are discussed, and a summary of important conclusions which may be drawn from the experimental work of this dissertation is presented. The chapter concludes with a discussion of further experimentation which shall be conducted on this valve.

6.1 Steady State Ion Current

The steady state ion current is the same current as would be expected to be flowing during CW operation of this valve. Measurements of the Faraday Cage current were shown to require two corrections before they could be considered an accurate determination of the total ion current drainage to the cathode. The first of these is a reduction of the measured current to account for secondary electrons which may escape the cage and thus cause a larger current to be measured than is that due to ions, and the second is an increase which accounts for the efficiency of the collection hole and collector. The efficiency determination is difficult to make accurately, and the determination that it lies between 45 and 50% is a conservative estimate, with some evidence that it might be as low as about 30%. Figure 58 shows the result of applying these the two corrections to the original data indicated in Figure 27.

A curve representing a theoretical calculation of the ion current from Equation 3.1 is also shown in Figure 58. This curve includes a 20 cm path length in the collector, which is a fairly accurate estimate based upon the data obtained on the spatial distribution of ion current formation. Included in this data is the account which had to be taken for a pressure differential which was believed to exist in the tube. Although impossible to verify, when this pressure differential is included in the theoretical calculations, a good agreement

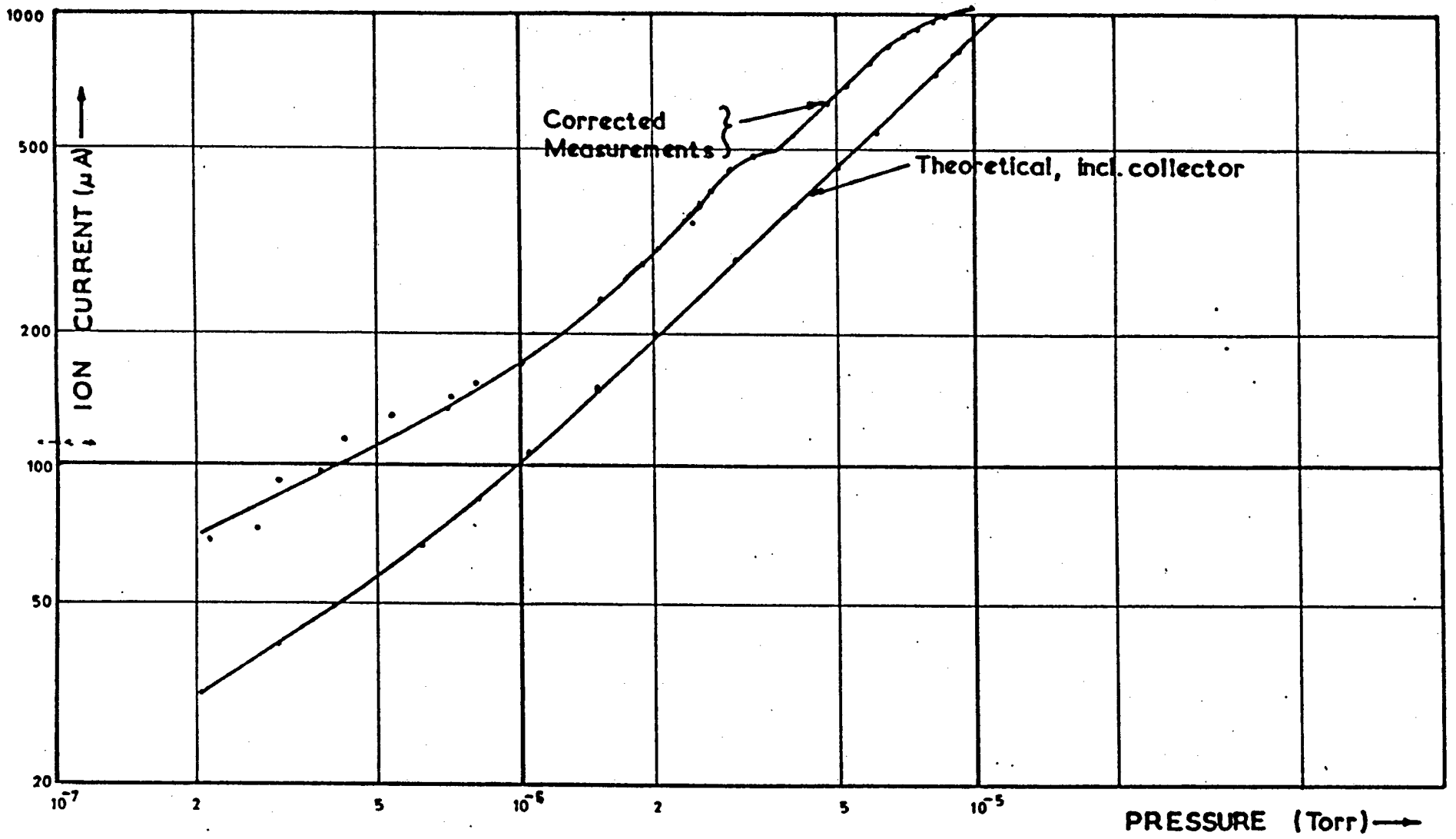

FIG. 58 ION CURRENT vs PRESSURE

between the measurements and theory is seen insofar as the pressure dependence of ion current is concerned. In comparing the magnitude of the two curves, however, it is apparent that the measured values of ion current are about 50% greater than those predicted by the modified Equation 3.1. The only extensive published measurements with which this value can be compared are those of Hines, et al (24), in which the measured values are smaller than predicted (75%). The valve on which their experiments were performed, however, only had a 2 KV, 14.5 ma beam.

An explanation for this larger current may be found in the combination of a variety of effects, and the emphasis should be laid on those which would serve to distinguish low and high power valves. The first of these has been mentioned in Section 5.2.2.3. Ejected electrons are shown by the analysis of Chapter 3 to be trapped within the beam or close to the beam, and possess sufficient velocity to have ionising collisions. Once a steady state is reached, these electrons drain longitudinally as quickly as they are created, but it would seem that a number may migrate to areas of high potential when the beam is first turned on and remain there, just as ions are seen to fill the scallop potential wells. A sufficient number of electrons could be trapped in this way to cause a reasonable increase in the beam current, as demonstrated by the calculations of Section 5.2.2.3. Furthermore, these ejected electrons would serve to explain the ion current increase at small negative biases on the collector.

Further explanation for the large ion current may be sought in our lack of knowledge concerning the constituents of the residual gas. In particular, copper atoms may be present in the valve. The determination of the distribution of ion formation, however, does preclude any explanations that this increase may be due to outgassing of the collector, since ion production is shown to be closely proportional to the path

length of the electron beam. Since the determination of ion current magnitude includes the conservative estimate made of efficiency, it is possible that the magnitude of ion current is greater than that determined here. In any case, this research indicates that larger ion effects than would be predicted from Equation 3.1, which is the commonly accepted theory, will be found in high power klystrons. Thus, for example, greater cathode damage may be expected.

6.2. Ion Current Build-Up Time

The observation of the build-up time of ion current draining to the cathode was made over almost two decades of pressure, between 3×10^{-7} and $1.5. \times 10^{-5}$ Torr, and it was found to be characterised by a gradual rise from zero starting at the same time as the beam pulse, and rising to 90% of its final value in times between 500 and 50 μsecs. The rise time decreased with increasing pressure, approximately as $1/\sqrt{p}$ over most of the range. The gradual rise from zero was not expected in light of the work of Sutherland (3) and Hartnagel (22) who have predicted a filling of the potential well near the cathode before any ion flow takes place. It may be that such a potential well does not exist in this valve, or that the pressure is too high for these effects to be observed. It is, however, certain that scalloping does exist, and Hartnagel has suggested that in cases of the residual gas pressure being too high, the behaviour to be expected is for an initial filling to take place, followed by a release of a large number of ions, and a settling down to a constant flow of ion current which is too high to allow oscillations of the type which he examined (Chapter 1). This would suggest that a peaking of ion current would be observed some time after the start of the pulse. However, the only pressure at which similar behaviour was seen was at 3.5×10^{-6} Torr (Figure 34a), and when the pressures was dropped below this point, no oscillations, or tendency to oscillation was observed although pulses as long as 1 msec were used. Conclusive

investigation of this type of oscillation could only be done by placing measurement equipment of the type employed here in a valve in which the oscillation is known to occur. It is the conclusion of this experimental work that the ion drainage current is observed to build-up gradually from the start of the pulse to the plateau value. Since some filling of the potential wells caused by scalloping must take place, it is concluded that the smooth rise is due to the axial velocity of some ions which allows them to drain before the wells are filled. Experiments did indicate that the axial potentials draining the ions may be on the order of a few hundred volts, rather than the lower value predicted by previous work (24).

The long rise and fall times which were measured mean that high power pulsed valves will not suffer the same amount of cathode damage as CW tubes of the same average power, but at the same time the changing beam transmission during the pulse can be expected to have significant undesirable effects in the RF amplitude and phase. This effect is best reduced by minimizing scallops, which is done in any case, but the amount of beam charge storage which takes place in even smooth beams indicates that the problem will be present to some extent.

6.3. Charge Storage in the Beam

Integration of the amount of ion current which was kept in the beam during the build-up time of the ion current was used to find the amount of ionic charge storage in the beam and collector. It is shown that a very large amount of charge is stored in the collector, in fact slightly more than is stored in the whole drift tube. This is thought to be due to a large potential well which exists within the collector in the absence of residual gases, and which is filled by ionic charge in beams with gas present. This well suggests that the flow of ions during a pulse may be different than that which occurs in the CW or steady state case.

By biasing the collector negative, it was possible to examine the charge storage which exists in the cathode half of the drift tube, thus eliminating collector storage. These experiments revealed that unless the ion current is adjusted upward by the Faraday Cage efficiency discussed above, unreasonably low values are found at pressures where neutralization is known to occur. This work agrees with the drift tube bias experiments in showing that efficiency is between 30 and 50%.

Figure 59 shows the charge storage in the cathode half of the drift tube, and differs from Figure 47 in that the data includes a correction factor of 2, corresponding to 50% Faraday Cage efficiency. It is apparent that a minimum of charge storage is reached at a pressure of about 6×10^{-7} Torr, and that for this particular valve, reduction of the pressure below that point will not reduce the number of ions in the beam. The data here indicates that the beam is 24% neutralised at even the lowest pressures. This neutralisation, of course, may have the beneficial effect of increasing beam transmission. Study of the RF performance of the valve must be done before the impact this may have on noise performance is known.

6.4. Oscillations

As the gas pressure was increased to about 3×10^{-6} Torr, small amplitude oscillations could be observed in the ion drainage current at frequencies between 8 and 33 KHz. As the pressure was further increased, these oscillations vanish, and larger oscillations at a frequency of about 20 KHz appear at a pressure of about 9×10^{-6} Torr. These oscillations cause a rise and fall of about 25% of the average ion drainage current. A large DC component of the current flows while the oscillations are observed. Further increase of the pressure finally squelches the oscillations. Experiments show that a large collector depression has the effect of raising the pressure for onset of these large oscillations, and apparently makes the boundary conditions

for their occurence far more critical. In the case of all oscillations, it is assumed that they are caused by alternate collapse and re-building of the beam potential well as it is neutralised. Measurements of the body interception current support this suggestion.

6.5. Spatial Distribution of Ion Formation

Pulsed biasing of drift tubes made it possible to determine the spatial distribution of the ion formation process. The result of these experiments was that the ion production rate is approximately directly proportional to the beam path length, as the model of Chapter 3 had supposed, and that no areas of extraordinarily large ion formation were found. Measurements with a negative collector showed agreement with these results.

6.6. Suggestions for Further Research

It was the intention of the experimental work covered in this dissertation to analyse the ion drainage in a high power klystron by direct measurement, and to design equipment to provide for a second series of measurements which would relate the measured ion effects and the RF noise which they produce. This natural progression of the work is clearly very important in understanding the RF effects of the large number of ions which have been shown to drain from the valve, and the large number which remain in it. The very sensitive techniques which have been developed (25) provide an accurate method to relate ion created noise and modulations. In particular, experiments which distinguish between RF performance at the beginning and end of the pulse would be of great importance in determining ionic effects. Changes in the beam diameter, ionic charge storage and direction of ion flow during the pulse will affect the RF measurements.

The findings of this experimentation include some unexpected results which could probably best further examined in an apparatus specially designed to assure higher Faraday Cage efficiency, etc., but not

necessarily capable of RF modulation. The apparatus would, of course, have to be capable of operating with the high current beams which are a significant part of the phenomena observed in these experiments. Further confirmation must be sought of the ion currents, which were 50% or more larger than those which have been assumed so far. An important part of this research would be the confirmation of the effectiveness of the ejected electrons in creating a significant amount of further ionisation. This could be examined in an apparatus which could vary the number of these which are trapped in the beam by varying the scallop depth. Such equipment already exists in the form of beam analyzers, but it has not been adapted to ion measurement. It is also clear that a more thorough analysis of the velocities which ions draining to the cathode attain during their travel in the drift tube would be a great interest in improving present theoretical work concerning the drift tube potential depression with ionic charge.

The findings with regard to ion build-up time were surprising in light of the explanations of low frequency oscillations presented by Hartnagel (22), but a proper investigation of the relationship of ion drainage and these low frequency oscillations would require the installation of experimental equipment such as that designed for this disseration in a valve in which these oscillations are known to occur. The work which has been reported concerning these oscillations has been for the case of low power valves, and it may be that the greater ion current in some way changes the conditions necessary for these oscillations to occur. Methods such as the one used here, however, are necessary for a proper investigation of these explanations.

It would seem that the great ion currents which have been discovered in this research do deserve more attention experimentally, in spite of the cost and time inherent in experiments with high power beams. The work discussed in this dissertation demonstrates that greater cathode

damage than would be expected will occur in high power valves, and that ion effects will be more significant in high power valves than in low power valves. The research on the build-up time of the ion current would indicate that special care must be taken in the construction of valves which are pulsed and have difficult phase linearity and amplitude flatness specifications. Minimization of beam scalloping is important not only for reasons of good beam transmission, but also to reduce ion effects during the pulse.

Results from the second stage of this research are looked forward to.

APPENDIX 1

CIRCUIT DIAGRAMS FOR ION MEASUREMENTS

Figure 60 20 KV Modulator

Figure 61 Rogowski Belt Amplifier

Figure 62 Sample and Hold Circuitry

Figure 63 Sample Pulse Generator

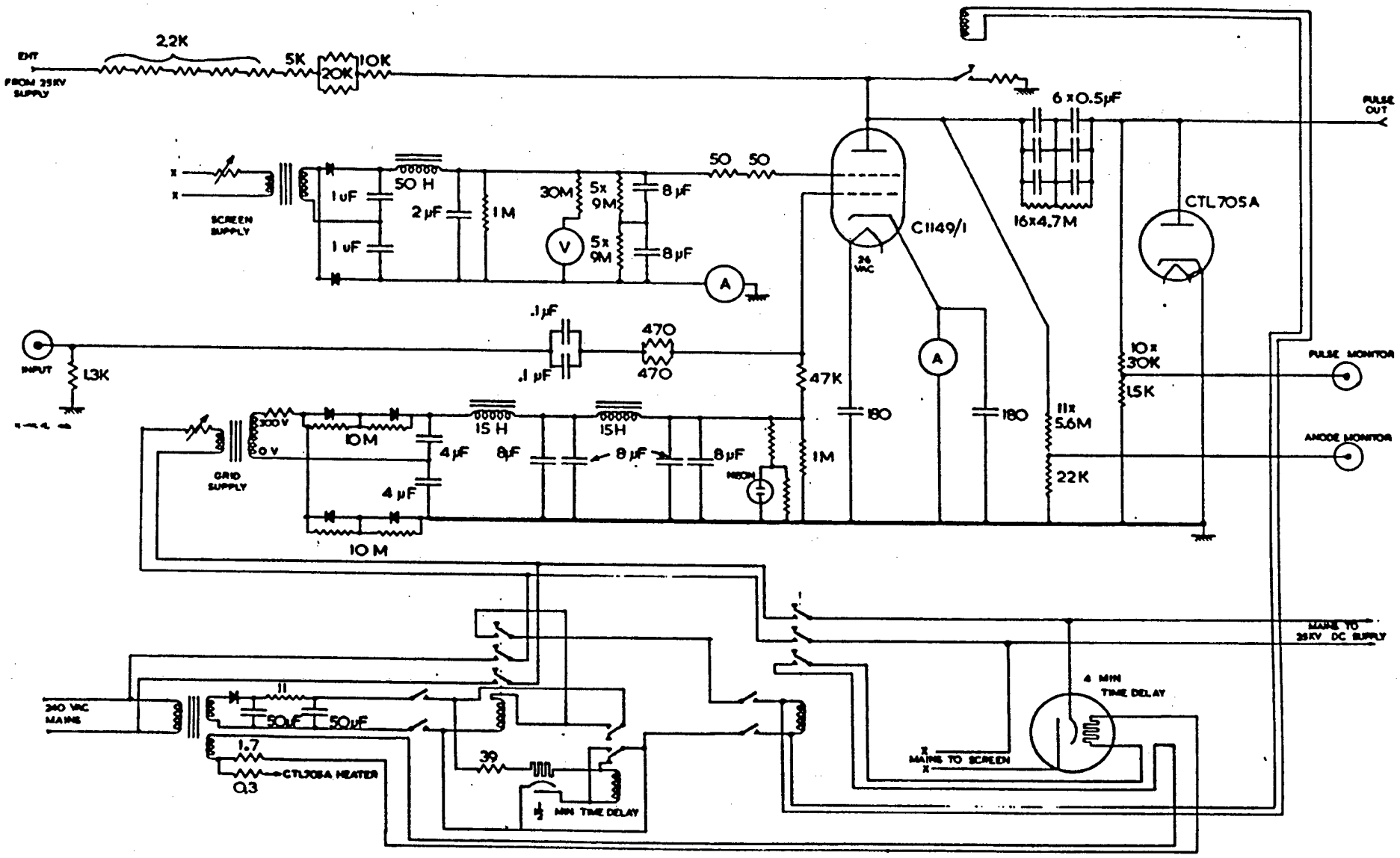

FIG. 60 20 KV MODULATOR

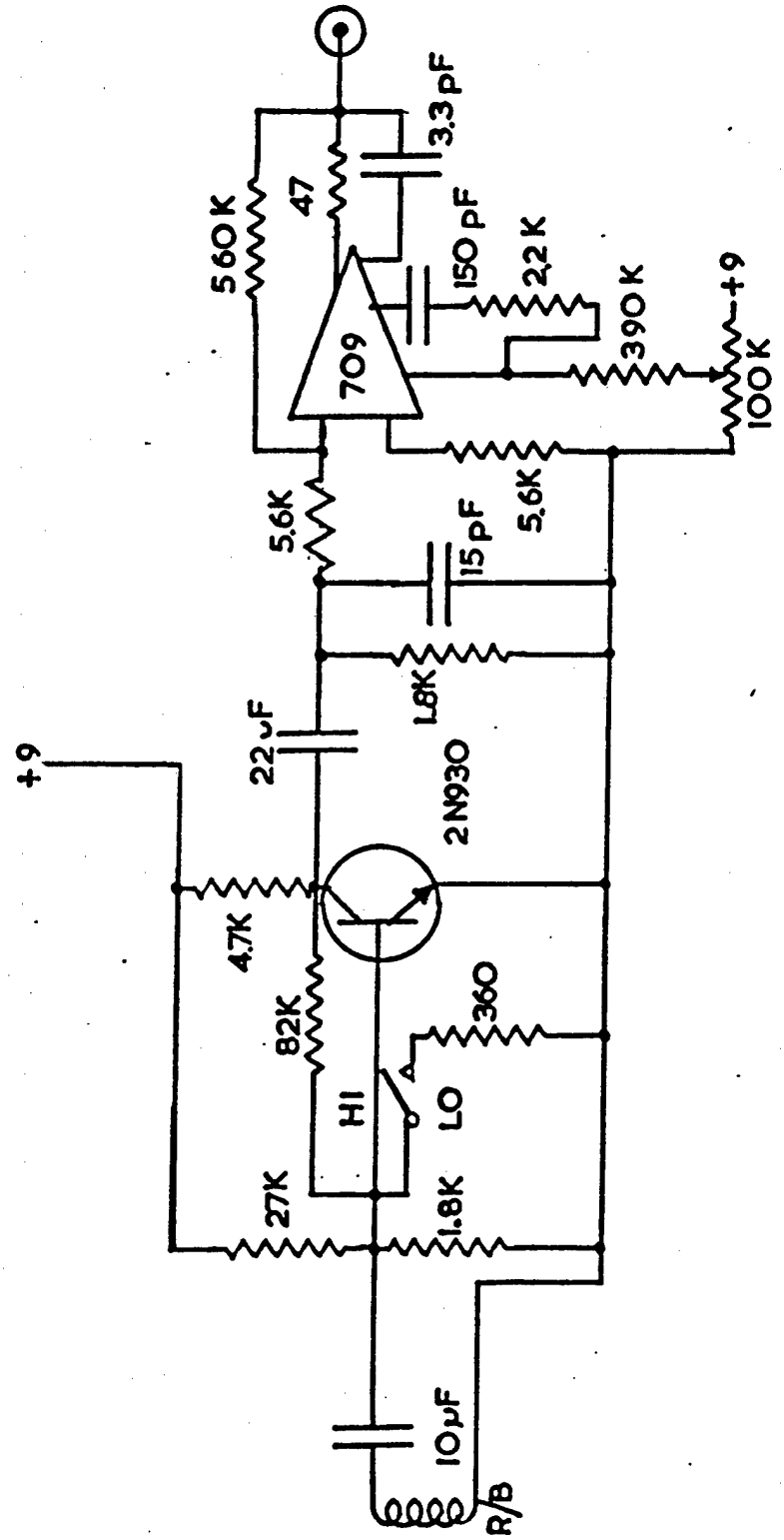

FIG.61 ROGOWSKI BELT AMPLIFIER

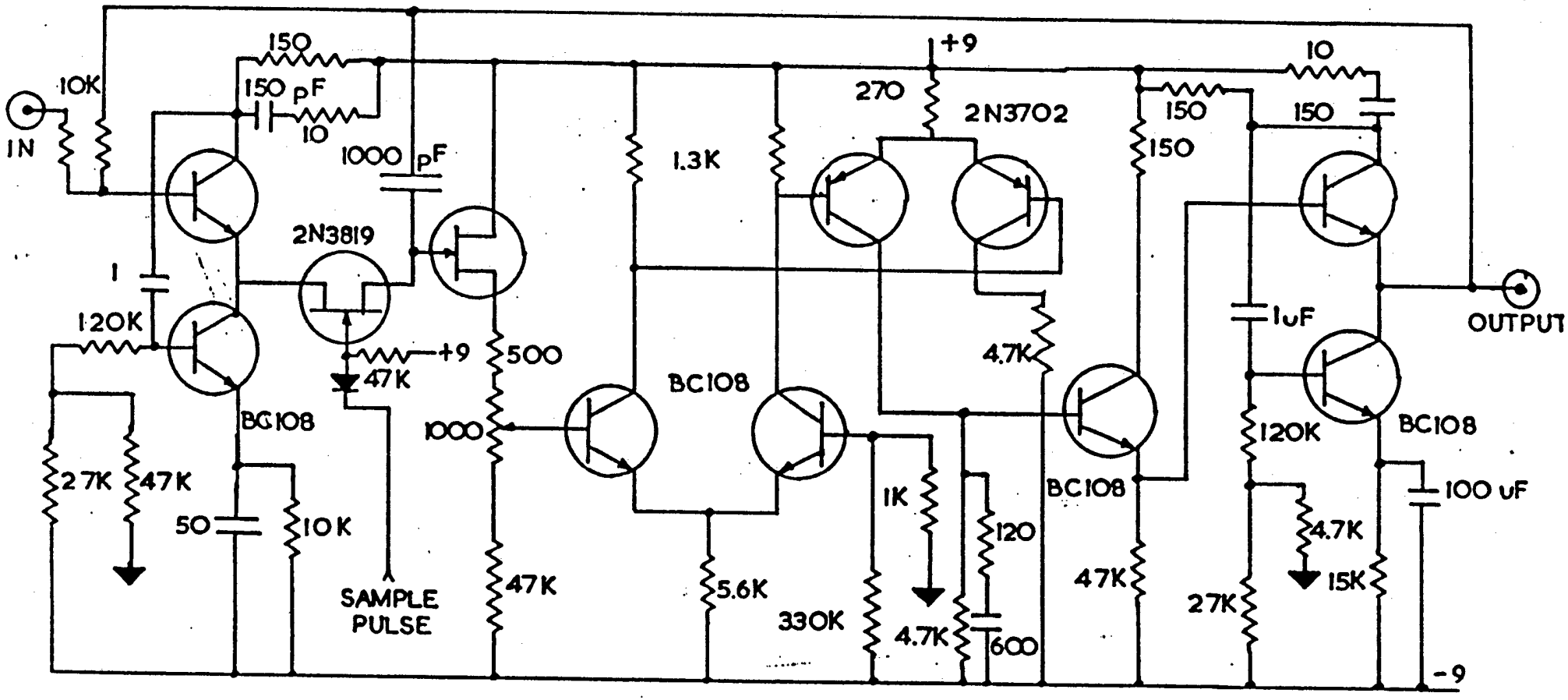

FIG.62 SAMPLE AND HOLD

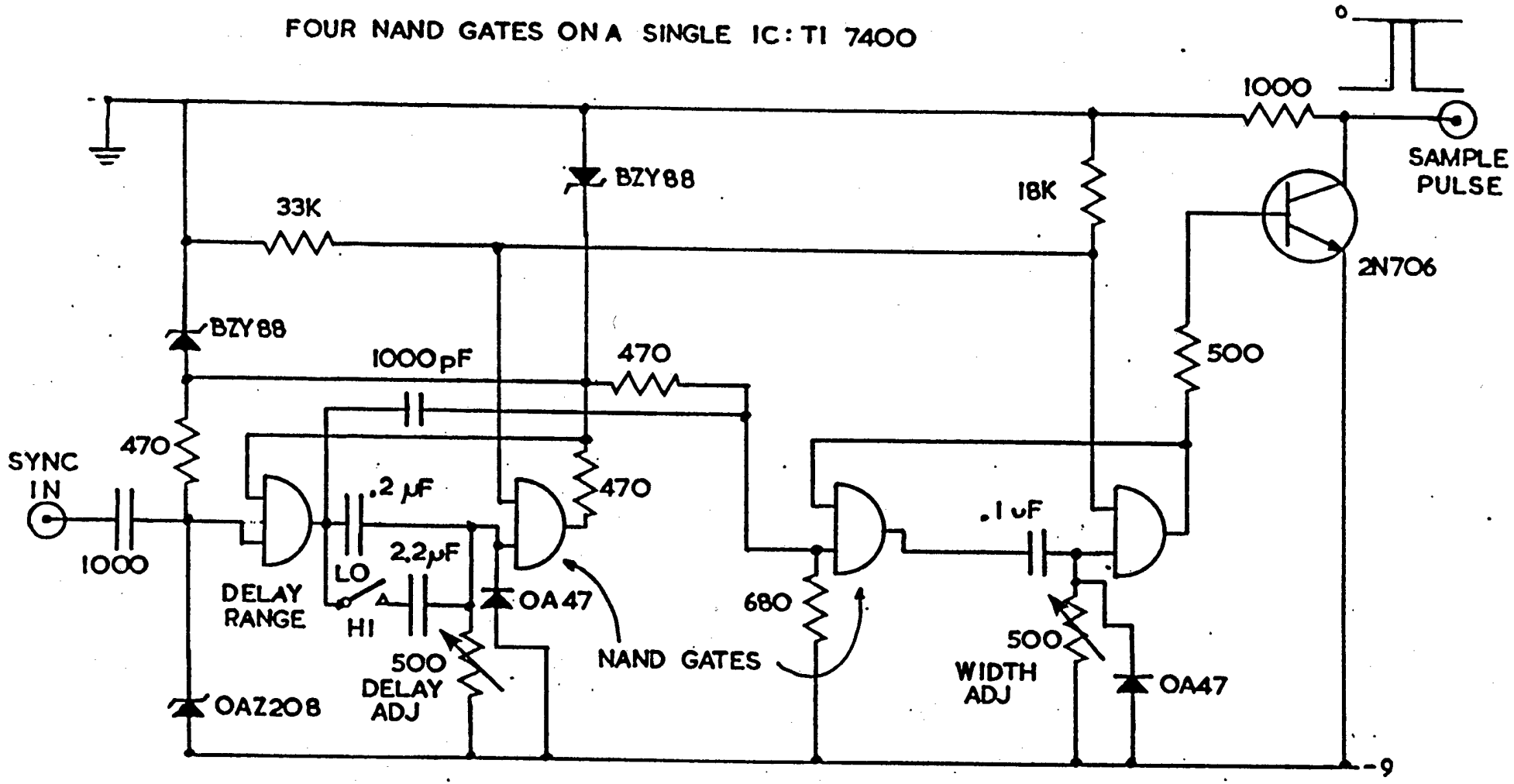

FIG.63 SAMPLE PULSE GENERATOR

Appendix II Rogowski Belt Construction

The Rogowski Belt is a magnetic pick-up loop which measures the current in a wire passing through it. Figure 64 illustrates the belt. If the solenoid cross-section is A, the torus average radius R_{av}, the number of turns N, then it may easily be shown from first principles that a voltage V

$$V = \frac{NAu_o}{2\pi R_{av}} \frac{dI}{dt} \qquad \text{Eq. II.1}$$

will be generated in the belt due to a current I in the wire passing through it. Furthermore, the inductance of the belt will be L:

$$L = \frac{u_o N^2 A}{2\pi R_{av}} \qquad \text{Eq. II.2}$$

The voltage output of the coil is thus proportional to the derivative of the current which is of interest. To obtain the integral of this voltage, two methods may be used. Figure 64 b and c illustrate equivalent circuit diagrams of these two methods and the belt itself. Here the belt and wire are regarded as coupled inductances. R_s is the inherent series resistance of the belt due to resistance in the wire. The method of Figure 64 b, which uses a large resistance to couple to an integrating negative feedback amplifier, is suitable for low frequencies, but the large value of R required for the frequency response needed would be sensitive to pick-up. Figure 64 c depicts an alternate method which uses low resistances and allows the induction of the belt itself to provide the integration. This method has a high frequency response which is limited only by the internal capacitance of the Rogowski Belt itself (combined with the coil inductance, which limits the maximum numbers of turns). The low frequency response is improved by making L as large as possible. This is more clear if the following analysis is considered. Neglecting inductance and resistance in the primary circuit, which is allowable at the frequencies of interest here (less than 1 MHz), one may write:

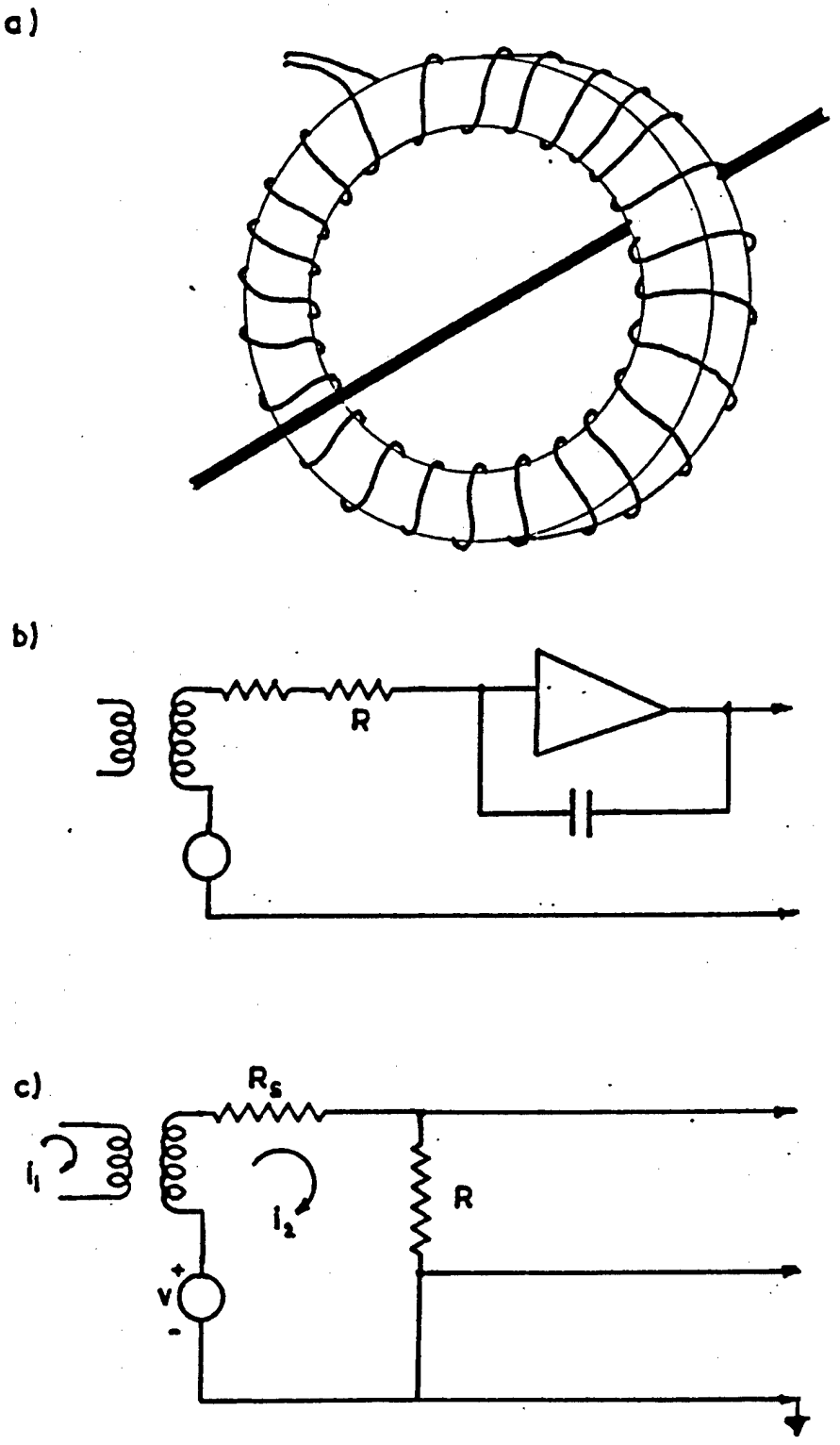

FIG. 64 ROGOWSKI BELT AND EQUIVALENT CIRCUITS

$$M\frac{di_1}{dt} = L_2\frac{di_2}{dt} + (R_s + R)i_2 \qquad \text{Eq. II.3}$$

A full Laplace solution would be:

$$I_2(s) = \frac{V_1 Ms}{(sL_1 + R_1)(sL_2 + R_2) - M^2s^2} \qquad \text{Eq. II.4}$$

The following useful observation be made about this equation: if it is assumed that the current being measured rises from zero to its maximum value, I_{max}, in t seconds, then I_{max}/t will be the approximate value of di_2/dt. Thus if $L/t \gg R_s + R$, the second term in Equation II.3 may be neglected, and both sides integrated to show that the current in the circuit will be:

$$i_2 = V/L = \left(\frac{NAu_o}{2\pi R_{av}}\right) \Big/ \left(\frac{u_o N^2 A}{2\pi R_{av}}\right) = i_1/N \qquad \text{Eq. II.5}$$

where $L/t \gg R_s + R$. This inequality is more applicable to this pulse case than that given in other sources which describe this belt (27). For the belt for this application, the choice of components was made after considerable experimentation, and is best understood by considering the response of the belt to a unit step function, $u_o(t)$:

$$i_2 = \frac{1}{N}(1 - \exp(-(R_s + R)t/L)) \qquad \text{Eq. II.6}$$

A droop in response with time constant $(R_s + R)/L$ will occur on long pulses. Since the output voltage measured across R will be larger for larger R, and smaller with increasing N, it is clear that a compromise must be sought. The final design had a switch providing two values of R, the smaller one for long pulses, and the following parameters:

L/R	High R	2.5 msec
	Low R	7.5 msec
N		2000 T
R_{av}		2 cm
A		3×10^{-4} cm^2
Rise time (10%-90%)		2 μsecs
R_s		27 ohms

Appendix III Drift Tube Pressure Differential

It was suggested in Chapter 4 that the ion gauge readings of pressure might not accurately reflect the true pressure in the drift tube due to the small conductance of the drift tube. If this were the case, the pressure readings would tend to underestimate the pressure in the collector end of the drift tube, and a pressure gradient along the drift tube would exist. It is the intention of this appendix to determine what estimate of this effect is possible, and to calculate the predicted ion current flow from a drift tube with a pressure gradient.

It is important to first record the pressure measurements which are made as the tube is brought from cold to normal beam pulsing. Pressure in the cold tube was observed to be 3×10^{-8} Torr. When the heater has been turned on and the pressure has had time to stabilise, a pressure of 1.6×10^{-7} Torr is observed. This pressure rise is caused by outgassing of the cathode and the ceramic wall sections adjacent to it, which become quite hot, even with forced air cooling (the temperature was observed to be in the neighbourhood of 100^{0}C. on the outside). When the beam is turned on in repeated trials, a very fast pressure rise to 2.5×10^{-7} is observed (within 1 minute) and this is followed by a slow pressure rise to 2.7×10^{-7} Torr, which is reached in 5 minutes. Further pressure rises and falls during long duration experiments are very small and are attributed to changes in the ambient temperature in the laboratory.

It is believed that the additional gas which is present after the beam has been turned on comes mainly from two locations: the cathode and the collector. In the case of the cathode, it is thought that additional conversion of $BaCO_3$ and $Ba(OH)_2$ to BaO, which occurs only while beam current is being drawn, would be a source some quantity of gas. The cathode is never made to deliver the full beam current under cw conditions during its activation, and reconversion of $Ba(OH)_2$ to BaO

it thought to be taking place continuously at a slow rate during the operation of the valve under these pulsed conditions.

The collector would be the other large source of gas emission since more beam current strikes the collector than anywhere else, and some gas would be expected to be evolved because of the resultant heating. It is worthwhile to review at this point what assumptions can be made concerning this gas evolution. Experimental work indicates that at temperatures up to 300^{0}K a monolayer of adsorbed gas will remain on the collector material. At temperatures above 700^{0}K., however, most of the other monolayers will have been stripped away (36). It would seem reasonable to assume that some removal of gas from the collector takes place during the beam pulse, and due to the average heating of the collector. Because the monolayer which continues to remain will lower the sticking probability, it also seems likely that only an insignificant amount of re-sticking takes place during interpulse periods, and that the net result of the beam heating of the collector is to produce an evolution of gas. The difference in mass between the electron and the gas molecules would seem to rule out any molecules being ejected due to collision phenomenon alone.

Because of the inability in this experimental configuration to measure the pressure close to the collector, it is impossible to apportion the observed pressure rise with pulsing between the cathode and the collector with accuracy. However, because the pressure is observed to rise quickly at first and more slowly until reaching a level value in five minutes, it seems not unreasonable to associate pressure rises which occur quickly with cathode outgassing, and to associate a slower rise with a thermal effect, and thus with the collector. It is clear that no significant temperature change will take place in the cathode. If this separation of gas sources can be made, it then becomes possible to determine the gas throughput from each of these regions, and thus

calculate the pressure gradient which the beam would be likely to see. To cover all extremes, a second calculation will be made which will assume that all gas throughput due to the beam originates in the collector, and thus a maximum value of the pressure gradient can be determined.

Making use of methods discussed in Van Atta (37), the following conductances were calculated for the low pressure regime :

Tube between pump and tee piece	370 l/sec
Passage between gauge and back of modified header plate	660
Annular ring formed by cathode pot and wall	470
Drift tube Section No. 1	10.7
2	8.5
3	9.7
4	11.7
5	12.5
Total drift tube conductance	2.1

It is assumed that pump speed is constant over the small ranges of pressure which are involved in this calculation of gas throughput, and that the beam pumping speed is negligible. The beam speed is 15.4 l/sec instantaneous, but this must be multiplied by the duty cycle, which is 1/100 or less. Denoting the gas throughput to the pump when the beam and heater are off as Q_{op}, the throughput with the heater on as Q_{hp}, and the throughput with heater and beam on as Q_{hbp}, and calculating that the 33 l/sec pump speed is reduced to a speed S_g of 30 l/sec at the pressure gauge, the same subscripts as used above may be used to write the results of pressure measurements:

$$P_{og} = 3 \times 10^{-8} \text{ Torr}$$

$$P_{hg} = 1.6 \times 10^{-7}$$

Since for steady flow, Q=PS,

$$Q_h + P_{hg} S_g = 4.8 \times 10^{-6} \text{ Torr-l/sec}$$

When the beam is turned on the pressure rises quickly to $P_{hbgi} = 2.5 \times 10^{-7}$, and finally stabilises in 5 minutes to $P_{hbgf} = 2.7 \times 10^{-7}$. These correspond to throughputs of 7.5×10^{-6} and 8.1×10^{-6} respectively. If it is assumed that all the gas measured in the first pressure rise

originates in the cathode, and the collector is only responsible for the gas which causes the second rise, it is concluded by subtracting Q_n from the above throughputs that 6×10^{-7} Torr-l/sec comes from the collector. Assuming that all the gas which flows after the beam is turned on comes from the collector, a gas flow of 3.3×10^{-6} Torr-l/sec is calculated.

If P_a is the pressure at the anode and P_c the pressure at the collector, the difference between them may be calculated from the equation :

$$Q = (P_c - P_a)C_d \quad (P_c - P_a) = Q/C_d$$

where C_d is the drift tube conductance, 2.1 l/sec. For the first assumption this pressure difference is 3×10^{-7}, and for the assumption that all gas flows from the collector, 1.7×10^{-6} Torr. Thus the pressure gradients for the two hypotheses chosen have been calculated and it remains to determine the ion current which is predicted to flow from a system with such a pressure gradient.

A calculation using the conductances between the modulating anode and the pressure gauge shows that with the full throughput with beam and heater on, a pressure drop of only 2.9×10^{-8} Torr occurs between these two points, and this can be neglected, and pressure at the anode can be taken to be the same pressure as that indicated on the pressure gauge.

For each length along the drift tube, dx, an ion current, dI is generated.

$$dI = p(x)P_1 I_B dx$$

The pressure starts at p_a and increases to a maximum of $p_a + (\Delta p)$. Because of the uniformity of the drift tube dimensions, a linear change in pressure along the length of the drift tube will be assumed, easing calculations. The pressure at any point along the drift tube is therefore

$$p(x) = p_a + \frac{x\,(\Delta p)}{I_D}$$

where I_D is the drift tube length. The total ion current may then be computed from the integral (or a simple average with the linear assumption)

$$I_i = \int p(x) P_I I_B dx = P_I I_B I_D \left(p_a + \frac{\Delta p}{2}\right)$$

Referring to the first part of this appendix, two values of Δp are shown to be of interest: 1) 3×10^{-7} Torr and 2) 1.7×10^{-6} Torr. For P_I = 26 ion-electrons pairs/meter-Torr, which is the coefficient for CO and other common gases at 15 KV beam volts, calculations have been made and are shown on Figure 65.

Also shown on Figure 65 are the ion current measurements from Figure 27, and a theoretical curve assuming no pressure differential. Although the absolute values of all three curves are different, it is important to observe that the shape of the measured curve is more closely matched by the curve which relates to a pressure differential of 3×10^{-7} Torr, which was the one arrived at by separating gas throughput from the cathode and the collector on the basis of differences in their times to steady flow. Inclusion of the pressure differential along the drift tube thus proves to be adequate to explain the shape of the curve of observed ion current vs pressure. This would indicate that no undesirable effects such as focussing of the ion current on the Faraday cage for low pressures are taking place. From the match of the curves it would seem that the true value of the pressure differential along the drift tube might be slightly higher than 3×10^{-7} Torr but this value shall be retained as being one which offers a good estimate. Thus the curve for $p = 3 \times 10^{-7}$ Torr in Figure 65 is taken as the prediction which a simple extension of Equation 3.1 leads to, and is therefore reproduced in Figure 27 for the purposes of comparison with the experimental data. It may be concluded from this discussion that in spite of the low conductance of the drift

tube, the pressure measured at the ionization gauge may be taken as an accurate figure for pressure throughout the valve, except at very low pressures.

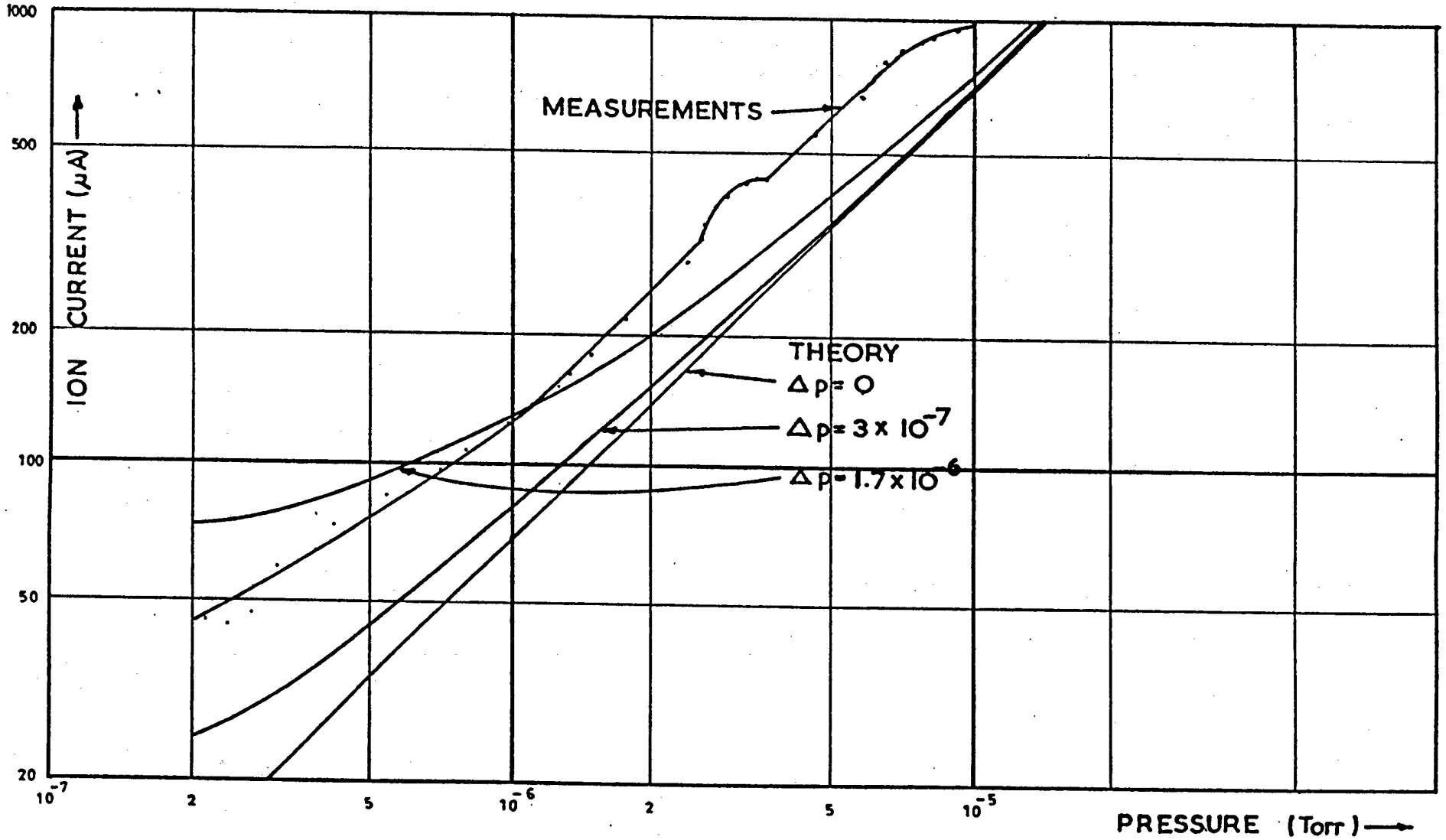

FIG. 65 ION CURRENT vs PRESSURE

Appendix IV Axial Potential Distribution in Drift Tube Biasing

The axial potential distribution in the drift tubes may be easily calculated by making use of the work done on coaxial cylinders in standard works on electron optics. Grivet (38) gives the formula for axial potential between two cylinders of the same diameter separated by a distance d as:

$$\phi = \frac{\phi_1 + \phi_2}{2}\left(1 + \frac{1-\lambda}{1+\lambda}\ \frac{1}{2\pi d}\ln\frac{\cosh \pi(z+d)}{\cosh \pi(z-d)}\right)$$

where all distances are measured in units of the drift tube radius. Then, since all but the final gap between tubes are 1", d = 2. Allowing $\phi_1 = 0$ one may write:

$$\phi(z) = \left(\frac{\phi_2}{1}\right)\left(\frac{1}{2}\right)\left(1 + \frac{1}{4W}\ \ln\frac{\cosh (z+2)W}{\cosh (z-2)W}\right) \qquad \text{Eq. IV.1}$$

where $W = \frac{\tanh (1.318)d}{d} = 0.494929$

This function was computed and the results are shown below:

AXIAL POTENTIAL DISTRIBUTION : TWO COAXIAL CYLINDERS

Z (radial units)	Fraction of Potential
0.0	.500000
0.5	.593809
1.0	.682770
1.5	.762480
2.0	.829615
2.5	.882607
3.0	.921889
3.5	.949443
4.0	.967936
4.5	.979948
5.0	.987577
5.5	.992349
6.0	.995306
6.5	.997126
7.0	.998244
7.5	.998927
8.0	.999345
8.5	.999601
9.0	.999756
9.5	.999851

BIBLIOGRAPHY

1. C.C. Cutler, "Spurious Modulation of Electron Beams," Proc. IRE, 1956, p. 16

2. L.D. Clough, K. Evans, H. L. Hartnagel, O. C Kendall, " Low-frequency Output fluctuations of microwave Tubes," Int. J. Electronics, 1969, 27, p. 195

3. A. D. Sutherland, "Relaxation Instabilities in High-Perveance Electron Beams," IRE Trans. on Electron Devices, Octobaer, 1960, p. 268

4. R.L. Jepson, " Ion Oscillations in Electron Beam Tubes, Ion Motion and Energy Transfer," Proc. IRE, 1957, p. 1069

5. J.R. Pierce, "Possible Fluctuations in Electron Streams Due to Ions," J. Appl. Physics, vol. 19, 1951, p. 231

6. H. Bohlen and V. Dubravec, "Signalstörungen Durch Ionen, Langsame Electronen und Multipactorentladungen bei UHF-Fernsehklystrons," 7th Int. Conf. of Microwave and Optical Gen. and Ampl., 1968, VDE-Verlag, Berlin

7. R. Anand, "An Electron Gun for Reducing Ion Oscillation in TWT's," Proc. IEEE, Electron Dev., 1964, p. 75

8. B. Laico, Mc Dowell, and Moster, " A Medium Power TWT for 6000 MHz Radio Relay," Bell Syst. Tech. J., Nov., 1956, p. 1285

9. C.C. Cutler and J. A. Saloom, " Pin-hole Investigation of Electron Beams," Proc. IRE, 1955, p. 299

10. Conversations with M. Esterston and R. Heppinstall, EEV, Chelmsford.

11. L. M. Field, K. Spangenberg, and R. Helm, "Control of Electron-Beam Dispersion at High Vacuum by Ions," Electrical Communications, 24, 1947, p. 108

12. B. H. Wadia, "Influence of Positive Ions on Electron Beam Profiles," PhD Thesis, Stanford University, California, Feb., 1954

13. E. L. Ginzton and B. H. Wadia, "Positive Ion Trapping in Electron Beams," Proc. IRE, 1954, p. 1548

14. G. Dunn and Self, "Static Theory of Density and Potential Distribution in a Beam-generated Plasma," J. Appl. Phys., 35, 1964, p.113

15. E.G. Linder and K.G. Hernqvist, "Space Charge Effects in Electron Beams and Their Reduction by Positive Ion Trapping," J. Appl. Phys., 21, 1950, p. 1088

16. K. G. Hernqvist, "Plasma Ion Oscillations in Electron Beams," J. Appl. Phys., 26, 1955, p. 544

17. J. E. Hopson, "Beam-generated Beam Plasma System," J. Appl. Phys., 34, 1963, p. 2425

18. N.S. Zinchenko and B. A. Zhigailo, "Effect of Ion Focusing in Velocity Modulated Electron Beams," Sov. Phys-Tech. Phys. 9, Jan. 1965, p. 1008

19. N. C. Barford, "Space Charge Neutralisation by Ions in Linear Flow Electron Beams," J. Electr. and Contr., Vol. 3, 1957, p. 63

20. V. I. Volosok and B. V. Chirikov, "Space Charge Compensation in an Electron Beam," Sov. Phys-Tech. Phys., 2, p. 2437

21. H. Hartnagel, "Ion Distribution in the Drift Region of Tubular Electron Beams," Int. J. Electr., 18, 1965, p. 431

22. University of Sheffield, Dept. of Electronic and Electrical Engrg., Final Report, Oct. 1969 - Sept. 1970, Res. Proj. RU 10-15, "Ions Trapped by Electron Beam Potentials," K. Evans

23. J. T. Senise, "Note of Positive-Ion Effects in Pulsed Electron Beams," J. Appl. Phys.,29, 1958, p. 839

24. M. E. Hines, G. W. Hoffman, and J. A. Saloom, "Positive Ion Drainage in Magnetically-focused Electron Beams," J. Appl. Phys.,26, p. 1157

25. K. Sann,"The Measurement of Near-Carrier Noise in Microwave Amplifiers, IEEE, MTT-16, Sept. 1968, p. 761

26. Principles of Radar, J. F. Reintjes and G.T. Coate, 3rd ed, 1952 Mc Graw-Hill, New York

27. R. H. Huddlestone and S.T. Leonard, Plasma Diagnostic Techniques, Academic Press, New York, 1965

28. R.P. Little and S.T. Smith,"Electrical Breakdown in Vacuum," IEEE Trans. on Elect. Dev., Feb. 1965, p. 77

29. H.S.W. Massey, E.H.S. Burhop, and H.B. Gilbody, Electronic and Ionic Impact Phenomena, Clarendon Press, Oxford 1969

30. A. von Engel, Ionized Gases, Claredon Press, Oxford, 1965

31. L.J.Kieffer and G. H. Dunn,"Electron Impact Ionization Cross-Section Data for Atoms, Atomic Ions, and Diatomic Molecules: I.Experimental Data," Rev. Mod. Phys., 38, 1966, p. 1

32. N.F. Mott and H.S.W. Massey, The Theory of Atomic Collisions, Claredon Press, Oxford, 1965

33. C.H. Bachman, Hull, and Silberg, "Positive and Negative Ions in Cathode Ray Tubes," J. Appl. Phys., 1953, p. 427

34. P. Hedvall, "Properties of a Plasma Created by an Ion Beam," J. Appl. Phys., 33, 1962, p. 2427

35. M. Kaminsky, Atomic and Ionic Impact Phenomena on Metal Surfaces, Springer-Verlag, Berlin, 1965

36. E. W. McDaniel, Collision Phenomena in Ionized Gases, J. Wiley & Sons, New York, 1964

37. C.M. Van Atta, Vacuum Science and Engineering, McGraw-Hill, New York, 1965

BIBLIOGRAPHY

1. C.C. Cutler,"Spurious Modulation of Electron Beams," Proc. IRE, 1956, p. 16

2. L.D. Clough, K. Evans, H. L. Hartnagel, O. C Kendall, " Low-frequency Output fluctuations of microwave Tubes," Int. J. Electronics, 1969, 27, p. 195

3. A. D. Sutherland, "Relaxation Instabilities in High-Perveance Electron Beams," IRE Trans. on Electron Devices, Octobaer, 1960, p. 268

4. R.L. Jepson, " Ion Oscillations in Electron Beam Tubes, Ion Motion and Energy Transfer," Proc. IRE, 1957, p. 1069

5. J.R. Pierce, "Possible Fluctuations in Electron Streams Due to Ions," J. Appl. Physics, vol. 19, 1951, p. 231

6. H. Bohlen and V. Dubravec, "Signalstörungen Durch Ionen, Langsame Electronen und Multipactorentladungen bei UHF-Fernsehklystrons," 7th Int. Conf. of Microwave and Optical Gen. and Ampl., 1968, VDE-Verlag, Berlin

7. R. Anand, "An Electron Gun for Reducing Ion Oscillation in TWT's," Proc. IEEE, Electron Dev., 1964, p. 75

8. B. Laico, Mc Dowell, and Moster, " A Medium Power TWT for 6000 MHz Radio Relay," Bell Syst. Tech. J., Nov., 1956, p. 1285

9. C.C. Cutler and J. A. Saloom, " Pin-hole Investigation of Electron Beams," Proc. IRE, 1955, p. 299

10. Conversations with M. Esterston and R. Heppinstall, EEV, Chelmsford.

11. L. M. Field, K. Spangenberg, and R. Helm, "Control of Electron-Beam Dispersion at High Vacuum by Ions," Electrical Communications, 24, 1947,p. 108

12. B. H. Wadia, "Influence of Positive Ions on Electron Beam Profiles," PhD Thesis, Stanford University, California, Feb., 1954

13. E. L. Ginzton and B. H. Wadia, "Positive Ion Trapping in Electron Beams," Proc. IRE, 1954, p. 1548

14. G. Dunn and Self, "Static Theory of Density and Potential Distribution in a Beam-generated Plasma," J. Appl. Phys., 35, 1964, p.113

15. E.G. Linder and K.G. Hernqvist, "Space Charge Effects in Electron Beams and Their Reduction by Positive Ion Trapping," J. Appl. Phys., 21 , 1950, p. 1088

16. K. G. Hernqvist,"Plasma Ion Oscillations in Electron Beams," J. Appl. Phys., 26, 1955, p. 544

17. J. E. Hopson,"Beam-generated Beam Plasma System," J. Appl. Phys.,34, 1963, p. 2425

18. N.S. Zinchenko and B. A. Zhigailo, "Effect of Ion Focusing in Velocity Modulated Electron Beams," Sov. Phys-Tech. Phys. 9, Jan. 1965, p. 1008

19. N. C. Barford, "Space Charge Neutralisation by Ions in Linear Flow Electron Beams," J. Electr. and Contr., Vol. 3, 1957, p. 63

20. V. I. Volosok and B. V. Chirikov, "Space Charge Compensation in an Electron Beam," Sov. Phys-Tech. Phys., 2, p. 2437

21. H. Hartnagel, "Ion Distribution in the Drift Region of Tubular Electron Beams," Int. J. Electr., 18, 1965, p. 431

22. University of Sheffield, Dept. of Electronic and Electrical Engrg., Final Report, Oct. 1969 - Sept. 1970, Res. Proj. RU 10-15, "Ions Trapped by Electron Beam Potentials," K. Evans

23. J. T. Senise, "Note of Positive-Ion Effects in Pulsed Electron Beams," J. Appl. Phys.,29, 1958, p. 839

24. M. E. Hines, G. W. Hoffman, and J. A. Saloom, "Positive Ion Drainage in Magnetically-focused Electron Beams," J. Appl. Phys.,26, p. 1157

25. K. Sann,"The Measurement of Near-Carrier Noise in Microwave Amplifiers, IEEE, MTT-16, Sept. 1968, p. 761

26. Principles of Radar, J. F. Reintjes and G.T. Coate, 3rd ed, 1952 Mc Graw-Hill, New York

27. R. H. Huddlestone and S.T. Leonard, Plasma Diagnostic Techniques, Academic Press, New York, 1965

28. R.P. Little and S.T. Smith,"Electrical Breakdown in Vacuum," IEEE Trans. on Elect. Dev., Feb. 1965, p. 77

29. H.S.W. Massey, E.H.S. Burhop, and H.B. Gilbody, Electronic and Ionic Impact Phenomena, Clarendon Press, Oxford 1969

30. A. von Engel, Ionized Gases, Claredon Press, Oxford, 1965

31. L.J.Kieffer and G. H. Dunn,"Electron Impact Ionization Cross-Section Data for Atoms, Atomic Ions, and Diatomic Molecules: I.Experimental Data," Rev. Mod. Phys., 38, 1966, p. 1

32. N.F. Mott and H.S.W. Massey, The Theory of Atomic Collisions, Claredon Press, Oxford, 1965

33. C.H. Bachman, Hull, and Silberg, "Positive and Negative Ions in Cathode Ray Tubes," J. Appl. Phys., 1953, p. 427

34. P. Hedvall, "Properties of a Plasma Created by an Ion Beam," J. Appl. Phys., 33, 1962, p. 2427

35. M. Kaminsky, Atomic and Ionic Impact Phenomena on Metal Surfaces, Springer-Verlag, Berlin, 1965

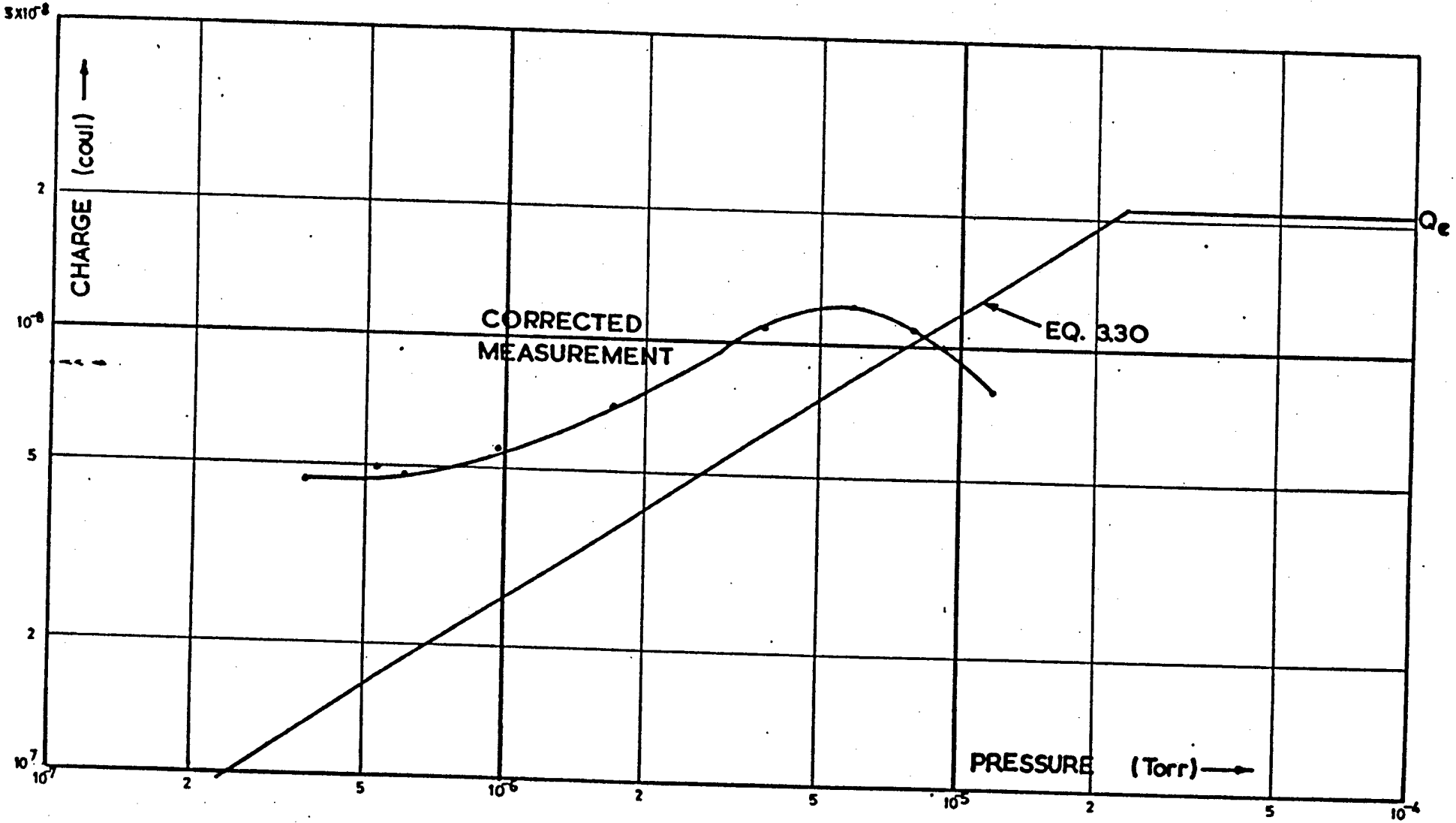

FIG. 59 IONIC CHARGE STORAGE WITH NEGATIVE COLLECTOR

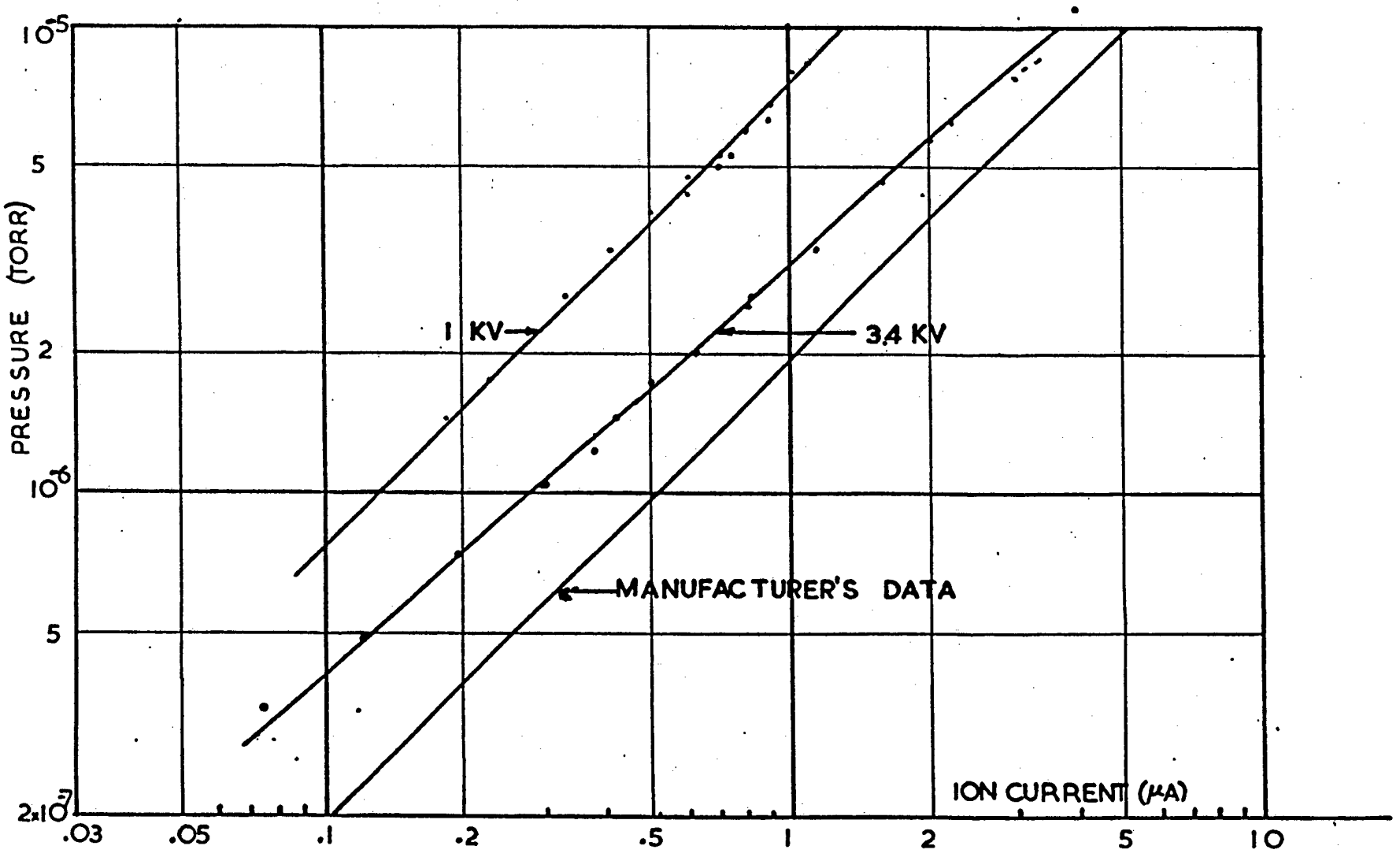

FIG. 11 ION PUMP CHARACTERISTICS